The Dissertation Committee for Bryan James Kaehr Certifies that this is the approved version of the following dissertation:

Defining Cellular Microenvironments using Multiphoton Lithography

Committee:

Jason B. Shear, Supervisor

Andrew D. Ellington

Dean R. Appling

Jennifer S. Brodbelt

Krishnendu Roy

Defining Cellular Microenvironments using Multiphoton Lithography

by

Bryan James Kaehr, B.S.

Dissertation

Presented to the Faculty of the Graduate School of

The University of Texas at Austin

in Partial Fulfillment

of the Requirements

for the Degree of

Doctor of Philosophy

The University of Texas at Austin

August 2007

Dedication

This dissertation is dedicated to my parents, Jim and Terri Kaehr

Acknowledgements

I sincerely thank my advisor, Jason Shear, for his guidance and support. I thank my IGERT co-advisor Andy Ellington for his advice and enthusiasm, and my sincere thanks to my committee members, Profs. Dean Appling, Jennifer Brodbelt and Krishnendu Roy, for their time and consideration. I owe many thanks to my labmates, past and present. Dr. Richard Allen and I worked together on developing a strategy for biocompatible microfabrication and much of our efforts are presented in Chapter 2. Dr. Nusret Ertas and I worked together and independently to characterize a low-cost laser for photofabrication. Rex Nielson and I collaborated on the development of a method to micro(re)construct virtually anything one might ever want micro(re)constructed, and our efforts are presented in the second half of Chapter 3. I owe Drs. Ryan Hill, Dana Wise, and Matt Plenert much thanks for their friendship, assistance and overall good times during our years spent together. I thank current lab members Eric Ritschdorff, Samira Moorjani, Stephanie Seidlets, Eric Spivey, Todd Hoppe, and Jodi Connell for their tolerance (of me) and their scientific enthusiasm (and wiffle ball skills). I thank Dwight Romanovicz for much technical and creative advice regarding microscopy. I thank Dr. Sandy Parkinson at the Univeristy of Utah for imparting some of his vast knowledge (both technical and scientific) of microbiology. I thank the NSF for an IGERT fellowship

Defining Cellular Microenvironments using Multiphoton Lithography

Publication No._____

Bryan James Kaehr, Ph.D.

The University of Texas at Austin, 2007

Supervisor: Jason B. Shear

To understand the chemistry of life processes in detail is largely a challenge of resolving them in their native, cellular environment. Cell culture, first developed a century ago, has proven to be an essential tool for reductionist studies of cellular biochemistry and development. However, for the technology of cell culture to move forward and address increasingly complex problems, *in vitro* environments must be refined to better reflect the cellular environment *in vivo*. This dissertation work has focused on the development of methods to define cellular microenvironments using the high resolution, 3D capabilities of multiphoton lithography. Here, site-specific photochemistry using multiphoton excitation is applied to the photocrosslinking of proteins, providing the means to organize bioactive species into well-defined 3D microenvironments. Further, conditions have been identified that enable microfabrication to be performed in the presence of cells — allowing cell outgrowth and motility to be directed in real time. In addition to the intrinsic chemical functionality of microfabricated protein structures, 3D protein matrices are shown to respond mechanically to changes in the chemical environment, enabling new avenues for micro-scale actuation to be

explored. Complex 2D and 3D protein photocrosslinking is further facilitated by integrating transparency and automated reflectance photomasks into the fabrication system. These advances could be transformative in efforts to fabricate precise cellular scaffolding that replicates the morphological (and potentially biochemical) features of *in vivo* tissue microenvironments. Finally, these methods are applied to the study of microorganism behavior with single-cell resolution. Microarchitectures are designed that allow the position and motion of motile bacterial to generate directional microfluidic flow — providing a foundation to develop micro-scale devices powered by cells.

Table of Contents

List of Figures

Chapter 1: Integrating Cell Biology to Microtechnology

1.1 INTRODUCTION

For over a century, much of the study of biology at the cellular level has taken place outside of a cell's 'natural' setting — in the laboratory environments of culture flasks and Petri dishes. Until recently, the methods developed to study microorganisms, dissociated tissue cultures and immortalized cells lines had evolved slowly in the many decades since the laboratory cell staples of *E. coli* K-12 and *HeLa* were harvested from their human environment[*]. Recent attention from the physical and chemical sciences to questions regarding human health and biology has begun to bring new approaches and technologies that, combined with the advances of modern genetic engineering, may revolutionize the study of cellular biology. For example, the high resolution 3D imaging technologies of multiphoton and confocal fluorescence microscopy are particularly well-suited to illuminate subcellular environments detailed by genetically encoded light-responsive molecules. This has enabled not only a clearer window into the elaborate spatial and temporally dynamic biochemistry of cells, but the means to perturb and analyze cellular behavior by increasingly precise and potentially less invasive means [1-3].

The current multidisciplinary approach to biology corresponds to an increased focus of scientific attention at the level of the cell. It is now clear that knowledge of the genetic program of cells, a molecular understanding of genetic material and mechanisms,

---

[*] *E. coli* K-12 was isolated from a diphtheria patient in 1922 and maintained at Stanford University beginning in 1925. *Hela* was isolated from Henrietta Lacks, who died of cervical cancer in 1951.

does not provide enough insight to address the current challenges faced in the basic and applied biosciences [4]. As both the questions and applications for cell biology become more complex and demanding, there is increased need for experimental platforms that better mimic the *in vivo* setting.

Microtechnology offers a means to address these challenges through the miniaturization of tissue culture platforms [5-7]. Culturing cells in miniaturized and microfluidic environments can offer a more precise means to dictate and assay the cellular and subcellular microenvironment with appropriate spatial and temporal resolution. It is along these lines that research in the Shear Lab has concentrated efforts toward developing methods of analysis and microfabrication that enable complex, spatially constricted and temporally dynamic biological phenomenon (e.g., neuronal outgrowth and synaptic transmission) to be interrogated.

Toward these ends, this dissertation outlines the development of novel microfabrication strategies that enable the 3D assembly of chemically and mechanically responsive biomaterials in the presence of developing cell populations at prescribed points in time. The new fabrication methods and 3D assemblage of materials described here stand as both an alternative and complementary technology for other relevant micropatterning strategies including hard and soft lithography. Further, the ability to define the 3D, *in vitro* microenvironment with biological materials may enable a more practical interface between the organic material of biochemical systems and cells to that of increasingly sophisticated microanalysis tools.

The realization of a truly 3D biocompatible microfabrication strategy outlined here could enable significant problems in cell biology to be addressed practically and

under short time scales. Important areas of research where the *in vitro* study of cells remains essential include the analysis and engineering of stem cell development and differentiation [8, 9], neural network function and regeneration [10, 11], and the population-directed behaviors of pathogenic microorganisms in ecologically complex environments [6, 12]. By interfacing well-defined 3D substrate cues with high subcellular and temporal resolution, the foundational studies outlined here should enable the further development of more precise strategies to achieve highly discrete cellular development and differentiation for specific cell types and applications.

1.2 MICROFABRICATION FOR CELLULAR STUDIES

Much of the microfabrication technology in practice today was developed for microelectronics and micro-electro-mechanical systems (MEMs) manufacturing. The increasing need for microfabricated platforms that cannot be manufactured under the strict demands imposed by these industries, which are optimized for planar surfaces and non-biocompatible materials, stems largely from the recent trend towards miniaturization of the chemical and biological laboratory. The micro-laboratory or the 'lab on a chip' has increased sensitivity and resolution for chemical analysis and diagnostics applications and is envisioned to revolutionize the fields of chemical synthesis, cell biology, and bio-micromechanical systems (BioMEMs) [7, 13-15]. An additional prohibitive factor of microchip fabrication technology for research purposes is simply the sophistication and expense of industrial-grade equipment and infrastructure needed to perform microscale lithography under vacuum. Thus a suite of non-conventional lithographic techniques including soft lithography, molecular self assembly, ink-jet printing, and multiphoton

lithography have emerged to provide attractive and potentially less expensive alternatives to prototype microplatforms for research applications [16-18]. Of these, only multiphoton lithography is an intrinsically 3D technique and thus potentially suitable to replicate the geometrically complex microenvironments of tissues — a capability that allows the development of the necessary 3D culture environments for stem cell scaffolding and engineered tissue replacement.

1.3 MULTIPHOTON EXCITATION (MPE)

The strategies developed in this work take advantage of intrinsic 3D photochemistry using the technique of multiphoton excitation (MPE), a photon absorption process initially described by Maria Goeppert-Mayer in 1931 [19]. MPE was observed experimentally in 1961 [20] only months after the invention of the laser but it was not until the early 1990s, with the development of the first two-photon laser scanning fluorescence microscope, that the technique garnered widespread attention outside of the fields of theoretical and applied physics and gas-phase physical chemistry. In this 1991 report, Webb and colleagues used a pulsed dye laser to demonstrate the exceptional 3D resolution of MPE fluorescence for biological microscopy and site-specific photochemistry [21].

The process of MPE can be spatially restricted in three dimensions using focused laser light (Figure 1.1). Whereas one-photon excitation (1PE) requires the energy of the absorbed photon be equivalent to the energy spacing between electronic energy levels in MPE, the excited state can be reached via two (or more) less energetic photons under very stringent temporal constraints. The first photon excites the molecule to a (virtual)

intermediate state which persists for several femtoseconds (as prescribed by Heisenberg's Uncertainty Principle). The second photon must arrive before the decay of this state to achieve two-photon excitation (2PE). Both one- and two- photon processes can be related in terms of a chemical reaction [22] where

$$M + n(h\nu) \leftrightarrow M^*$$ (1.1)

Where M and M^* are the ground and excited state of the chromophore, $h\nu$ is a photon and n is the number of absorbed photons to reach the excited state. The reaction rate for formation of M^* can be stated in terms of reactant concentrations:

$$d[M^*]/dt = k[h\nu]^n\,[M] = \delta I^n[M]$$ (1.2)

Where k is the rate constant for the forward reaction, I is the instantaneous intensity (in units of photons/s·cm^2) and δ is the excitation cross section (in units cm^{2n}(s/photon)$^{n-1}$). There is generally no distinction between one- and two-photon excitation upon energy dissipation processes; for instance there is no spectral shift of emission in the case of fluorescence (Figure 1.1a). The dependence on I^n for a multiphoton process can be used to impose spatial constraints on the excited state by bounding the threshold for MPE to regions of greatest photon intensity (i.e., near the 'waist', or focal point of a focused laser beam; Figure 1.1b). Under the nonlinear excitation regime of MPE, the probability of excitation and ultimately fluorescence decreases sharply for a given molecule as one

5

moves further from the focal point. For 1PE there is equal excitation for all planes throughout the axis of beam propagation (Figure 1.1b).
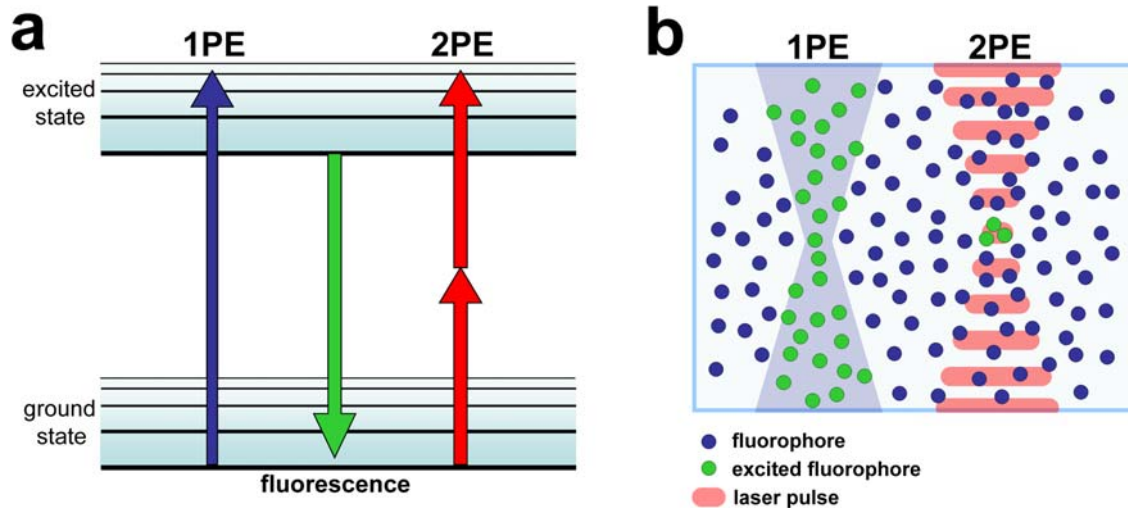
Figure 1.1:   One and two-photon excitation (1PE vs 2PE). (a) The absorption of a single, high energy photon (blue) or two photons (red) of half the energy results in an excited state that can relax via fluorescence (green). (b) Whereas 1PE occurs along the entire axis of light propagation (area of shaded blue), 2PE can be restricted to the region of greatest light intensity (corresponding to the focal point) by using high-NA focusing optics and high peak intensity pulsed laser light.

MPE requires such high intensities of light that its use as a practical technique did not come about until the commercial availability of turn-key, solid-state femtosecond pulsed laser sources, such as the titanium:sapphire (Ti:S) oscillator, in the 1990s. Pulsed lasers concentrate photons into discrete temporal packets providing high instantaneous intensities at low average powers; a situation that decreases the likelihood of damage from heating (an important consideration for biological applications such as fluorescence imaging of tissue). Further, restriction of excitation to the focal point using MPE

alleviates out of plane photodamage. In addition, Ti:S oscillators offer a high degree of tunability, from ~700-1000 nm, enabling greater penetration into biological tissue due to the ~1 order of magnitude less absorbance for biological specimens at these wavelengths compared to the UV and visible regions [23].

For a Ti:S operating at 10 mW and generating pulse durations of ~100 fs separated by ~15 ns, the instantaneous intensity can reach ~10^{11} W cm^{-2} at the beam waist using a high numerical aperture (NA) objective. These conditions permit photochemical reaction volumes (or 'voxels') to be confined to < 1 μm^3. Thus, photoexcitation for fluorescence, photo-uncaging, photopolymerization and photocrosslinking can be prescribed to highly resolved 3D points in space and time. Under most conditions, MPE voxels are not spherical but resemble a prolate spheroid with dimensions proportional to the square of light intensity (SLI) at the focal volume [24].

The majority of work presented here was performed using a Ti:S oscillator — an excellent light source for the MPE application of 3D photolithography. However, the cost of commercial femtosecond laser sources such as the Ti:S remain prohibitive for most individual users. Therefore, the capacity of a low-cost laser to promote multiphoton photochemical reactions for microfabrication was also evaluated. This small-footprint, Q-switched, frequency-doubled (532-nm) Nd:YAG laser produces subnanosecond (~600 ps) pulses with energies of up to several microjoules and peak powers comparable to those needed to initiate photochemical crosslinking with femtosecond Ti:S laser light.

1.4 MPE PROTEIN PHOTOCROSSLINKING

The use of MPE for lithographical patterning was suggested by Webb and colleagues shortly after their demonstration of two-photon laser scanning microscopy [25]. However, the 3D capabilities for microfabrication were not demonstrated until the late 1990's in a number of studies using photopolymerization of acrylate-based resins. In these reports, fabrication of arbitrary forms and microsculptures [26, 27], 3D optical data storage devices [28] and photonic lattices [29] demonstrated the unique capabilities for high resolution, 3D fabrication beyond traditional layer by layer photolithographic methods.

Unfortunately, the organic resins and solvents used in those studies are not conducive for the patterning of most biomaterials — clearly a desirable capability for biological applications. Around the same time, however, Pitts *et al.* demonstrated that the photocrosslinking of proteins, such as bovine serum albumin (BSA) and alkaline phosphatase, could be accomplished in aqueous conditions using two-photon initiated photocrosslinking [30]. These initial studies suggested that protein matrices could be fabricated under conditions that would enable *in situ* microfabrication in cellular environments. With this goal in mind, a system was developed to explore the fabrication of 'free-form' microstructures from aqueous solutions of proteins in order to influence neuronal outgrowth and interactions.

Protein photocrosslinking is a widely used biochemical tool often used to study protein interactions with other biomolecules [31-33]. Crosslinking can be initiated through excitation of photosensitizing molecules to triplet states that act directly upon oxidizable moieties (a type I process) through, for instance, a hydrogen abstraction

8

mechanism or by transferring energy to ground state molecular oxygen (a type II process) forming reactive oxygen species such as singlet oxygen ($^1O_2$) [34]. In either case, excited-state intermediates can catalyze the inter- or intramolecular covalent crosslinking of oxidizable protein residues [35]. Additionally, photooxidizable residues including Tyr, Trp, His, Cys, can absorb UV light to form reactive or ionized species capable of crosslinking to other oxidizable moieties — mechanisms that appear to play a role in formation of some types of cataracts [36] as well as the aging of skin [37]. Given the toxicity of radical and singlet oxygen generating chemistries on cells (a mechanism exploited to destroy cancerous cells in the technique of photodynamic therapy; PDT) the latter mechanism — potentially accessed via a three-photon absorption of Ti:S laser light or through 2PE using the 532 nm YAG laser — might decrease the generation of toxic species and thus enhance the biocompatibility of the fabrication process.

The system developed for direct-writing of matrices composed of crosslinked proteins is shown in Figure 1.2. By tightly focusing a high peak-power laser beam to a submicrometer focal spot, protein lines can be fabricated onto a glass substrate by translating the substrate relative to the beam focus. The vast number and character of potential intermolecular crosslinks between oxidizable residues accessible to photo-generated species currently inhibits the molecular resolution of protein matrices which is best approximated as amorphous (circular inset). However, the nature of intermolecular crosslinking for both photocatalyzed radical and singlet oxygen generating pathways has been investigated using model proteins and amino acids [34, 38-41] (Figure 1.3).

Using the approach illustrated in Figure 1.2, matrices of various proteins could be patterned sequentially and imaged with standard microscopy (differential interference

contrast [DIC], and fluorescence microscopy). Here lines comprised of bovine serum albumin (BSA) and the biotin-binding protein avidin were patterned side by side and washed with a biotinylated fluorophore. The localization of fluorescence signal demonstrates the capabilities of this approach for site-specific targeting and scaffolding of molecular effectors — a topic discussed in greater detail in Chapter 2.

Further, by focusing into reagent solution above the glass substrate, structures can be fabricated at the point of focus — independent of the substrate. Figure 1.4 shows a sequence of images tracking the construction of an interlocking chain link comprised of crosslinked BSA. Here, the chain is fabricated entirely in a concentrated protein solution (i.e., with no mooring to a surface). This sequence demonstrates the ability to fabricate well defined 3D micro-objects under the temporal constraints imposed by interlocking the chain links before the nascent structure experiences significant drift through Brownian motion.
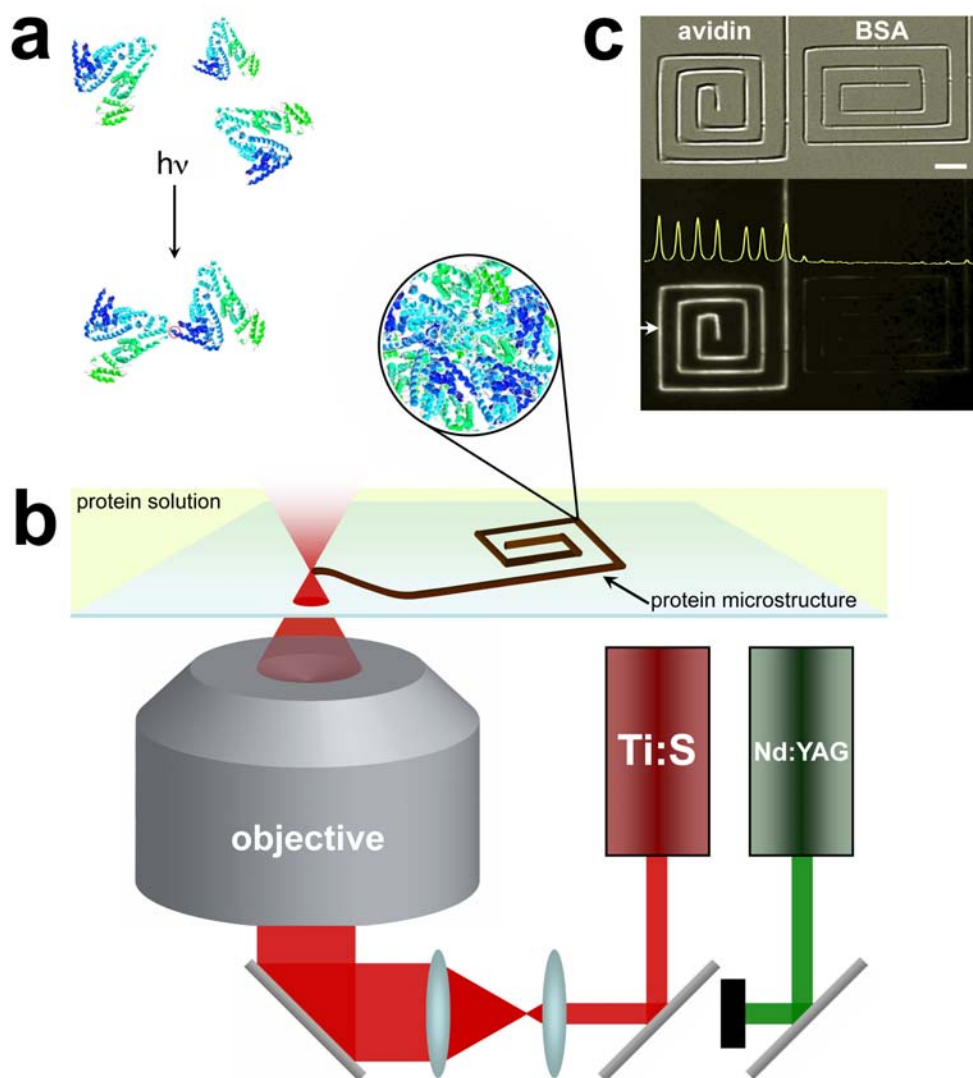
Figure 1.2: A strategy for the microfabrication of 3D protein structures. (a) Proteins can undergo light-induced intermolecular crosslinking initiated either by direct photon absorption or photosensitizer mediated pathways. (b) Microstructures composed of crosslinked proteins are fabricated onto transparent substrates using light from a Ti:S (730-800 nm) or a frequency doubled Nd:YAG (532 nm) coupled to a high NA objective, inverted microscope system. (c) Images of spiral microstructures (fabricated using the Q-switched YAG laser) comprised of crosslinked avidin (left images) and BSA (right images) and following the application of 2-µM biotin-fluorescein (lower panel). Fluorescence intensity versus horizontal position (from the arrow) is plotted on the upper portion of the fluorescence image. Scale bar, 5 µm.

11
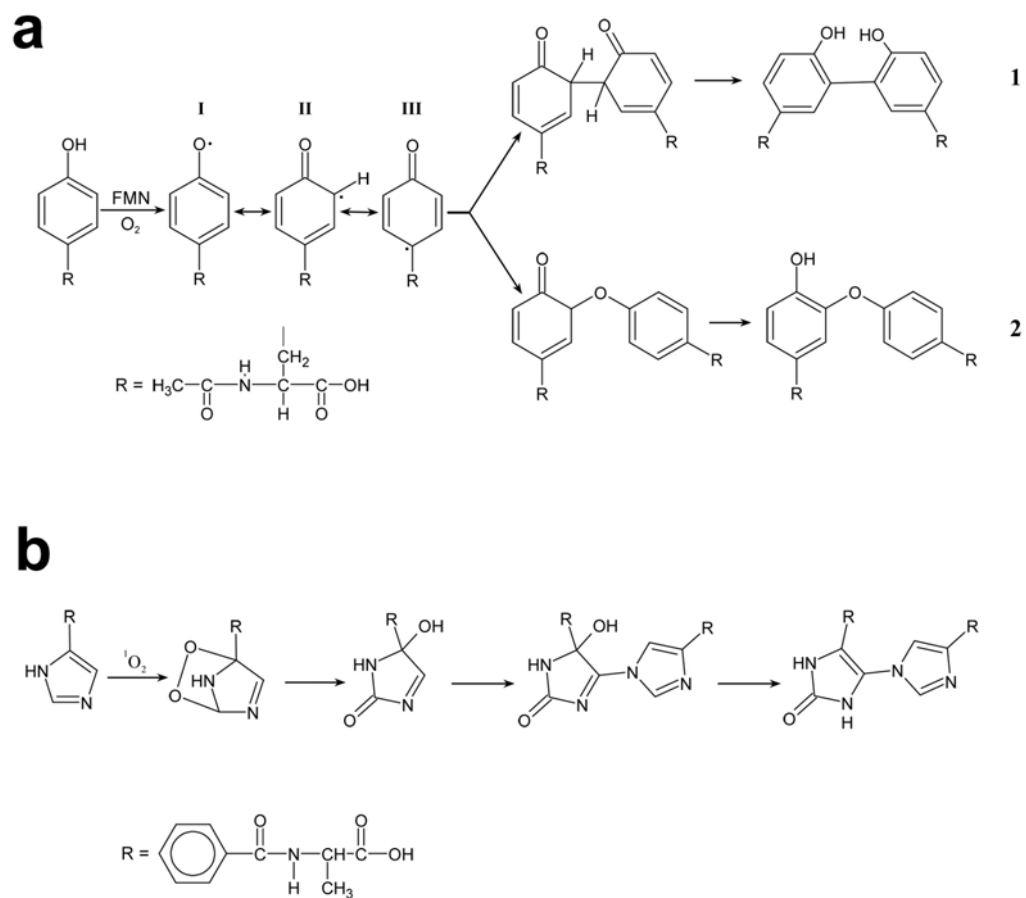
Figure 1.3: Proposed mechanism for the formation of tyrosine (a) and histidine (b) dimers in protein photocrosslinking using photosensitizers operating through Type I (FMN, a) and Type II mechanisms (Rose Bengal, b). Adapted from [40, 41].
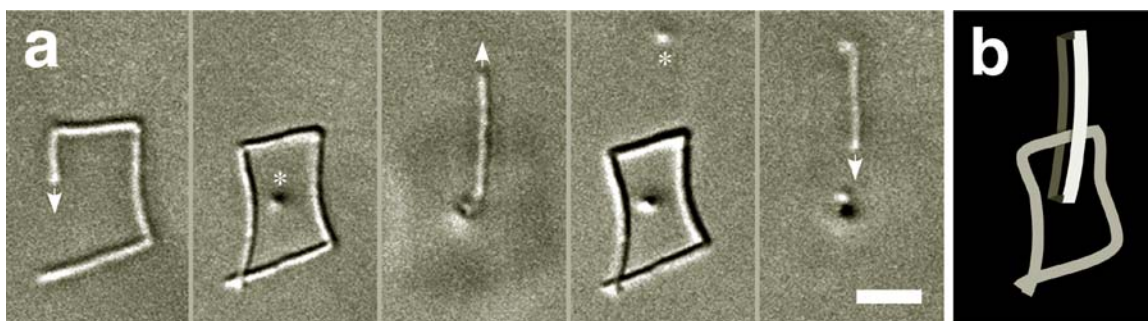
Figure 1.4: Direct-write of a free-floating three-dimensional object using the Q-switched YAG laser. (a) A DIC image sequence acquired over ~40 s demonstrating fabrication of interlocking chain links from a solution of BSA (400 mg ml^{-1} protein with no additional photosensitizer; average power, 1.7 mW). Arrows in the first, third, and fifth panels indicate the direction of protein structure fabrication in planes orthogonal to the optical axis; asterisks in the second and fourth panels identify protein matrix as it is fabricated along the optical axis. Scale bar, 5 μm. (b) Schematic representation of the interlocking links.

Combining the volume-limited photochemistry of MPE to photocrosslinking of proteins provides countless avenues of exploration for basic and applied research. For instance, the vast range of physical and chemical identities of proteins (in addition to the ability to engineer new protein functionalities [42, 43]) that could be incorporated into microstructures using this approach may enable 3D cell-substrate interactions, that would otherwise be inaccessible *in vitro,* to be well-defined and examined. Here we have concentrated on the development of methodologies and instrumentation for the site-specific tailoring of cellular microenvironments using a relatively small number of proteins. Nevertheless, strategies have been developed that allow microstructures composed of readily available proteins to act as 3D scaffolding for affinity-directed binding (through ligand and electrostatic mechanisms) of virtually an unlimited range of biologically active species [44, 45].

13

1.5 CONCLUSION AND SUMMARY OF CHAPTERS

In this work, the development of methods for MPE protein photocrosslinking to define cellular microenvironments with high temporal and spatial resolution is presented. These studies provide a foundation for a highly versatile microfabrication strategy that may enable currently inaccessible problems in cell and microbiology to be addressed. For instance, the ability to construct simple, interrogatable neuronal circuits *in vitro* is an important step towards understanding the basic mechanisms of neuronal development, signal processing and regeneration. Current strategies for defining neuronal interactions *in vitro* largely rely on the lithographic patterning of substrates (in an effort to bias the desired growth pathways and interconnects) before cells are seeded. By providing what is essentially a static cell-substrate interaction, 'pre-patterning' technologies are unable to achieve the temporal and spatial dexterity necessary for interaction with neurons undergoing development and differentiation.

Chapter 2 describes initial studies to address these shortcomings through the development of a microfabrication approach that can be performed *in situ*, in the presence of cells. By selecting suitable sensitizers and fabrication conditions, microstructures can be fabricated in the vicinity of developing neuronal populations with little to no disruption of cellular processes. The neuritic architecture of cell from neuronal lines and primary cortical neurons is shown to be corralled and (re)directed to prescribed sites using protein matrix barriers. Additionally, the capacity of a low cost laser to perform MPE protein photocrosslinking is evaluated. Finally, the chemical functionality of proteins incorporated into photocrosslinked matrices is evaluated by assessing the binding properties of matrices comprised of avidin and concanavalin A, studies that

provided a foundation to develop more complex and elaborate functionalization strategies by others in the Shear Lab [45-47].

The techniques described in Chapter 2 provide only rudimentary microstructuration of the cellular environment. To fully realize the highly resolved 3D capabilities of MPE protein photocrosslinking requires a similarly high resolution, coordinated mechanism for voxel positioning. Chapter 3 describes the development and instrumentation of a novel method to address this issue and create complex 3D microstructures by coupling traditional, mask-directed photolithography to MPE protein photocrosslinking. In this way, arbitrary microstructural features can be applied to photocrosslinked protein matrices rapidly, without intensive computational effort. The rapid prototyping of 3D microcontainers and functional microgradients for cell and microbiological applications is presented. The strategy is further enhanced by integrating an automated reflectance element (a digital micromirror device; DMD) into the masking system. This allows microfabrication to be directed by coordinating image sequences to z-steps along the optical axis. This unique technology allows input of imaged biological tissue encoded by 3D imaging methods (e.g., confocal, CT, MRI) to be microreplicated, and further provides the capability to fabricate and therefore mimic the natural, *in vivo* 3D scaffolding of cellular microenvironments.

In Chapter 4, the mechanical functionality of MPE protein photocrosslinked matrices is assessed. Specifically, the hydrogel swelling properties of matrices are investigated under a range of environmental conditions (e.g., pH, ionic strength). The identity of incorporated proteins as well as the crosslinking density is shown to strongly influence the matrix swelling behavior. The mechanical properties of protein matrices for

15

prescribed microactuation and microparticle translocation in three dimensions is demonstrated.

Finally in Chapter 5, MPE protein photocrosslinking is evaluated as a high resolution tool for behavioral microbiology. Microchamber geometries, fabricated using the methods described in Chapter 3, are evaluated for the trapping, incubation and directed motility of microorganisms. Biocompatible fabrication strategies discussed in Chapter 2 are used here to trap and incubate motile bacteria with single cell resolution. The hydrogel properties of protein matrices discussed in Chapter 4 are exploited here as a mechanism of cell release from microchambers. Finally, microarchitectures that direct the position and motion paths of motile bacterial are evaluated for the production of controlled and directed microfluidic flow.

1.6 REFERENCES

[1]   F. Zhang, L. P. Wang, M. Brauner, J. F. Liewald, K. Kay, N. Watzke, P. G. Wood, E. Bamberg, G. Nagel, A. Gottschalk, and K. Deisseroth, "Multimodal fast optical interrogation of neural circuitry," *Nature*, vol. 446, pp. 633-9, 2007.

[2]   M. Banghart, K. Borges, E. Isacoff, D. Trauner, and R. H. Kramer, "Light-activated ion channels for remote control of neuronal firing," *Nat Neurosci*, vol. 7, pp. 1381-6, 2004.

[3]   M. Chalfie and S. Kain, *Green fluorescent protein : properties, applications, and protocols*, 2nd ed. Hoboken, N.J.: Wiley-Interscience, 2006.

[4]   A. Husain, X. Zhang, M. A. Doll, J. C. States, D. F. Barker, and D. W. Hein, "Functional Analysis of the Human N-Acetyltransferase 1 Major Promoter: Quantitation of Tissue Expression and Identification of Critical Sequence Elements," *Drug Metab Dispos*, 2007.

[5]   T. M. Pearce and J. C. Williams, "Microtechnology: meet neurobiology," *Lab Chip*, vol. 7, pp. 30-40, 2007.

[6]   D. B. Weibel, W. R. Diluzio, and G. M. Whitesides, "Microfabrication meets microbiology," *Nat Rev Microbiol*, vol. 5, pp. 209-18, 2007.

[7]   J. El-Ali, P. K. Sorger, and K. F. Jensen, "Cells on chips," *Nature*, vol. 442, pp. 403-11, 2006.

[8]   S. R. Khetani and S. N. Bhatia, "Engineering tissues for in vitro applications," *Current Opinion in Biotechnology*, vol. 17, pp. 524-531, 2006.

[9]   A. Khademhosseini, R. Langer, J. Borenstein, and J. P. Vacanti, "Microscale technologies for tissue engineering and biology," *Proceedings of the National Academy of Sciences of the United States of America*, vol. 103, pp. 2480-2487, 2006.

[10]   P. Fromherz, "Electrical interfacing of nerve cells and semiconductor chips," *Chemphyschem*, vol. 3, pp. 276-84, 2002.

[11]   A. M. Taylor, M. Blurton-Jones, S. W. Rhee, D. H. Cribbs, C. W. Cotman, and N. L. Jeon, "A microfluidic culture platform for CNS axonal injury, regeneration and transport," *Nat Methods*, vol. 2, pp. 599-605, 2005.

[12]   B. A. Hense, C. Kuttler, J. Muller, M. Rothballer, A. Hartmann, and J. U. Kreft, "Does efficiency sensing unify diffusion and quorum sensing?," *Nat Rev Microbiol*, vol. 5, pp. 230-9, 2007.

[13]   G. M. Whitesides, "The origins and the future of microfluidics," *Nature*, vol. 442, pp. 368-373, 2006.

[14]   A. J. DeMello, "Control and detection of chemical reactions in microfluidic systems," *Nature*, vol. 442, pp. 394-402, 2006.

[15]   H. Hess, "Materials science. Toward devices powered by biomolecular motors," *Science*, vol. 312, pp. 860-1, 2006.

[16]   D. G. Bucknall and Institute of Materials Minerals and Mining., *Nanolithography and patterning techniques in microelectonics*. Cambridge: CRC Press, 2005.

[17]   Y. N. Xia and G. M. Whitesides, "Soft lithography," *Angewandte Chemie-International Edition*, vol. 37, pp. 551-575, 1998.

[18]   H. B. Sun and S. Kawata, "Two-photon photopolymerization and 3D lithographic microfabrication," *Nmr - 3d Analysis - Photopolymerization*, vol. 170, pp. 169-273, 2004.

[19]   M. Goppert-Mayer, "Elementary processes with two quantum jumps," *Annalen der Physik (Berlin, Germany)*, vol. 9, pp. 273-94, 1931.

[20]   W. Kaiser and C. G. B. Garrett, "Two-photon excitation in CaF2:Eu++," *Physical Review Letters*, vol. 7, pp. 229-31, 1961.

[21]   W. Denk, J. H. Strickler, and W. W. Webb, "2-Photon Laser Scanning Fluorescence Microscopy," *Science*, vol. 248, pp. 73-76, 1990.

[22]   J. B. Shear, "Multiphoton-excited fluorescence in bioanalytical chemistry," *Analytical Chemistry*, vol. 71, pp. 598A-605A, 1999.

[23]   F. A. Duck, *Physical properties of tissue: a comprehensive reference book*, U.S. ed. London ; San Diego: Academic Press, 1990.

[24]   H. B. Sun, T. Tanaka, and S. Kawata, "Three-dimensional focal spots related to two-photon excitation," *Applied Physics Letters*, vol. 80, pp. 3673-3675, 2002.

[25]   E. S. Wu, J. H. Strickler, W. R. Harrell, and W. W. Webb, "Two-photon lithography for microelectronic application," *Proceedings of SPIE-The International Society for Optical Engineering*, vol. 1674, pp. 776-82, 1992.

[26]   S. Maruo, O. Nakamura, and S. Kawata, "Three-dimensional microfabrication with two-photon-absorbed photopolymerization," *Optics Letters*, vol. 22, pp. 132-134, 1997.

[27]   S. Kawata, H. B. Sun, T. Tanaka, and K. Takada, "Finer features for functional microdevices," *Nature*, vol. 412, pp. 697-8, 2001.

[28]   B. H. Cumpston, S. P. Ananthavel, S. Barlow, D. L. Dyer, J. E. Ehrlich, L. L. Erskine, A. A. Heikal, S. M. Kuebler, I. Y. S. Lee, D. McCord-Maughon, J. Qin, H. Rockel, M. Rumi, X.-L. Wu, S. R. Marder, and J. W. Perry, "Two-photon polymerization initiators for three-dimensional optical data storage and microfabrication," *Nature (London)*, vol. 398, pp. 51-54, 1999.

[29]   M. Deubel, G. von Freymann, M. Wegener, S. Pereira, K. Busch, and C. M. Soukoulis, "Direct laser writing of three-dimensional photonic-crystal templates for telecommunications," *Nature Materials*, vol. 3, pp. 444-447, 2004.

[30] J. D. Pitts, P. J. Campagnola, G. A. Epling, and S. L. Goodman, "Submicron Multiphoton Free-Form Fabrication of Proteins and Polymers: Studies of Reaction Efficiencies and Applications in Sustained Release," *Macromolecules*, vol. 33, pp. 1514-1523, 2000.

[31] G. Bitan, "Structural study of metastable amyloidogenic protein oligomers by photo-induced cross-linking of unmodified proteins," *Methods in Enzymology*, vol. 413, pp. 217-236, 2006.

[32] H. J. Lin and T. Kodadek, "Photo-induced oxidative cross-linking as a method to evaluate the specificity of protein-ligand interactions," *Journal of Peptide Research*, vol. 65, pp. 221-228, 2005.

[33] Z.-R. Liu, B. Sargueil, and C. W. J. Smith, "Methylene blue-mediated cross-linking of proteins to double-stranded RNA," *Methods in Enzymology*, vol. 318, pp. 22-33, 2000.

[34] J. D. Spikes, H.-R. Shen, P. Kopeckova, and J. Kopecek, "Photodynamic crosslinking of proteins. III. Kinetics of the FMN- and rose bengal-sensitized photooxidation and intermolecular crosslinking of model tyrosine-containing N-(2-hydroxypropyl)methacrylamide copolymers," *Photochemistry and Photobiology*, vol. 70, pp. 130-137, 1999.

[35] R. C. Straight and J. D. Spikes, "Photosensitized oxidation of biomolecules," *Singlet O2*, vol. 4, pp. 91-143, 1985.

[36] M. J. Davies and R. J. W. Truscott, "Photo-oxidation of proteins and its role in cataractogenesis," *Journal of Photochemistry and Photobiology, B: Biology*, vol. 63, pp. 114-125, 2001.

[37] M. J. Davies, "Reactive species formed on proteins exposed to singlet oxygen," *Photochemical & Photobiological Sciences*, vol. 3, pp. 17-25, 2004.

[38] H. R. Shen, J. D. Spikes, P. Kopecekova, and J. Kopecek, "Photodynamic crosslinking of proteins. I. Model studies using histidine- and lysine-containing N-(2-hydroxypropyl)methacrylamide copolymers,"*Journal of photochemistry and photobiology. B, Biology,* vol. 34, pp. 203-10, 1996.

[39] H.-R. Shen, J. D. Spikes, P. Kopeckova, and J. Kopecek, "Photodynamic crosslinking of proteins. II. Photocrosslinking of a model protein-ribonuclease A," *Journal of Photochemistry and Photobiology, B: Biology*, vol. 35, pp. 213-219, 1996.

[40] H. R. Shen, J. D. Spikes, C. J. Smith, and J. Kopecek, "Photodynamic crosslinking of proteins IV. Nature of the His-His bond(s) formed in the Rose bengal-photosensitized crosslinking of N-benzoyl-L-histidine," *Journal of Photochemistry and Photobiology, A: Chemistry*, vol. 130, pp. 1-6, 2000.

[41]   H. R. Shen, J. D. Spikes, C. J. Smith, and J. Kopecek, "Photodynamic crosslinking of proteins V. Nature of the tyrosine-tyrosine bonds formed in the FMN-sensitized intermolecular crosslinking of N-acetyl-L-tyrosine," *Journal of Photochemistry and Photobiology, A: Chemistry*, vol. 133, pp. 115-122, 2000.

[42]   Y. Yoshikuni and J. D. Keasling, "Pathway engineering by designed divergent evolution," *Current Opinion in Chemical Biology*, vol. 11, pp. 233-239, 2007.

[43]   Y. Mazor, T. Van Blarcom, R. Mabry, B. L. Iverson, and G. Georgiou, "Isolation of engineered, full-length antibodies from libraries expressed in Escherichia coli," *Nature Biotechnology*, vol. 25, pp. 563-565, 2007.

[44]   B. Kaehr, R. Allen, D. J. Javier, J. Currie, and J. B. Shear, "Guiding neuronal development with in situ microfabrication," *Proceedings of the National Academy of Sciences of the United States of America*, vol. 101, pp. 16104-16108, 2004.

[45]   R. T. Hill and J. B. Shear, "Enzyme-nanoparticle functionalization of three-dimensional protein scaffolds," *Anal Chem*, vol. 78, pp. 7022-6, 2006.

[46]   R. Allen, R. Nielson, D. D. Wise, and J. B. Shear, "Catalytic three-dimensional protein architectures," *Anal Chem*, vol. 77, pp. 5089-95, 2005.

[47]   R. T. Hill, J. L. Lyon, R. Allen, K. J. Stevenson, and J. B. Shear, "Microfabrication of three-dimensional bioelectronic architectures," *J Am Chem Soc*, vol. 127, pp. 10707-11, 2005.

Chapter 2: Microfabrication in the Presence of Cells

2.1 INTRODUCTION

In 1907, the embryologist Ross Harrison extracted tissue from a frog embryo and then transferred the sample to a substrate composed of lymph-derived protein matrix. As he watched growth cones extend from neuronal cell bodies and elongate over the matrix terrain (the first to witness such an event over time), it puzzled him as to what mechanisms guide these outgrowths to specified targets during developement. This remarkable experiment helped to prove the controversial 'neuron doctrine', the idea that neurons were the 'main ingredient' of the nervous system. Of perhaps greater historical significance however, Harrison's demonstration marked the birth of modern tissue culture [1].

Though much progress has been made identifying many of the molecules and mechanisms that guide axons to targets, the task of providing and predicting the appropriate cues at the appropriate time points *in vitro* — an arena were there is still much to learn — remains challenging. The ability to dictate the behavior and communication networks of neurons in cell culture potentially provides a foothold towards understanding the dauntingly complex circuitry of the brain, the delineation of regeneration pathways after neuronal damage in injury and disease states, and routes towards interfacing the ion conduction mechanisms of neurons to the electrical conduction of modern microelectronics — an endeavor geared towards potentially realizing neuronally driven prosthesis and other mechanical devices.

A first step to define the interaction between cultured cells and the substrate is to determine the proper substrate for a given cell type. This was Harrison's breakthrough that allowed tissue culture to flourish as a technique in cell biology. However, to truly

tackle the challenge of prescribing highly specific and tractable neuronal interactions, substrate patterning must be scaled down to the resolution of subcelluar features. Patterning can involve defining positive and/or negative cues that a developing cell encounters as it explores the substrate. Yet only recently have strategies for substrate patterning with milli- to microscale resolution been explored for cell and neurobiology applications.

Borrowing largely from photolithographic methods developed for the microelectronics industry as well as soft lithographic methods (i.e., molding, printing or embossing using elastomeric materials) cell culture environments can be tailored with complex physical and biochemical cues with increasingly fine resolution necessary for single cell and subcellular interrogation [2]. Finely etched topographies [3], growth channels [4, 5], and electronic substrates [6] have been shown to provide physical restraint and electrophysiological access for neuronal cultures. The patterning of chemical cues that define adhesive (e.g., poly-lysine) and non-adhesive substrates (e.g., polyethylene glycol) [7, 8], in addition to bioactive extracellular matrix proteins [9, 10], have been employed to generate arbitrary patterns of many cell types. Unfortunately, these pre-defined environments are generally static — providing limited opportunity to respond to developing cells or to select cells for experimental interrogation based on phenotypic criteria such as neurite arborization.

However, a variety of techniques have emerged that are capable of generating transient and continuous stimulation of neurons in real-time. Neurotropins dispensed by micropipette [11] or attached to physically addressable beads (i.e., through optical or magnetic trapping; [12, 13]), have been used to probe the dynamics of developing neurons. Light-induced responses using infrared light [14] and photo-lysis of effectors [15] have allowed neurons to be stimulated with precise temporal control. Though these

approaches can provide some control of the chemical gradient presented to the neuronal environment these techniques offer only limited (subcellular) spatial resolution and are inadequate for prescribing neuronal architectures and interconnectivity.

Certainly a combination of approaches could be used to address specific questions. However many of these techniques, especially those involving complicated surface preparation, require lengthy multistep procedures using highly specialized equipment. Thus, we set out to develop a biocompatible microfabrication system using MPE protein photocrosslinking that would be capable of presenting both chemical and topographical cues to developing cell cultures. By using a variety of proteins and endogenous sensitizers such as flavins, crosslinking conditions were determined that allowed fabrication of microstructures to be performed in the presence of cells while minimizing disruption to the cellular environment. We evaluated a number of sensitizers including flavin mononucleotide (FMN), flavin adenine dinucleotide (FAD), nicotinamide adenine dinucleotide (NAD), and serotonin as well as synthetic dyes such as Rose Bengal and methylene blue. In general, the biologically derived sensitizers proved less toxic to cells than the synthetic dyes. These differences can, in part, be attributed to the mechanism of photosensitization. Sensitizers operating primarily through type I (radical generating) mechanisms such as the flavins [16] were found to inflict little to no damage to cellular environments when excited at distances ≥ 1.5 μm from cells. Type II sensitizers (singlet oxygen generating) such as Rose Bengal [16] and methylene blue [17] were, in general, found to be much more damaging to cells which reflects their use as photosensitizers for targeted tumor cell death in the technique of photodynamic therapy [18, 19]. FAD proved to be a robust sensitizer for biocompatible fabrication and is used in the majority of experiments presented here.

23

As discussed in Chapter 1, pulsed laser light (Ti:S, Nd:YAG) is focused into reagent solution to excite photosensitizer molecules via nonlinear absorption of two or more, low-energy photons. Fabrication of protein microstructures follows the formation of intermolecular crosslinks occurring between oxidizable residue side chains (e.g., tyrosine, cysteine, histidine, lysine). The superlinear dependence of excitation rate on laser intensity allows one to confine photochemistry not only in the two radial dimensions, but also axially (along the laser propagation axis). By tightly focusing a high peak-power laser beam to a submicrometer focal spot, it is feasible to create complex three-dimensional protein matrices with minimum feature sizes of several hundred nanometers.

A demonstration of the capabilities of both the biocompatibility of the fabrication process as well as the time scale and spatial precision in which microstructures can be formed is shown in Figure 2.1. Here a motile bacterium, bathed in a fabrication solution containing BSA and methylene blue, is corralled in real time by the developing microstructure. Though, in this case, the bacterium eventually escapes the protein fence by swimming above the low-profile microstructure, surface-adhered protein lines such as these were often suitable to affect neuronal development over much longer timescales.
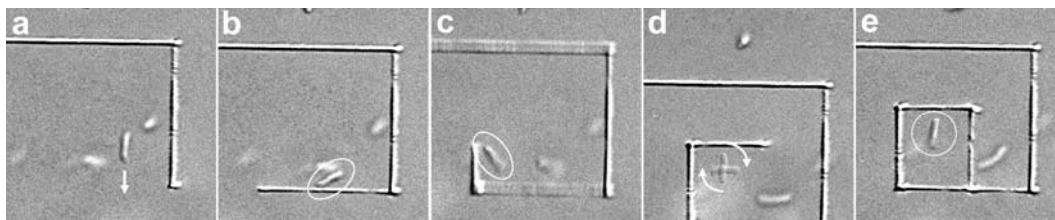
Figure 2.1: Real-time (DIC) image sequence of the photofabrication of a surface-adherent protein microstructure (from a solution of 200 mg ml^{-1}BSA and 0.6 mM MB), a process that ultimately boxes in an *E. coli* bacterium. The diameter of the protein line is < 0.5 μm, and the elapsed time for the image sequence (a-e) is 5 seconds.

2.2 EXPERIMENTAL METHODS

2.2.1 Materials

Methylene blue (M-4159) and rose bengal (330000) were purchased from from Sigma-Aldrich (St. Louis, MO). Bovine serum albumin (BSA, BAH64-0100; Equitech-Bio, Kerrville, TX) was stored undessicated at 4 °C. Concentrated stock solutions of fluorescein-biotin (Fl-biotin, B-1370; Molecular Probes, Eugene, OR) in DMSO were stored at 4 °C. Bovine heart cytochrome c (cyt c, C3131; Sigma-Aldrich, St. Louis, MO), avidin (A-887; Molecular Probes), and flavin adenine dinucleotide (FAD, F-6625; Sigma-Aldrich) were stored desiccated at -20 °C.

2.2.2 Cell Culture

Neuroblastoma-glioma (NG108-15) cells were cultured in DMEM supplemented with 10% FBS, penicillin (100mg/liter), and streptomycin (100 kilounits/liter). Flasks were maintained at 37°C in a 10% CO_2 atmosphere with saturated H_2O. Cells were seeded on 0.01% poly-L-lysine coated glass coverslips and incubated for 1–3 days in a low-serum (1% FBS) growth medium. In the periods immediately before and after microfabrication, cells were maintained in a supplemented pH 7.4 Hepes buffer (10 mM Hepes, 140 mM NaCl, 5 mM KCl, 1 mM $MgCl_2$, 1 mM $CaCl_2$, 10 mM D-glucose).

Rat brain cortical cells (embryonic days 18–19) were harvested by QBM Cell Science (Ottawa) and cultured according to standard procedures. Briefly, cryopreserved neurons were transferred to poly-L-lysine or uncoated flame-treated coverslips and incubated in neurobasal medium (Invitrogen) with L-glutamine, 1 unit/ml penicillin-streptomycin, and 2% B27 serum-free culture supplement. Microfabrication experiments were performed 1–3 days after plating.

2.2.3 Matrix Fabrication

Fabrication of crosslinked BSA structures was performed in Hepes buffer (pH 7.4) containing 1–4 mM FAD and 50–200 mg ml^{-1} BSA. Cell exposure to this solution was 1 min or less, but longer periods do not appear to be detrimental to NG108-15 cells or cortical neurons. Protein lines were written on a Zeiss Axiovert microscope using a femtosecond titanium:sapphire laser (Coherent Mira, Santa Clara, CA; Tsunami, Spectra Physics, Mountain View, CA) with the output tuned to 740 or 780 nm (~12 nm bandwidth). The laser output was adjusted to approximately fill the back aperture of a high-power objective (Zeiss 100X Fluar, 1.3 numerical aperture, oil immersion). Desired powers were obtained by attenuating the laser beam using a half-wave plate/polarizing beamsplitter pair. Lines were written by scanning the position of the sample with a motorized XY stage (ProScan; Prior Scientific, Cambridge, U.K.) and rectangular platforms were created by raster scanning the focused laser beam within the focal plane with a confocal scanner (BioRad MRC600). In cases where structures extended along the z-dimension (i.e., along the optical axis), the position of the laser focus was translated manually within sample solution using the microscope's fine focus adjustment. Microstructures comprised of proteins other than BSA were fabricated by using similar procedures. Biotin binding of avidin matrices was assessed by applying fluorescein-biotin (B1370, Molecular Probes) to structures postfabrication at a concentration of 1.2 μM, with labeled structures subjected to 10–15 rinses with Hepes (pH 7.4) to minimize nonspecific binding. A laminin A-chain peptide (Cys-Ser-Arg-Ala-Arg-Lys-Gln-Ala-Ala-Ser-Ile-Lys-Val-Ala-Val-Ser-Ala-Asp-Arg; American Peptide Company) was reacted with biotin sulfo-N-hydroxysuccinimide ester containing a hexanoic spacer (B1022, Sigma-Aldrich) at 5:4 molar ratio (peptide to biotin-SSE) for 3 hours (pH 8.3, 25

°C). The labeled peptide was diluted to a final concentration of 2.5 µM and incubated for 10 minutes on avidin microstructures before rinsing (10 X).

In addition to studies using the Ti:S laser, a low-cost MPE light source was also used in a similar configuration. This frequency-doubled (532-nm) diode-pumped Q-switched Nd:YAG laser (NG10320-110; JDS Uniphase, San Jose, CA) provided an average power output of > 25 mW, a pulse width of ~600 ps, and a repetition rate of 7.65 kHz. These values correspond to a peak power of ~7 kW and a pulse energy of ~3.5 µJ. Powers used to crosslink were measured immediately before the objective, and were generally between 0.5 and 3 mW. Desired powers were obtained by attenuating the laser beam using a half-wave plate/polarizing beamsplitter pair.

Figure 2.2 compares BSA structures fabricated from a solution of 200 mg mL^{-1} BSA and 4 mM Rose Bengal using the YAG laser (Figure 2.2a) and a Ti:S source (Figure 2.2b). Although differences in grain characteristics of the structures is evident from these SEM images, in both cases, protein matrixes could be fabricated with similar gross morphologies and high structural integrity — both proving useful for cell guidance and retention of functionality studies.
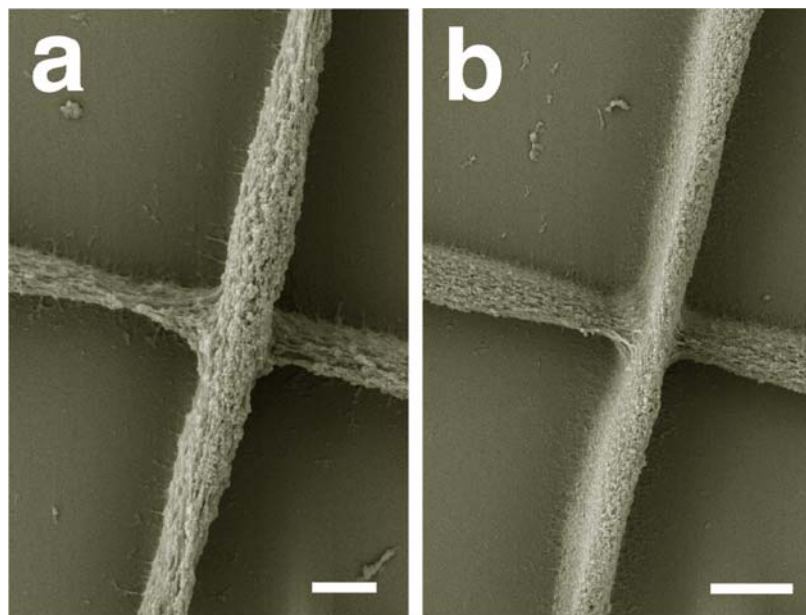
Figure 2.2: Scanning electron micrographs (SEMs) of microstructures fabricated from bovine serum albumin (BSA) using multiphoton-excited crosslinking. (a) An intersection of two lines fabricated from BSA and Rose Bengal using the Q-switched YAG laser (average power, 0.5 mW). Scale bar, 1 μm. (b) A structure fabricated in the same manner as that described in part (a) except that a femtosecond titanium:sapphire was used as the photofabrication source (average power, 11 mW). Scale bar, 2 μm.

2.2.4 Scanning Electron Microscopy (SEM) Preparation

Samples were fixed in 3.5-5% gluteraldehyde solution for 20 min, dehydrated by using 10-min sequential washes [2:1 ethanol/H_2O; twice in 100% ethanol; 1:1 ethanol/methanol; 100% methanol; all solutions stated as vol/vol; methanol was occasionally replaced with hexamethyldisilazane (HMDS)], allowed to air dry for 3 h., and sputter-coated to nominal thicknesses of 10-20 nm with Au/Pd.

2.2.5 Fluorescence and DIC Microscopy

Widefield fluorescence imaging was performed on the Axiovert microscope, which was equipped with a mercury-arc lamp and standard "Red" and "Green" filter sets

(Chroma, Rockingham, VT). Fluorescence emission was collected using the Fluar 100x objective and detected using a 12-bit 1392 x 1040-element CCD (Cool Snap HQ; Photometrics, Tucson, AZ). Data was processed using Image J and Metamorph (Universal Imaging, Sunnyvale, CA) image analysis software.

Unless otherwise stated, differential interference contrast (DIC) was used as the bright-field microscopy technique throughout this dissertation work. Microscopic imaging using DIC produces monochromatic 'shadowing' by (reference) light beam interference which greatly increases image contrast (without loss of light amplitude) and can allow 'optical sectioning' of transparent specimens.

2.3 RESULTS

Campagnola and colleagues were the first to demonstrate protein photocrosslinking using multiphoton absorption and thus were able to fabricate protein microstructures with defined 3D geometries [20]. Photocatalysis relied on potentially toxic photosensitizers such as benzophenone and the xanthene dye, Rose Bengal. However, this aqueous based crosslinking chemistry using protein "monomers" appeared to us to be a good starting point for developing microfabrication strategies that could be performed in the presence of living cells. Starting with a range of sensitizers (Figure 2.3) and the protein bovine serum albumin (BSA), we began experiments to test the feasibility for microfabrication under biocompatible conditions.
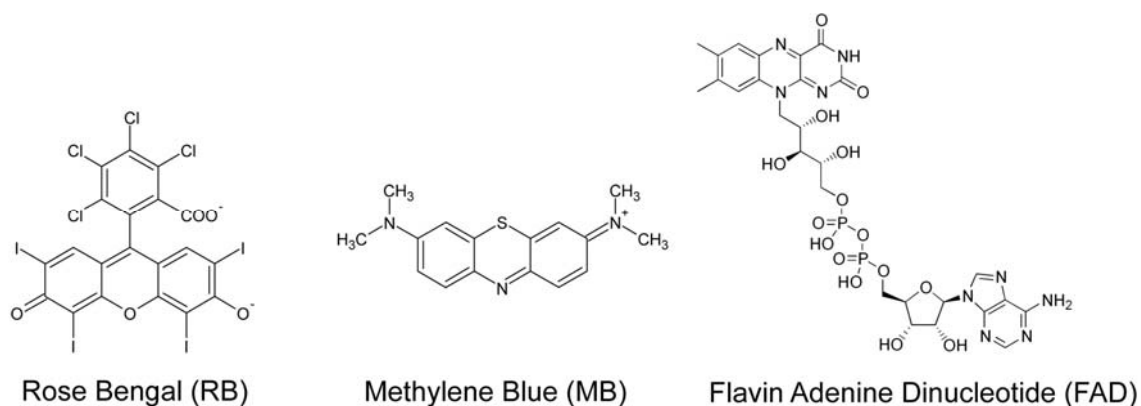
Figure 2.3: Structures of photosensitizers evaluated for biocompatible fabrication.

The toxicity of photosensitizers to cells occurs through the generation of harmful reactive photoproducts (phototoxicity) or by the chemical toxicity of the ground-state molecule (cytotoxicity). As stated previously, phototoxicity effects have been used therapeutically to target cancerous cells in photodynamic therapy. Rose Bengal, methylene blue, protoporphyrin and various analogues of these sensitizers have been evaluated for this purpose [18, 19, 21]. Rose Bengal (RB) is a highly efficient sensitizer with reported quantum yields of formation for reactive oxygen nearing 1.0 [22], and therefore could potentially be used at low enough concentrations for minimal perturbation of cells. Indeed, fabrication of RB sensitized BSA microstructures proved straightforward at relatively low sensitizer concentrations (~100 μM). Yet even at these concentrations, RB-sensitized fabrication was found to compromise cell viability (Figure 2.4). The redox indicator and common biological dye, methylene blue (MB), was also examined and proved to sensitize structures under conditions where cell viability (NG108-15) was occasionally maintained. However, the broad binding of MB to a wide

30

range of biological species [23] as well as the lack of reproducible cell viability encouraged the exploration of alternative sensitization strategies.
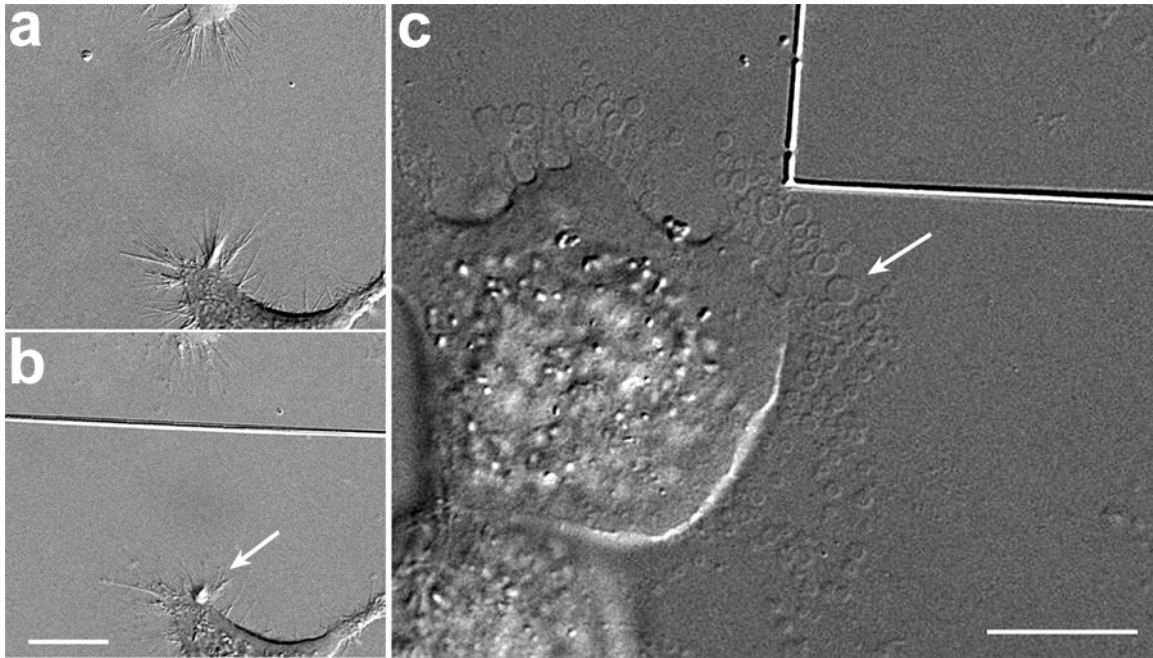
Figure 2.4: Microfabrication of BSA protein lines in the presence of NG108-15 cells using 250 µM Rose Bengal, a type II photosensitizer. (A) Before fabrication. After fabrication atrophy and blebbing of neuritic structures is observed, presumable through phototoxic mechanism (A, B; arrows). (C) Scale bars, 10 µm.

Various biological molecules have been known to photosensitize protein crosslinking [24] and generally have low cytotoxicity. Flavin mono nucleotide (FMN) previously has been characterized as an efficient photosensitizer for the oxidation of tyrosine and subsequent formation of tyrosine dimers [16] in addition to having a relatively large two photon cross-section [25]. Indeed, flavins, pyridine nucleotides, and the neurotransmitter serotonin proved capable of multiphoton sensitization of BSA

crosslinking. Of these, FAD was adopted as the primary photosensitizer for further studies due to its low cost, high purity and reduced hygroscopicity compared to FMN.

Typical fabrication of crosslinked BSA structures was performed in Hepes buffer (pH 7.4) containing 1–4 mM FAD and 100–200 mg/ml BSA. Cells were generally exposed to this solution for 1 min or less followed by thorough washing in cellular buffer. However, longer exposure periods (up to ~1 hour) did not appear to be detrimental to either NG108-15 cells or cortical neurons. Previous work had shown that the photoexcitation of flavins can produce a number of reactive compounds such as superoxide, singlet oxygen, and flavin radicals [16], species that can be detrimental to cellular structures, proteins, and biopolymers. To assess the phototoxicity of FAD-sensitized fabrication of BSA microstructures on primary cortical neurons, calcium homeostasis was monitored throughout the fabrication process using the intracellular calcium chelating dye x-Rhod-1. No detectible transient (i.e within the resolution of a 2.4-Hz frame rate) or long lasting (> 10s) change in calcium homeostasis was observed when microstructures were fabrictated to within 1.5 μm of the plasma membrane. In addition, fabrication of close proximity lines did not appear detrimental to delicate cellular features such as axonal-type and dendritic structures (Figure 2.5) and cells were capable of normal growth and depolarization responses for minutes up to days post-fabrication. Overall, these experiments show that both the aqueous solution for fabrication as well as the process itself can be minimally disruptive to developing cell culture environments.
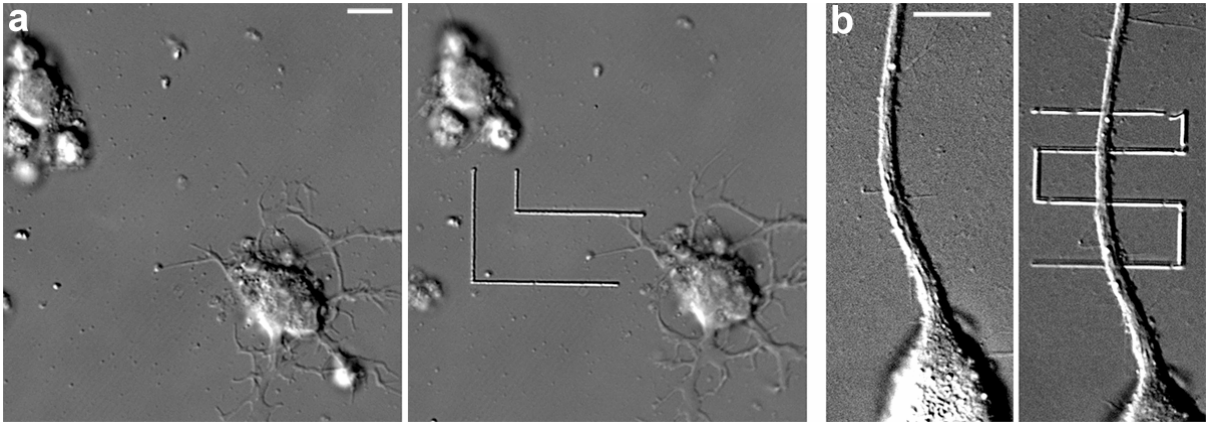
Figure 2.5:   Microfabrication of BSA protein lines in the presence of rat cortical neurons (a) and NG108-15 cells (b) using FAD as a photosensitizer. Cellular features appear unperturbed following fabrication. Scale bars, 5μm.

The nonlinear dependence of two-photon photosensitizer excitation on laser intensity restricts the crosslinking reaction both radially (i.e., in the focal plane) and axially (i.e., along the optical axis), resulting in a protein crosslinking voxel of <1 fl (1 μm^3). By translating the relative position of the voxel within crosslinking solution, a continuous matrix can be fabricated in, for instance, the form of a line (Figure 2.5). Surface adhered lines can be fabricated such that the radial and axial dimensions are roughly equivalent — an effect that can be attributed to truncation of the spinning ellipsoid-shaped voxel by the glass substrate — and these low profile lines (~ 250 nm) could be fabricated underneath cellular structures (Figure 2.6).
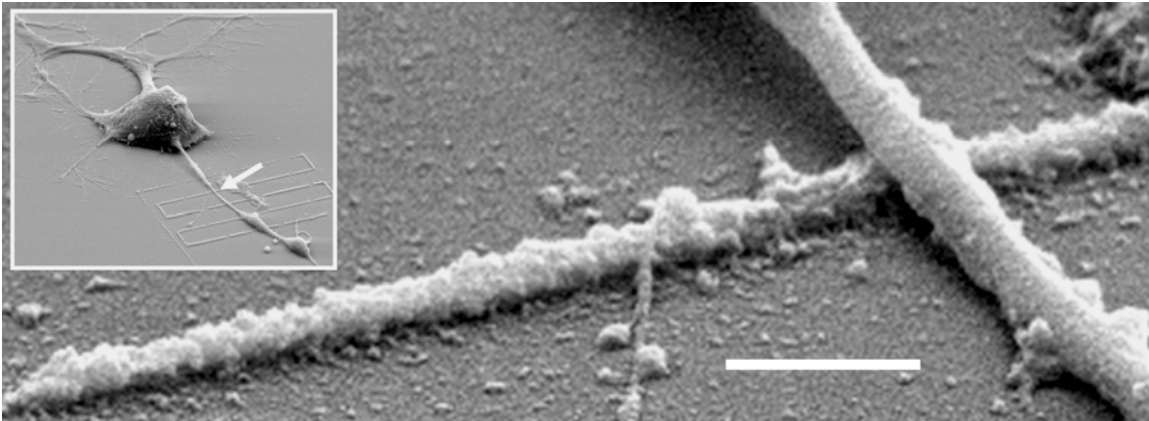
Figure 2.6:   SEM of a low-profile protein line fabricated underneath an NG108-15 neurite that is descending from the cell body (inset, arrow) to the glass substrate. Scale bar, 1μm.

It was of interest to determine whether such subtle topographical features could influence neurite elaboration or pathfinding. Figure 2.7 demonstrates that neurite pathfinding can be redirected by a BSA protein corral. A BSA line was fabricated near an NG108-15 cell undergoing differentiation and over the course of the experiment, the confined neuritic architecture formed an elaborate set of self interactions (Figure 2.7, arrows). Unfortunately, these initial FAD-sensitized BSA lines lacked the uniformity and reproducibility of microstructures fabricated with more robust sensitizers (e.g., RB, MB) and in some areas were insufficient to prevent neurite overgrowth (Figure 2.7, lower portion of panels).
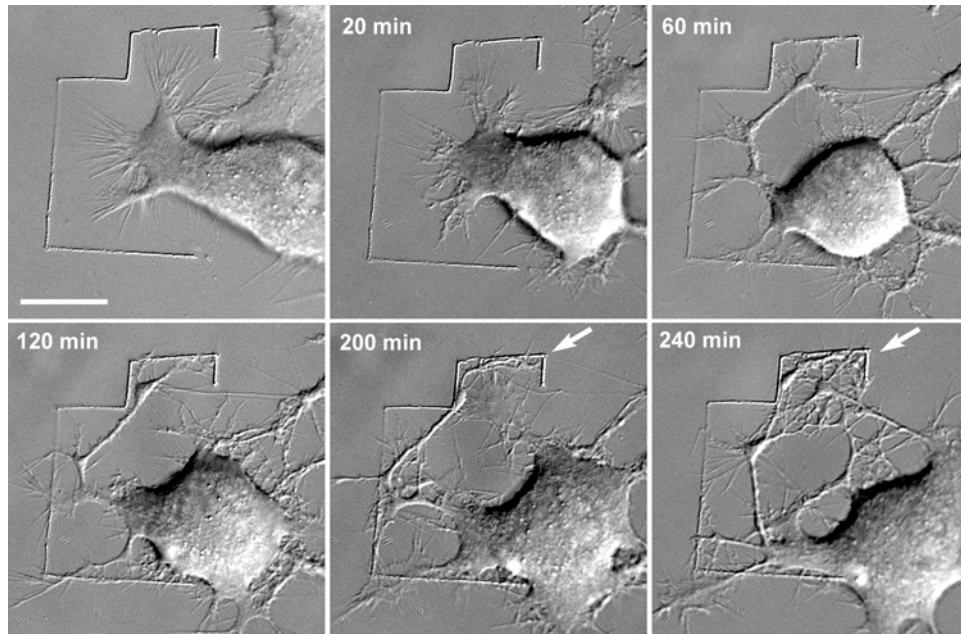
Figure 2.7: Confinement of neurite outgrowth. Here an NG108-15 neuroblastoma-glioma cell is seen interacting with protein lines comprised of BSA and sensitized using the biological co-factor flavin adenine dinucleotide (FAD). The structure is generated by scanning the stage relative to the focused laser beam to create a <1 micron tall corral. Subsequent growth of the developing cell was significantly constrained by the protein barrier (arrows). Scale bar, 10 μm.

It is not surprising that barriers of various heights are needed to constrain or redirect different neuritic features. Fine features such as fillapodia could be readily contained by low profile protein barriers whereas growth cones, especially those extending from broad diameter neurites were less likely deterred by similar protein lines. Using this approach, structures of significant height should be achievable by using focusing optics with longer working distances (to extend the axial MPE voxel dimensions), layering or otherwise stacking lines vertically using multiple scan passes. These approaches were only briefly explored but generally resulted in decreased viability of cells post-fabrication. Although this issue is not fully reconciled, it is likely in part a

consequence of extended exposure time to high concentrations of photo-generated reactive species and could potentially be overcome by directing solution flow away from cells during the fabrication process.

This issue of matching feature height to contain a given cellular outgrowth could potentially be circumvented with the ability to pin cellular structures to the glass substrate. Interestingly, fabrication of protein structures over, or into integral contact with the soma and neuritic plasma membrane does not comprise cell or neurite viability beyond that of photocrosslinking in general. Thus cell migration and morphology could be constrained at specific coordinates for extended periods of time while still allowing differentiation and development on either side of the barrier (Figure 2.8). It is still unclear what cytosolic damage may occur with brief exposure to focused Ti:S light but damage would be influenced by factors such as duration of exposure as well as the concentration of endogenous chromophore. Nevertheless, the ability to direct integral contacts to subcellular locations potentially enables precise electrical stimulation and measurement at multiple sites with high temporal control. This has motivated others in the Shear Lab to develop strategies to functionalize protein lines with conductive materials. It has been shown that photocrosslinked avidin, cytochrome C, and lysozyme can act as scaffolds for functionalized nanoparticles [26]. Photocrosslinked cytochrome c structures targeted with gold nanoparticles were silver stained and shown to conduct electricity across gaps on indium-tin-oxide coated surfaces [27]. Current work in this area is aimed towards particle deposition and staining strategies under biocompatible conditions.
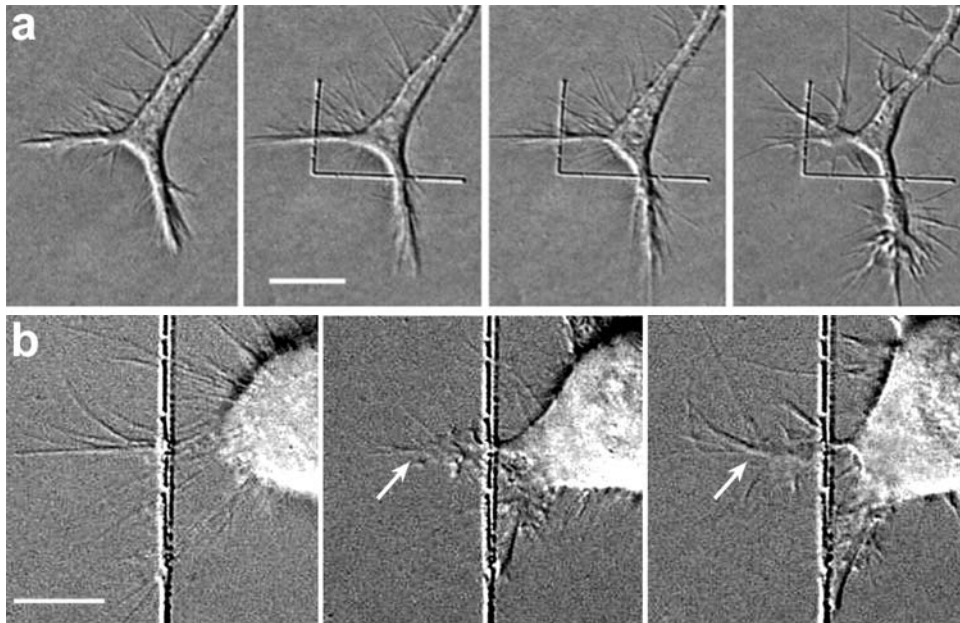
Figure 2.8: FAD-sensitized BSA protein lines fabricated into direct contact with NG108-15 neuritic structures. (a) A bifurcating neurite continues outgrowth and differentiation after microstructure fabrication. By 75 minutes post-fabrication, significant growth cone development has occurred on the lower right branch (right panel). (b) Neurites from an NG108-15 cell are pinned following fabrication of a BSA line (left panel). Growth cone development continues (arrow, middle panel) eventually bifurcating (arrow, right panel). Scale bars, 5μm.

In addition to studies using neuron-like cell lines (e.g., NG108-15), rat cortical neurons could also be influenced by low profile protein microstructures as shown in Figure 2.9. The top panel shows the guiding of an extending neurite after a short period following fabrication of the BSA line. The bottom panels demonstrate use of a single barrier to direct inter-cell contacts. Here, the photofabrication path of a narrow protein line is passed over an existing process (cell 1) causing partial retraction of the neurite. After 30 minutes, the neurite re-extends to form the desired contact point on cell 2. Though contacts between cells do not ensure formation of an active synapse, in this study

37

the interaction remained stable for the duration of the experiment (~100 additional minutes).
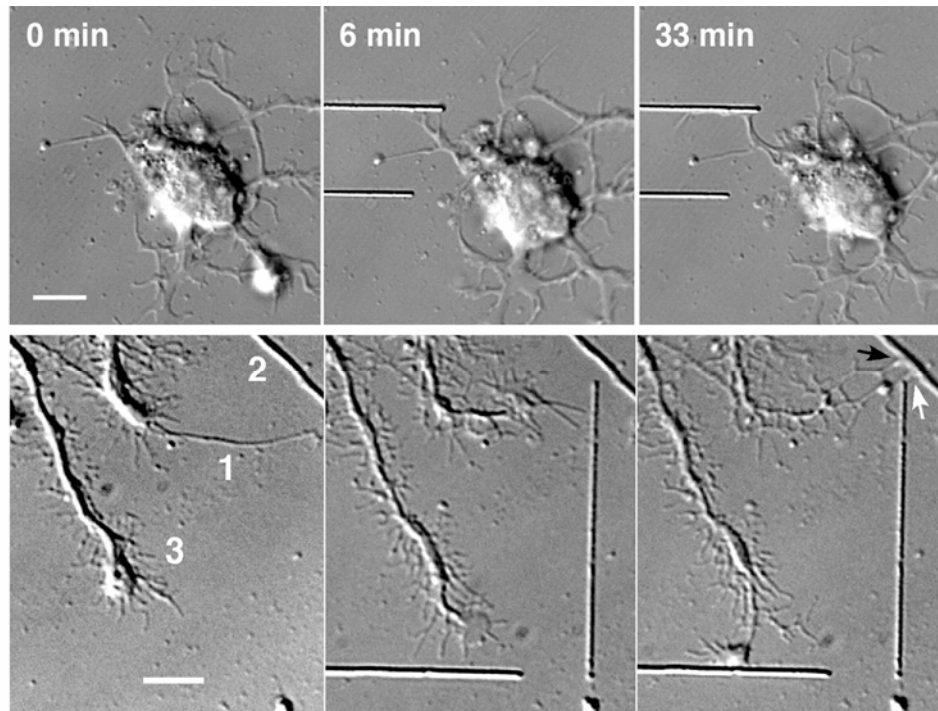
Figure 2.9: Cortical neuron targeting: (top) Re-direction of cortical process outgrowth using FAD/BSA microfabrication. The left image was acquired immediately before fabrication of microstructures. (bottom) The left panel shows neurites from three separate rat cortical neurons (1 – 3) before photofabrication. The horizontal and vertical lines in the last two panels were fabricated 5 min and 42 min, respectively, after acquisition of the first image. The middle panel reveals filopodia from Cell 1 interrogating the vertical line as the neurite undergoes re-extension (15 min post-fabrication). Within another 12 min, one of the filopodia had successfully navigated this barrier (not shown), forming a contact with Cell 2 just beyond the terminus of the line. This contact site persisted for at least tens of minutes, and is identified by an arrow in the right panel (acquired 61 min post-fabrication). Scale bar, 5 μm.

As shown, for FAD photosensitized BSA crosslinking, low-profile lines could be fabricated that re-directed and confined axonal outgrowth without compromising cell viability. Similar capabilities were obtained using the Q-switched YAG laser

38

(Figure 2.10). Here, a low-profile protein fence was constructed in the presence of a cultured rat cortical neuron using a solution of BSA (200 mg ml^{-1}, pH 7.4) containing no additional sensitizer, rinsed, and observed over a period of more than 1.5 h. The neurite extended to the protein microstructure within ~17 minutes but did not scale the barrier for the duration of the experiment (~78 additional min).

In general, the outgrowth of primary neurons in these studies showed greater sensitivity to photocrosslinked structures compared to that of cancer derived cell lines which tend to grow more rapidly and erratically. The axon corralling capabilities shown here represent a basic but important step toward more sophisticated cellular manipulations such as the fabrication of neuronal networks. Further, biocompatible fabrication using near-IR Ti:S light (which penetrates deeply within tissue) or non-sensitized photocrosslinking chemistry (Nd:YAG) may enable cellular manipulation *in vivo*; although studies to determine photoxicity and other potential side effects of protein photocrosslinking on biological tissue are needed.
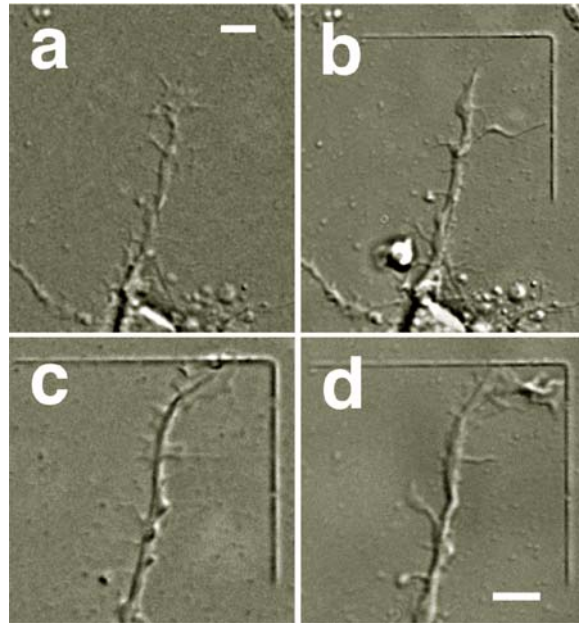
Figure 2.10: Confinement of neurite outgrowth from a cultured rat cortical neuron *in situ* using the YAG laser as an MPE light source. The low-profile (less than 1 μm high) lines were fabricated from a solution of 200 mg ml^{-1} BSA without additional sensitizer using an average laser power of 1.5 mW. (a) DIC micrographs immediately before microstructure fabrication. (b) 10 min. after fabrication. (c) 26 min after fabrication. (d) 95 min after fabrication. Scale bars, 5 μm.

It is presumed that the interaction of BSA-composed microstructues with cells is primary mechanical, comparable to neurite interactions with micropatterned surfaces, barriers, and finely etched quartz coverslips [3, 5]. An advantage of fabricating structures comprised of proteins is the potentially unlimited range of chemical identities inherent in the incorporated molecules or that can be targeted to ligand binding proteins. An excellent protein to examine for matrix incorporation is the biotin-binding protein, avidin. Avidin and its bacterial derivative, strepavidin, have been greatly exploited for biotechnology applications owing to the tight binding between avidin and biotin (K_d ~10^{-15}). Moreover, biotin can be readily conjugated to secondary molecules enabling virtually limitless targeting strategies.

It proved straightforward to fabricate avidin matrices with tunable binding properties (Figure 2.11). Here, avidin containing fabrication solutions were cut with the 'inert' protein BSA and microstructures were photocrosslinked side by side. The fluorescence signal from matrices after rinsing with biotin-fluorescein essentially scaled with the ratio of avidin in the fabrication solution indicating that ratio concentrations of solution are maintained in the matrix. To determine the biotin-binding capacity of avidin structures, multiple multiphoton point measurements of uniform ($\sim$ 1 μm tall) avidin structures were recorded following labeling with biotin-fluorescein and compared to standard solutions. These structures provided low to mid-micromolar range of biotin-binding activity ($\sim 10^3$ molecules μm^{-2} of surface). This study was performed using 200 mg ml^{-1} avidin and factors such as crosslinking density — a tunable property through laser exposure and solution concentrations — can effect both matrix diffusion properties [28] and functional densities [29]. Therefore, assessing binding capacity under a range of protein concentrations and laser exposures should enable even more precise tunability of functional matrices.
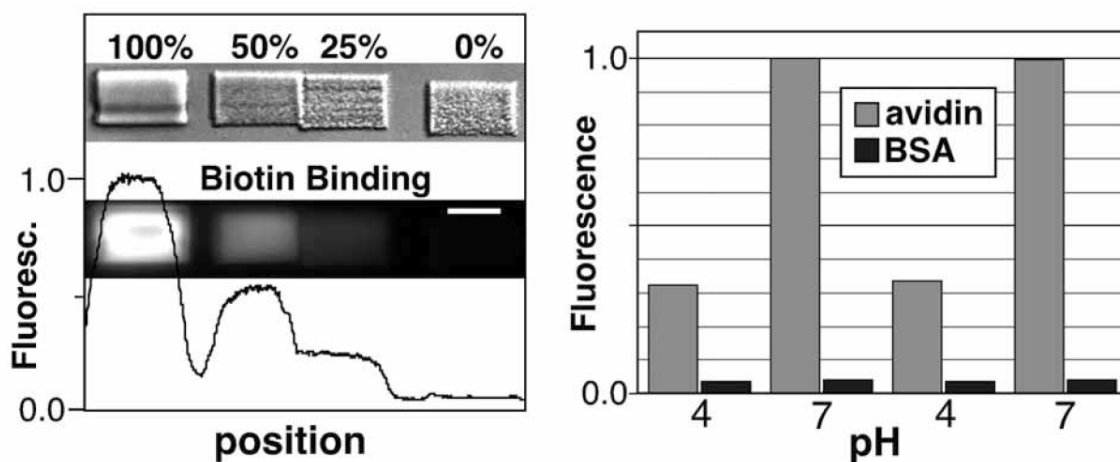
Figure 2.11: Biotin-binding capacity can be tuned by altering the composition of photocrosslinking solutions (Left). The top strip shows DIC images of 3D structures produced by using solutions containing methylene blue and 200 mg ml^{-1} of protein (avidin and BSA; percentage of avidin shown). After the structures were incubated in a fluorescein-biotin solution and rinsed, fluorescence imaging shows that photocrosslinked avidin retains the ability to capture biotin (lower strip) with a binding capacity that scales essentially as the ratio of avidin in the fabrication solution. Plotted data represents signal along a horizontal line drawn through the four structures (Scale bar, 10 μm). The matrices shown (left) were subjected to cycling between acidic (pH 4 acetate) and neutral (pH 7 Hepes) solutions, causing reversible and reproducible modulation in the fluorescence intensity of fluorescein. Bar plots represent normalized signal from the 100% and 0% avidin structures.

The retention of the functionality of a matrix-incorporated protein is an indication that the irradiation and subsequent photochemical crosslinking of proteins using MPE can be achieved under conditions that do not induce denaturation (e.g., through thermal mechanisms which would be expected to destroy protein function). It has been shown that irradiation of materials by femtosecond laser pulses results in photon energy deposition that is much faster than electrons can transfer it to the lattice [30]. Therefore multiphoton absorption using femtosecond laser sources is considered a heat insulation process [30-32], and any heating is restricted to the focal region. Some degree of

42

functional inactivation of incorporated proteins likely occurs following photochemical crosslinking. Indeed, prolonged irradiation of a single focal point or scan plane regularly induces what appear as 'micro-explosions' resulting in the gelation of material. Future studies should determine, under well-defined conditions, the degree to which functionality is maintained following photocrosslinking and the effect on the kinetics of ligand binding by matrix-incorporated avidin and strepavidin. Studies using both the Ti:S and the Nd:YAG clearly indicate that functionality of incorporated matrix proteins can be routinely retained [33-35]. However, given the different photonic energies, pulse widths and modes of non-linear photon absorption between the Ti:S and the microchip YAG laser, different photo-induced thermal processes for these MPE excitation sources would be expected.

The means to localize tunable densities of biotinylated compounds, including indicators, enzymes, and recognition peptides is valuable for a variety of cell biology applications such as the creation of substrate-bound neurotropic signals that affect growth cone extension. As an initial study of this concept, rat cortical neurons were plated on avidin structures labeled with the laminin-derived peptide IKVAV, a motif shown to facilitate neurite initiation and outgrowth [36]. Here, the neuritic outgrowth is maintained throughout the photofabricated line, deviating little if any from the protein scaffold, until reaching the end where undirected growth proceeds (Figure 2.12). It must be noted that the precise interaction between the extending axonal outgrowth and protein scaffold is unclear. Others in the lab have shown a high degree of avidin absorption to glass surfaces under these fabrication conditions indicating that even here, avidin and thus biotin-IKVAV should be present throughout the culture environment. In fact the global charge of 'bare' avidin (pI ~ 10.5) at neutral pH may provide stabilization of the cellular plasma membrane similar to other cationic surface treatments for cell culture. Therefore

numerous systems are currently being investigated in the Shear Lab to increase the signal-to-noise ratio for protein deposition targeting strategies; these include surface pre-treatments, laser-targeted functionalization (i.e., microfabrication and functionalization in a single step by using sensitizers with inherent ligand character such as biotin-benzophenone), and surface-free or 3D scaffolding.
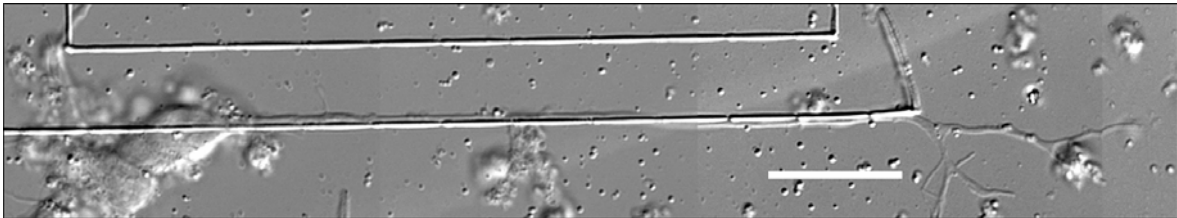
Figure 2.12: A rat cortical neurite develops along an avidin line exposed to biotinylated laminin peptide after fabrication. Scale bar, 20 μm.

Other ligand binding proteins also have been investigated using MPE protein photocrosslinking. Lectins are a class of carbohydrate-binding proteins with affinity for a range of glycan moieties. For instance, the jack bean derived lectin, concavalin A (Con A), has high binding affinity for terminal alpha-mannosyl groups [37]. Con A was photocrosslinked next to BSA microstructures and targeted with fluorescently labeled ovalbumen (Figure 2.13a) — a protein with glycan moieties that Con A binds with high affinity [37, 38]. The fluorescence intensity profile indicated capture of ovalbumin by Con A structures. Futher, fluorescence signal could be attenuated with addition of a competitive binder (D-mannose) — indicating the release of ovalbumin. This potentially provides the means to spatially target a range of effectors (given the vast range of lectin-ligand interactions; [37]) but with an element of temporal control not afforded using the largely irreversible binding of biotin to avidin. Biological effectors could be continually

44

released and rebound at precise time points in cell cultures using innocuous ('free' carbohydrate) competitors and novel methods, developed by others in the Shear lab [26, 34], that allow site specific downstream targeting of cells via upstream protein matrices. Additionally, interest in the study of cell-surface glycosylation, a determinant of pathogenic immunity, tumor metathesis and embryonic development, has resulted in the development of lectin patterning strategies for applications such as microarrays [37, 39]. These results may enable better resolution of array output in addition to the passive targeting of multiple chemical identities or even cells [39] to well-defined 3D coordinates.
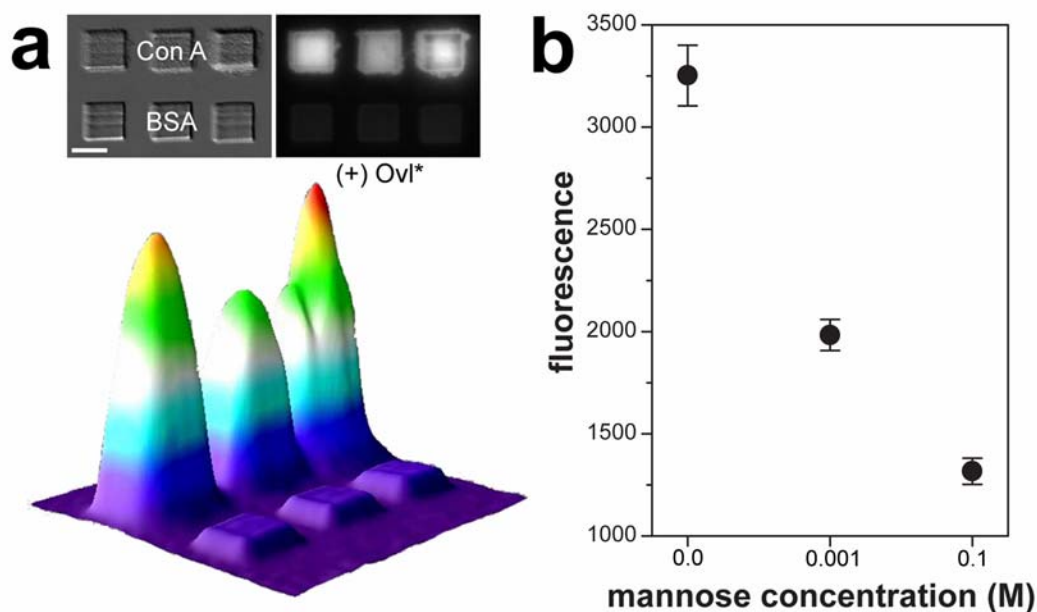
Figure 2.13: Ligand binding and release properties of photocrosslinked Con A protein matrices. (a) Matrices comprised of Con A and BSA fabricated and rinsed with fluorescein ovalbumin (Ovl*). The fluorescence intensity profile indicates capture of ovalbumin by Con A structures. Scale bar, 10 μm. (b) Ovalbumin release from Con A structures by rinsing with D-mannose (5 min per application), a competitive binder (data from similar structures to those shown in panel a. Error represents the standard deviation of the average fluorescence intensity from 3 structures).

2.3 CONCLUSION

These studies describe a new method for creating physically and chemically interactive microstructures within cell cultures, a technique that offers capabilities for interfacing with neuronal cells during development in fundamentally new ways. Multiphoton photocrosslinking of proteins is rapid, minimally intrusive to cells, and potentially accessible to a broad scientific community using an inexpensive YAG laser. The ability to remold and remodel the *in vitro* cell culture environment during the process of cell development and differentiation mirrors the development course *in vivo*. As a first step towards realizing a truly versatile and interactive experimental platform for cellular culture, these studies demonstrate basic abilities for microstructuration of the cellular environment. Methods to form more complex and elaborate microgeometries are explored in the following chapter.

2.4 REFERENCES

[1]   H. Keshishian, "Ross Harrison's "The outgrowth of the nerve fiber as a mode of protoplasmie movement"," *Journal of Experimental Zoology Part a-Comparative Experimental Biology*, vol. 301A, pp. 201-203, 2004.

[2]   D. R. Jung, R. Kapur, T. Adams, K. A. Giuliano, M. Mrksich, H. G. Craighead, and D. L. Taylor, "Topographical and physicochemical modification of material surface to enable patterning of living cells," *Critical Reviews in Biotechnology*, vol. 21, pp. 111-154, 2001.

[3]   A. M. Rajnicek and C. D. McCaig, "Guidance of CNS growth cones by substratum grooves and ridges: effects of inhibitors of the cytoskeleton, calcium channels and signal transduction pathways," *Journal of Cell Science*, vol. 110, pp. 2915-2924, 1997.

[4]   M. Merz and P. Fromherz, "Polyester microstructures for topographical control of outgrowth and synapse formation of snail neurons," *Advanced Materials (Weinheim, Germany)*, vol. 14, pp. 141-144, 2002.

[5]   M. J. Mahoney, R. R. Chen, J. Tan, and W. M. Saltzman, "The influence of microchannels on neurite growth and architecture," *Biomaterials*, vol. 26, pp. 771-8, 2005.

[6]   G. Zeck and P. Fromherz, "Noninvasive neuroelectronic interfacing with synaptically connected snail neurons immobilized on a semiconductor chip," *Proceedings of the National Academy of Sciences of the United States of America*, vol. 98, pp. 10457-10462, 2001.

[7]   E. Sanjana Neville and B. Fuller Sawyer, "A fast flexible ink-jet printing method for patterning dissociated neurons in culture,"*Journal of neuroscience methods*, vol. 136, pp. 151-63, 2004.

[8]   J. C. Chang, G. J. Brewer, and B. C. Wheeler, "A modified microstamping technique enhances polylysine transfer and neuronal cell patterning," *Biomaterials*, vol. 24, pp. 2863-2870, 2003.

[9]   C. K. Yeung, L. Lauer, A. Offenhausser, and W. Knoll, "Modulation of the growth and guidance of rat brain stem neurons using patterned extracellular matrix proteins," *Neuroscience letters*, vol. 301, pp. 147-50, 2001.

[10]   F. Turcu, K. Tratsk-Nitz, S. Thanos, W. Schuhmann, and P. Heiduschka, "Ink-jet printing for micropattern generation of laminin for neuronal adhesion," *Journal of Neuroscience Methods*, vol. 131, pp. 141-148, 2003.

[11]   G. L. Ming, S. T. Wong, J. Henley, X. B. Yuan, H. J. Song, N. C. Spitzer, and M. M. Poo, "Adaptation in the chemotactic guidance of nerve growth cones," *Nature*, vol. 417, pp. 411-8, 2002.

[12]   C. Weinl, N. Becker, and J. Loeschinger, "Responses of temporal retinal growth cones to ephrinA5-coated beads," *Journal of neurobiology*, vol. 62, pp. 219-30, 2005.

[13]   Y. Naka, A. Kitazawa, Y. Akaishi, and N. Shimizu, "Neurite outgrowths of neurons using neurotrophin-coated nanoscale magnetic beads,":*Journal of bioscience and bioengineering*, vol. 98, pp. 348-52, 2004.

[14]   A. Ehrlicher, T. Betz, B. Stuhrmann, D. Koch, V. Milner, M. G. Raizen, and J. Kas, "Guiding neuronal growth with light," *Proceedings of the National Academy of Sciences of the United States of America*, vol. 99, pp. 16024-16028, 2002.

[15]   H. Y. Chang, K. Takei, A. M. Sydor, T. Born, F. Rusnak, and D. G. Jay, "Asymmetric retraction of growth cone filopodia following focal inactivation of calcineurin," *Nature*, vol. 376, pp. 686-90, 1995.

[16]   J. D. Spikes, H.-R. Shen, P. Kopeckova, and J. Kopecek, "Photodynamic crosslinking of proteins. III. Kinetics of the FMN- and rose bengal-sensitized photooxidation and intermolecular crosslinking of model tyrosine-containing N-(2-hydroxypropyl)methacrylamide copolymers," *Photochemistry and Photobiology*, vol. 70, pp. 130-137, 1999.

[17]   C. Tanielian and R. Mechin, "Mechanism and kinetics of the methylene-blue-sensitized photo-oxygenation of polydienes," *Journal of Photochemistry and Photobiology, A: Chemistry*, vol. 48, pp. 43-51, 1989.

[18]   J. P. Tardivo, A. Del Giglio, C. Santos de Oliveira, D. S. Gabrielli, H. C. Junqueira, D. B. Tada, D. Severino, R. d. F. Turchiello, and M. S. Baptista, "Methylene blue in photodynamic therapy: From basic mechanisms to clinical applications," *Photodiagnosis and Photodynamic Therapy*, vol. 2, pp. 175-191, 2005.

[19]   T. Theodossiou, J. S. Hothersall, E. A. Woods, K. Okkenhaug, J. Jacobson, and A. J. MacRobert, "Firefly Luciferin-activated Rose Bengal: In Vitro Photodynamic Therapy by Intracellular Chemiluminescence in Transgenic NIH 3T3 Cells," *Cancer Research*, vol. 63, pp. 1818-1821, 2003.

[20]   J. D. Pitts, P. J. Campagnola, G. A. Epling, and S. L. Goodman, "Submicron Multiphoton Free-Form Fabrication of Proteins and Polymers: Studies of Reaction Efficiencies and Applications in Sustained Release," *Macromolecules*, vol. 33, pp. 1514-1523, 2000.

[21]   M. A. Herman, D. Fromm, and D. Kessel, "Tumor blood-flow changes following protoporphyrin IX-based photodynamic therapy in mice and humans," *Journal of Photochemistry and Photobiology, B: Biology*, vol. 52, pp. 99-104, 1999.

[22]   D. C. Neckers, "Rose Bengal," *Journal of Photochemistry and Photobiology, A: Chemistry*, vol. 47, pp. 1-29, 1989.

[23]   D. Gabrielli, E. Belisle, D. Severino, A. J. Kowaltowski, and M. S. Baptista, "Binding, aggregation and photochemical properties of methylene blue in mitochondrial suspensions," *Photochemistry and Photobiology*, vol. 79, pp. 227-232, 2004.

[24]   B. S. Cooperman, J. Dondon, J. Finelli, M. Grunberg-Manago, and A. M. Michelson, "Photosensitized cross-linking of IF-3 to Escherichia coli 30S subunits," *FEBS Letters*, vol. 76, pp. 59-63, 1977.

[25]   C. Xu, W. Zipfel, J. B. Shear, R. M. Williams, and W. W. Webb, "Multiphoton fluorescence excitation: new spectral windows for biological nonlinear microscopy," *Proc Natl Acad Sci U S A*, vol. 93, pp. 10763-8, 1996.

[26]   R. T. Hill and J. B. Shear, "Enzyme-nanoparticle functionalization of three-dimensional protein scaffolds," *Anal Chem*, vol. 78, pp. 7022-6, 2006.

[27]   R. T. Hill, J. L. Lyon, R. Allen, K. J. Stevenson, and J. B. Shear, "Microfabrication of three-dimensional bioelectronic architectures," *J Am Chem Soc*, vol. 127, pp. 10707-11, 2005.

[28]   S. Basu, C. W. Wolgemuth, and P. J. Campagnola, "Measurement of normal and anomalous diffusion of dyes within protein structures fabricated via multiphoton excited cross-linking," *Biomacromolecules*, vol. 5, pp. 2347-57, 2004.

[29]   B. Kaehr and J. B. Shear, "Mask-directed multiphoton lithography," *J Am Chem Soc*, vol. 129, pp. 1904-5, 2007.

[30]   P. Saeta, J. K. Wang, Y. Siegal, N. Bloembergen, and E. Mazur, "Ultrafast electronic disordering during femtosecond laser melting of gallium arsenide," *Physical Review Letters*, vol. 67, pp. 1023-6, 1991.

[31]   E. N. Glezer, M. Milosavljevic, L. Huang, R. J. Finlay, T. H. Her, J. P. Callan, and E. Mazur, "Three-dimensional optical storage inside transparent materials (vol 21, pg 2023, 1996)," *Optics Letters*, vol. 22, pp. 422-422, 1997.

[32]   E. N. Glezer and E. Mazur, "Ultrafast-laser driven micro-explosions in transparent materials," *Applied Physics Letters*, vol. 71, pp. 882-884, 1997.

[33]   B. Kaehr, R. Allen, D. J. Javier, J. Currie, and J. B. Shear, "Guiding neuronal development with in situ microfabrication," *Proceedings of the National Academy of Sciences of the United States of America*, vol. 101, pp. 16104-16108, 2004.

[34]   R. Allen, R. Nielson, D. D. Wise, and J. B. Shear, "Catalytic three-dimensional protein architectures," *Anal Chem*, vol. 77, pp. 5089-95, 2005.

[35]   B. Kaehr, N. Ertas, R. Nielson, R. Allen, R. T. Hill, M. Plenert, and J. B. Shear, "Direct-write fabrication of functional protein matrixes using a low-cost Q-switched laser," *Anal Chem*, vol. 78, pp. 3198-202, 2006.

[36]   G. A. Silva, C. Czeisler, K. L. Niece, E. Beniash, D. A. Harrington, J. A. Kessler, and S. I. Stupp, "Selective differentiation of neural progenitor cells by high-epitope density nanofibers," *Science*, vol. 303, pp. 1352-1355, 2004.

[37]   K. T. Pilobello, L. Krishnamoorthy, D. Slawek, and L. K. Mahal, "Development of a lectin microarray for the rapid analysis of protein glycopatterns," *Chembiochem*, vol. 6, pp. 985-989, 2005.

[38]   Y. Ohyama, K. Kasai, H. Nomoto, and Y. Inoue, "Frontal affinity chromatography of ovalbumin glycoasparagines on a concanavalin A-sepharose column. A quantitative study of the binding specificity of the lectin," *J Biol Chem*, vol. 260, pp. 6882-7, 1985.

[39]   K. L. Hsu, K. T. Pilobello, and L. K. Mahal, "Analyzing the dynamic bacterial glycome with a lectin microarray approach," *Nat Chem Biol*, vol. 2, pp. 153-7, 2006.

Chapter 3: Mask-Directed Multiphoton Lithography

3.1 INTRODUCTION

In the last 20 years, many new lithographic and microfabrication techniques have emerged as a consequence of the desire to miniaturize the chemical and biological laboratory. In comparison to strategies developed for microelectronic and microelectromechanical (MEMs) fabrication, soft lithography, ink-jet printing, molecular self assembly, direct ink writing and multiphoton lithography have been proposed as alternative and often more appropriate microfabrication strategies for many aspects in the development of 'labs on chips'[1-5]. These advances, occurring largely in the fields of material physics, chemistry and engineering should provide new avenues for discovery in the biosciences and more rapid, accurate, and inexpensive diagnostics in clinical settings [4]. Of these fabrication strategies, multiphoton lithography provides the greatest potential to render accurate and arbitrary 3D microgeometries from a variety of inert and functional materials [5]. In the previous chapter, MPE photocrosslinking of proteins was proposed as a biocompatible microfabrication strategy to affect cellular (specifically neuronal) development *in situ* — a capability that further separates this approach beyond other methods. Unquestionably a highly flexible microfabrication approach for a number of applications, there remains significant barriers to the widespread adoption of multiphoton lithography as a technique for cell biology.

First, femtosecond laser sources remain cost-prohibitive for most potential users in the biosciences. Therefore we evaluated a low-cost MPE light source, a sub-nanosecond Q-switched microchip laser, and demonstrated its ample performance for

MPE protein photocrosslinking in cellular environments [6]. Second, though MPE enables high resolution 3D microfabrication using tight focusing, a similarly high resolution beam or stage scanning methodology must be coordinated to the MPE voxel in order to fully take advantage of the 3D capabilities for microfabrication. This need has largely been met by pairing MPE light sources to piezo driven stage scanners — which can provide nanometer resolution of x,y,z coordinates — in addition to (or in place of) galvanometer mirror scanning of x,y dimensions [5]. These solutions, though suitable, can also be cost-prohibitive and often require significant programming expertise or additional investment in 3D scanning and rendering equipment/software. All of these considerations result in high initial investment for multiple components that require expertise in multiple areas (a situation indicative of any new technology).

In this chapter a more straightforward MPE photofabrication methodology is demonstrated. Here, the capabilities of 'free-form' microfabrication are extended to fabricate complex 3D microstructures and microgradients. In addition, these methods enable the rapid prototyping (tens of minutes per iteration) of microscale geometries for cell studies — a substantial improvement over current prototyping timescales using photolithographic or soft lithography methods (≥24 hours per iteration). The method outlined here is suitable for a wide variety of microprototyping applications including microfluidic and MEMs platform design as well as scaffolds for 3D cell and tissue engineering.

The first half of the chapter describes an approach for mask-directed multiphoton lithograpy (MDML) — a strategy that melds traditional photolithography using transparency photomasks and mask objects to multiphoton projection lithography. The

final section describes the replacement of the transmission-based photomask with an automated reflectance mask, a digital micromirror device (DMD; [7]) and demonstrates DMD-directed multiphoton lithography for applications such as the microreplication of biological specimens and tissue constructs. Microstructure design described here is optimized for microbiological studies, a topic to be addressed in detail in Chapter 5. Nevertheless, these methods should be readily extendable to virtually any cell and tissue culture application of interest.

3.2 EXPERIMENTAL METHODS

3.2.1 Materials

Methylene blue (M-4159) and flavin adenine dinucleotide (FAD, F-6625) was purchased from Sigma-Aldrich (St. Louis, MO). Bovine serum albumin (BSA, BAH64-0100) was supplied by Equitech-Bio (Kerrville, TX). Avidin (A-887) and fluorescein biotin (B-1370) were supplied by Molecular Probes, (Eugene, OR). All chemicals and solvents were stored according to supplier's specifications and used without further purification. Office grade transparency film for laser printers was used to produce photomasks on an HP Laser Jet 2100TN.

3.2.2 Strains

E. coli strains RP9535 (smooth-swimming, $\Delta cheA$), kindly provided by John S. Parkinson (Department of Biology, University of Utah), were grown aerobically in tryptone broth (32 °C) and harvested at mid-log phase. Cells were diluted 20-100 fold into PBS (10 mM potassium phosphate, pH 7.0) for experiments with fabricated microchambers (described in more detail in Chapter 5).

3.2.3 Matrix Fabrication

3.2.3.1 Transparency-Directed Fabrication

Matrices composed of photocrosslinked protein were fabricated onto untreated #1 microscope coverglass using the output of a mode-locked titanium:sapphire laser (Tsunami; Spectra Physics, Mountain View, CA) operating at 730 to 740 nm. The laser beam was raster scanned in rectangular patterns using a confocal scanner (BioRad MRC600) and brought to a focus between the scanbox and the microscope by the scanbox optics. Placing masks or automated reflectance elements in this focal plane (referred to in the text as the 'mask plane') allowed the greatest fidelity in the fabricated object since the mask plane is conjugate with the microscope specimen plane, although masks could be used (with less edge resolution) when placed at any position between the scanbox and the microscope. Transparency masks were aligned manually by adjusting the XY position of the mask during test photofabrication procedures. Moving masks were generally translated at a linear velocity of 100 to 200 μm s^{-1} using rectangular scan frequencies (the inverse of the time to complete a raster-scanned rectangle) of 3 Hz.

The laser output was adjusted to approximately fill the back aperture of high numerical aperture (NA) objective (Zeiss Fluar, 100x/1.3 NA, oil immersion) situated on a Zeiss Axiovert inverted microscope system. Desired powers (30-40 mW before the back aperture of the microscope objective) were obtained by attenuating the laser beam using a half-wave plate/polarizing beam splitter pair. To extend structures along the *z* dimension (i.e., along the optical axis), the position of the laser focus was translated manually within fabrication solutions using the microscope fine focus adjustment. By removing transparency masks once the desired structure height was attained, microchambers could be readily sealed from the top with closed rectangular roofs.

Typical microchambers having heights of 2 – 10 μm were produced by allowing two full scans to be rastered across the sample per micron of vertical travel.

Microstructures composed of photo-cross-linked BSA were fabricated from solutions containing protein at 320 – 400 mg mL^{-1} and 2 – 5 mM methylene blue as a photosensitizer.

3.2.3.2 DMD-Directed Fabrication

Digital micromirror devices are manufactured by Texas Instruments predominately for use in digital projectors and high definition televisions. The type of DMD used in these experiments (0.55SVGA) consists of an 848 x 600 array of aluminum mirrors 16.2 μm on a side. Each individual mirror switches between an "off" and "on" state corresponding to a ±10º tilt angle. The DMD utilized was a component of a partially dismantled business projector (Benq MP510). The projector's DMD was exposed by removing its optics, optics housing and light source. The individual mirrors were controlled by the intact projector electronics programmed to replicate (by modulating between the off and on states) graphic output of a computer. Focused laser light that scanned over approximately a quarter of the DMD mirrors was reflected into a beam block or directed further down the optical path according to the state of the individual mirrors. Light reflected down the optical path was collimated by a tube lens and sent into a microscope objective (Zeiss Fluar, 100x/1.3 NA, oil immersion, or; Olympus LUMPlanFl, 100x/1.0 NA, water immersion) mounted in a Zeiss Axiovert (inverted) microscope. Laser powers measured at the back aperture of the microscope objective typically were 50 – 60 mW. The irradiated area at the sample plane was ~60-μm by ~40-μm.

Most input data were adjusted using Adobe Photoshop to correct for an observed ~5º skew caused by the reflection geometry from the DMD. In addition, most

tomographic input data were processed to enhance contrast, typically converting grayscale information to binary data.

Structures were fabricated onto coverglass that was boosted over a lower coverglass by using microsphere or coverglass spacers. The low profile chamber was filled with the fabrication solution (BSA, 320 – 400 mg mL^{-1}; methylene blue, 2 – 5 mM). Structures were fabricated from the top coverglass (to avoid focusing through the nascent structure) using 60 to 150 planes separated by 0.1- to 1-µm steps (along the optical axis) controlled by a motorized focus driver (Prior, H122). Vertical heights of the structures could be extended to as much as 150 µm using this approach.

3.2.4 Wide-Field Fluorescence Microscopy

Wide-field fluorescence imaging was performed on the Axiovert microscope, which was equipped with a mercury-arc lamp and standard "red" and "green" filter sets (Chroma, Rockingham, VT). Fluorescence emission was collected using the Fluar 100x objective and detected using a 12-bit 1392 x 1040 element CCD (Cool Snap HQ; Photometrics, Tucson, AZ). Data were processed using Image J and Metamorph (Universal Imaging, Sunnyvale, CA) image-analysis software.

3.2.5 Scanning Electron Microscopy (SEM) Preparation

Samples were fixed in 3.5% gluteraldehyde solution for 20 min and dehydrated by using 10-min sequential washes (2:1 ethanol/H_2O; twice in 100% ethanol; 1:1 ethanol/methanol; 100% methanol; all solutions stated as v/v), allowed to air-dry for 3 h, and sputter-coated to a nominal thickness of 12 – 15 nm with Au/Pd.

3.3 RESULTS

The general approach for MDML is shown in Figure 3.1. Essentially it is an amalgamation of laser-scanning lithography [8] to microscope projection lithography [9] to direct MPE protein photocrosslinking. A Ti:S laser is sent through a confocal scan box to raster the beam in a rectangular pattern at a focal plane positioned between the scan box and an inverted microscope. This focal plane (mask plane) is conjugate with the front focal plane of the microscope objective. Figure 4.1 shows that an object such as an insect (in this case the common house fly, *Musca domestica*) placed within the mask plane directs the fabrication of a protein microstructure representing the negative of the object silhouette at the objective focal plane. The microfabricated structure composed of BSA records silhouette features of even minute fly structures such as the hairs protruding from the insect leg (shown in detail in panel 1). Objects fabricated in this manner display feature sizes of F_{mask}/M_{obj}, where F_{mask} is the feature size in the mask and M_{obj} is the magnification of the objective/lens system. Minimum achievable feature sizes are ultimately determined by the spatial confinement of multiphoton absorption processes and the diffusion distances of reactive intermediates [5]. From a practical standpoint, features of ~0.5 µm are readily attainable using mask objects and transparency photomasks — a scale appropriate for addressing a broad range of applications in cell biology [10].
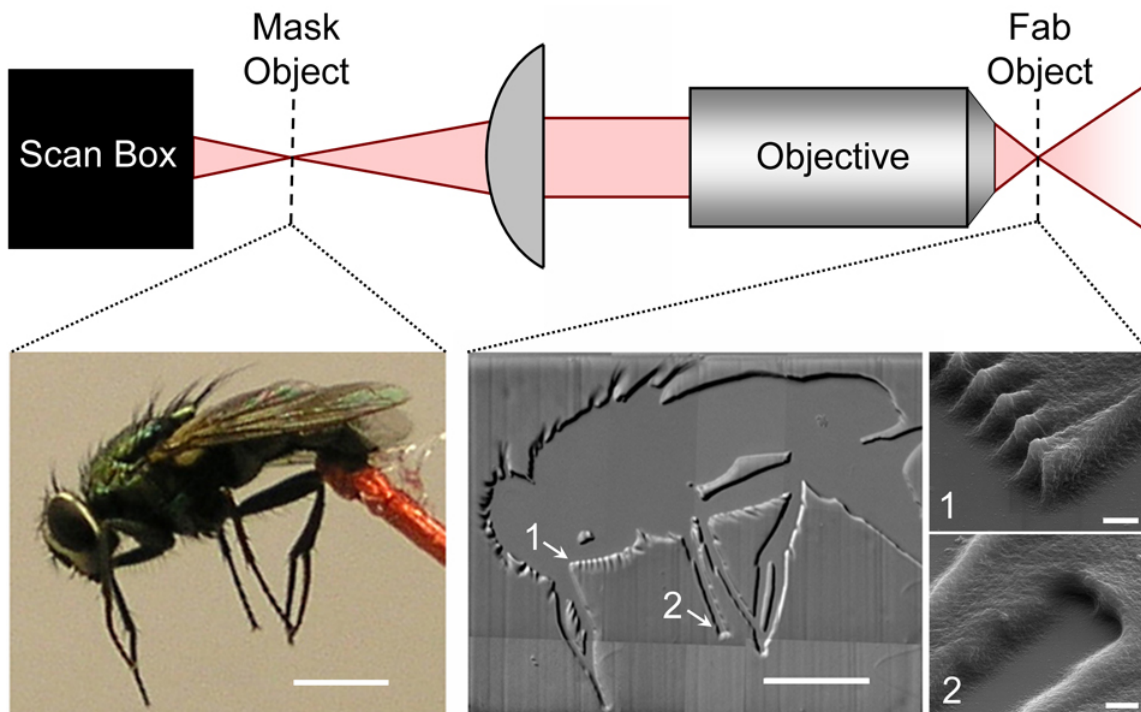
Figure 3.1: Mask-directed multiphoton lithography. (A) Placement of a mask object (left panel; scale bar, 2 mm) in a plane conjugate to the front focal plane of the microscope objective directs fabrication of the object negative (DIC image, center panel; scale bar, 20 μm) using multiphoton lithography. Regions demarked 1 and 2 in this image are shown in detail in SEMs (right panels; scale bar, 1 μm).

In addition to objects such as insects and small plants to direct fabrication of negative features, transparent materials such as glass and transparency photomasks were evaluated. Figure 4.2 illustrates fabrication of 'grooves' into protein microstructures corresponding to the edges of glass coverslips positioned in the mask plane. Edge effects occurring by light diffraction are an inescapable phenomenon in mask-based photolithography [11]. Disregarding the contributions of photochemistry on groove width at transparency mask edges, as well as refraction occurring at the air/glass interface, the

trench width is proportional to the limit of resolution R for the theoretical limit of resolution of $R = \lambda/2(NA)$; where NA is the numerical aperture of the objective.

Additionally, defects (or particles such as dust) in otherwise transparent materials were mapped into fabricated structures (Figure 3.2, arrows). This was considerably more apparent using transparency photomasks (as opposed to glass) printed from office printers as the spooling mechanics tend to add minor opacities to the transparency. However, in the development of 3D microstructures for cell entrapment and guidance, these defects in fabricated objects were of minor consequence as they only occasionally affected the desired structural features defined by the opaque geometries of the photomask.
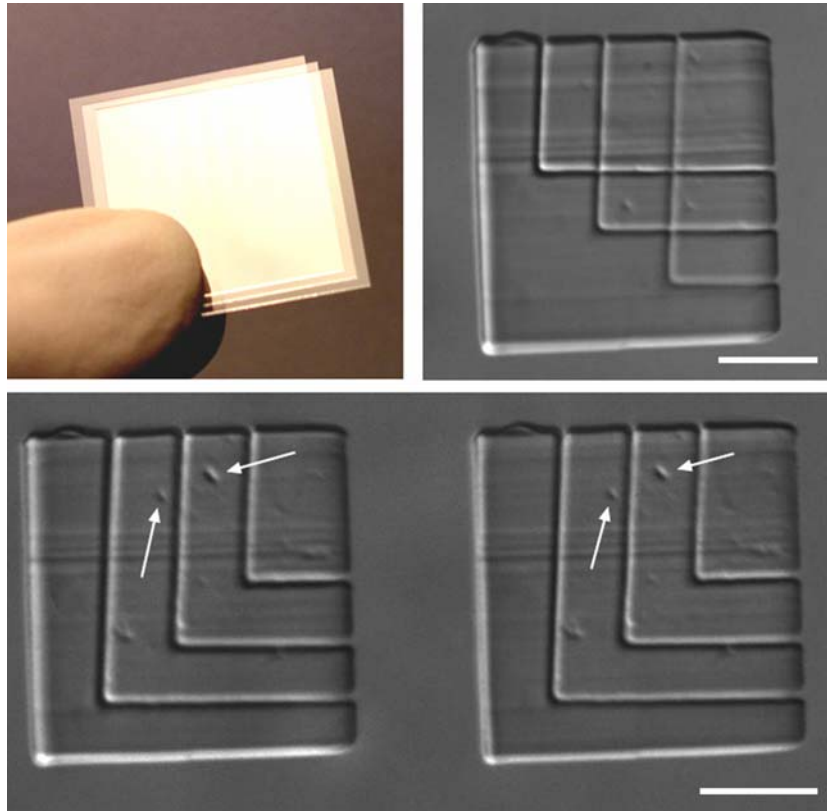
Figure 3.2: MDML using transparent masks. The edges of transparent photomasks (top left panel) define channel-like features in microstructures (top right panel). 'Defects' are replicated in microstructures (bottom panel, arrows). Scale bars, 5 μm.

The use of objects for photomasking — particularly objects with differing point-of-view profiles — is interesting to consider. A single mask object could be used to define a series of microstructures corresponding to the object sillouette from a given prospective. This is analogous to modern tomographic imaging (e.g., computerized tomography or CT), which relies not solely on imaging planes at different depths, but also from different perspectives. The utility of this approach was only briefly explored but could potentially offer, in combination with DMD-directed techniques discussed later in the chapter, an additional level of control over microstructure geometries.

Printed transparencies designed for office laser and inkjet printers proved invaluable for prototyping microstructures. Their low cost and the potential to print hundreds of usable photomasks per transparency, aided rapid iteration of prototype geometries. Typically, transparencies for laser printers were used for photomasks (ink jet transparencies are 'roughened' on the ink deposition side, increasing defects in fabricated structures) which were printed on an HP Laser Jet 2100TN at 600-1200 dpi. Figure 3.3 shows the effects of mask placement at different positions along the axis of beam propagation on sillouette feature size and resolution. The effective mask feature size outside of the focal plane increases by a factor proportional to the width of a laser beam spreading by $2Z\lambda/\pi\omega_0$ where ω_0 is the half width of the laser beam at the focal plane and and Z is the axial distance from the focal plane [11]. Thus, masks placed nearest the focal point after the scanbox produced the sillouette of best resolution and accuracy.
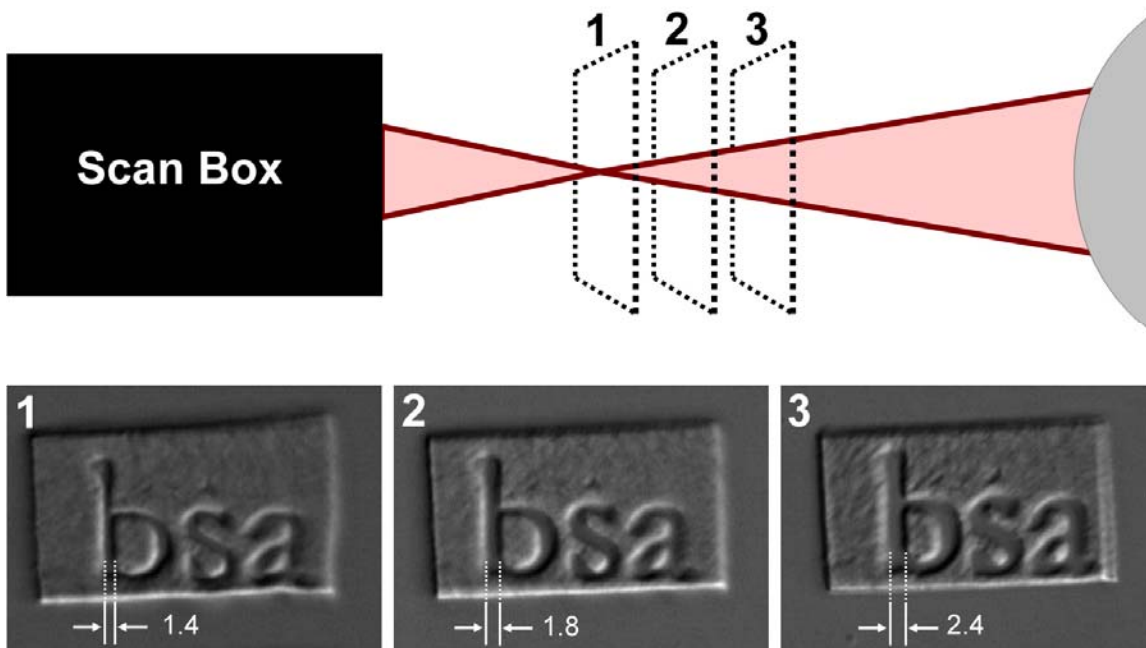
Figure 3.3: Optimizing mask placement. A transparency photomask was placed in different spatial locations (1-3 shown in the schematic, distances are not to scale) along the axis of the scanning laser beam. Panel 1 corresponds to mask placement closest to the focal point, resulting in the greatest accuracy and resolution of mask features in the fabricated microstructure (distances are in μm). The effective feature size of a mask feature ($\sim$ 150 μm width) placed $\sim$ 1 and 2 mm outside the focal plane (panel 2 and panel 3) is increased by a factor proportional to width of the laser beam (see text).

3.3.1 MDML for the Fabrication of Microgradients

Strict structural organization of biomolecules and materials is necessary to impart proper development and function of biological tissue. As a consequence, biomaterials research has been focused for quite some time on developing *in vitro* patterning techniques to mimic cell and tissue scaffolding such as the extracellular matrix [12]. Gradients of molecular cues presented to cells along their development paths are of crucial importance. Chemical gradients of soluble, immobilized and mechanical cues drive chemotaxic, haptotaxic and durotaxic cell behavior, respectively [13]. For instance,

neuronal outgrowths such as axons develop along soluble and immobilized gradient pathways to reach appropriate termination points [14].

In cell culture, soluble gradients can be produced using various methods that define directional fluid flow [15, 16], and including novel approaches developed in the Shear Lab [17, 18]. The patterning of immobilized or substrate-bound gradients can present greater challenges due in large part to the difficulty of establishing and 'freezing' into place substrate-bound gradients with desired gradient profiles. A number of strategies have been proposed for defining immobilized gradients in cell culture including those in which soluble spatial gradients, generated in complex microfluidic geometries, are adsorbed, dried, or photopolymerized in place [19-21]. As an alternative strategy, MDML using variable light exposure through translatable or movable masks was explored.

In the MDML configuration shown in Figure 3.1, it was straightforward to translate mask objects orthogonal to the optical axis. Orthogonal translation of an opaque mask during the fabrication process functioned to vary the laser exposure at the specimen plane over time. Using this principle, a functional substrate-bound microgradient could be fabricated from a protein solution containing, for instance, avidin washed with a biotinylated molecule as is shown in Figure 3.4. Further, microgradients could be defined with arbitrary boundaries, directionality and slope profiles (Figure 3.5). The simplicity and flexibility of this approach for generating microscale gradients cannot be overstated. Other strategies require elaborate microfluidic mixing geometries to generate gradients and thus the gradient length and direction are 'locked' into the outflow geometry [16, 20]. These methods are optimized to fabricate substrates to which cells are then seeded and therefore are limited in their capability to define gradients *in situ*.

63

As neurite outgrowth has been shown to proceed up substrate bound gradients *in vitro* [19], it should be straightforward to exploit these chemistries using MDML and movable masks. For instance, by guiding outgrowth from various cells to desired target points using linear or radial gradients (Figure 3.5A,B), the construction of neuronal circuits *in situ* — a goal proposed in Chapter 2 — should be attainable. Finally substrate-bound gradients such as these should further aid in the generation of even more complex soluble gradients from catalytically active microstructures — an extension of other work in the Shear Lab [17, 18]. For example, if an immobilized linear gradient of catalytic activity is addressed with an orthogonal laminar flow containing an enzymatic substrate, the product outflow would also be a gradient of linear slope. The relative ease of defining the slope and direction of substrate-bound gradients shown here should provide great flexibility for a broad number of applications.
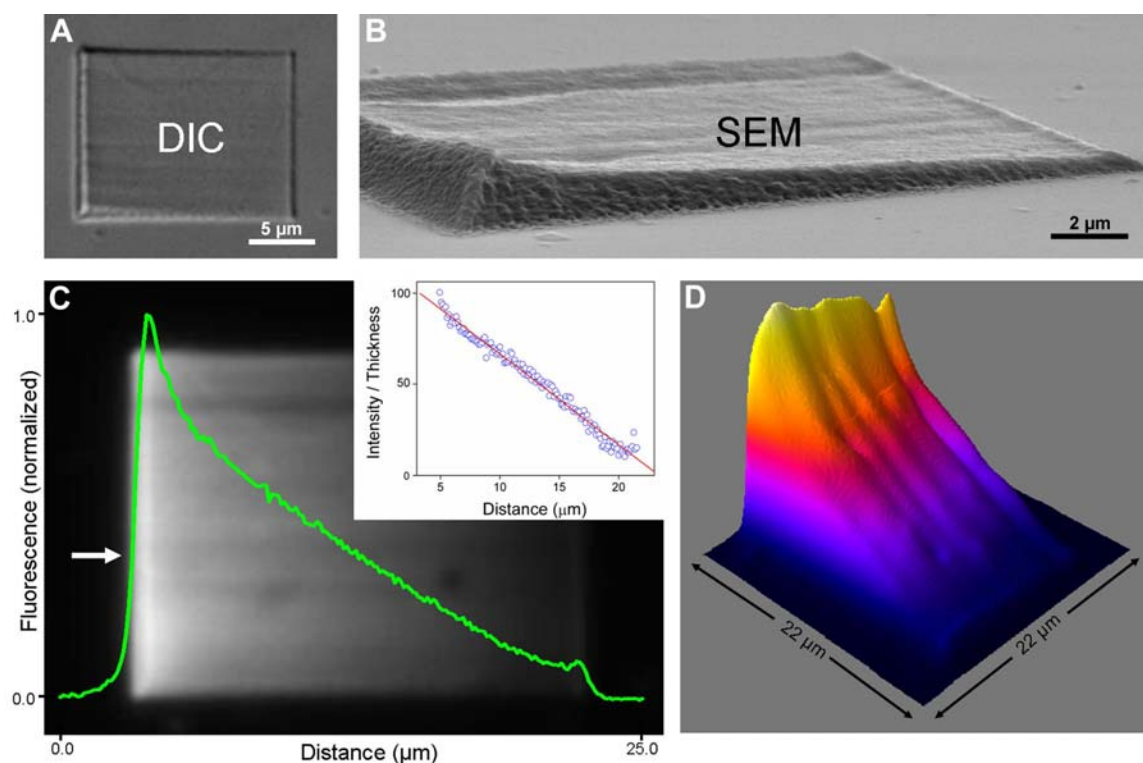
Figure 3.4: Use of a moving mask to create a gradient in both thickness and chemical functionalization across a protein microstructure. A gradient microstructure was fabricated from a solution containing 90% BSA and 10% avidin (wt/wt; total protein concentration was 320 mg ml^{-1}) and methylene blue (3 mM). During laser scanning, a fully opaque straight-edge mask was translated such that its image in the fabrication plane was swept at a rate of 2 μm s^{-1}. The resultant BSA/avidin microstructure was incubated in 2 μM fluorescein biotin for 10 min, rinsed 10 times in PBS (pH 7.0), and imaged via fluorescence. (A, B) DIC and SEM microscopy reveal that changes in laser exposure times across the protein structure cause a thickness gradient. (C) Plot (green line) representing the fluorescence intensity of a horizontal line drawn across the structure (from arrow). This intensity was divided by the thickness of the structure (inset) to yield the functional gradient density (i.e., normalized for structure thickness). From this data, the fluorescence intensity gradient is shown to be a convolution of structure thickness and functional density (i.e., biotin-binding capacity of avidin). Panel D is a 3D surface intensity plot of the fluorescent image in panel C and shows that the gradient is maintained across the surface of the microstructure.
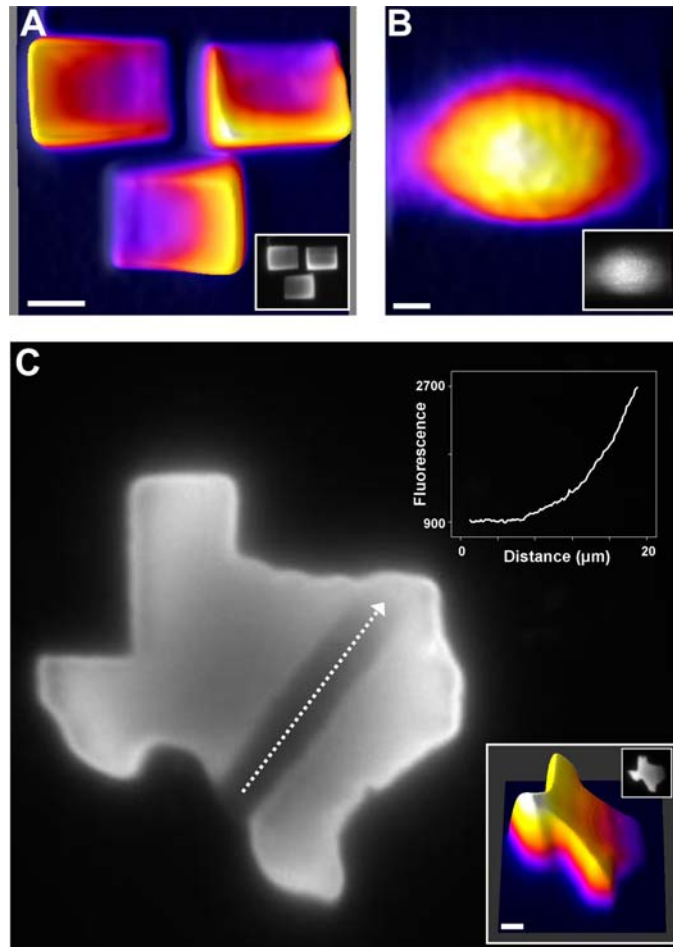
Figure 3.5: Translatable masks are a flexible strategy for fabrication of microgradients. (A) The direction of the gradient slope can be dictated by the direction of mask translation orthogonal to the beam axis (e.g., west to east, [left structure]; south to north, [right structure]; east to west, [bottom structure]. (B) Actuation (from closed to open) of a variable aperture iris during fabrication produces a radial microgradient. (C) Microgradient boundaries can be defined with a stationary negative mask. Here linear (lower inset) or nonlinear gradients (along the dotted arrow) are fabricated using masks translated at linear and accelerated velocities respectively. The plot shows the gradient profile along the direction of the dotted arrow in C, produced by translating an opaque mask of dimensions smaller than the negative transparency used to define the microstructure edges. All microstructures were fabricated from 400 mg ml^{-1} BSA photosensitized using 5 mM methylene blue. Fluorescence intensity is from entrapped photosensitzer. Scale bars, 5 μm.

66

3.3.2 MDML for Rapid Prototyping

MDML allows facile optimization of microfabricated structures by using CAD software (e.g., MS powerpoint, Adobe Illustrator, AutoCAD, etc.) and an office printer. Figure 3.7 shows a scheme to fabricate a microchamber designed to direct the movement of motile *E. coli* — the utility of which will be discussed in detail in Chapter 5. Rectangular scanning parameters were adjusted to the desired dimensions (by defining the laser scan area using the scan box software) and a transparency photomask defined the internal chamber dimensions. The structure is extended from the surface and along the z-axis (i.e., optical axis) by manually adjusting the microscope fine focus until the desired height was attained. This plane by plane layering approach can result in a 'seamless' vertical microstructure provided there is sufficient overlap between fabricated planes (the width of which is defined by the axial dimensions of the fabrication voxel) and spatial steps along the z-dimension. Typical microchambers having heights of 2 – 10 μm were produced by allowing two full scans to be rastered across the sample per micron of vertical travel. This procedure allows fully formed 3D objects to be fabricated on time scales of 10 – 30 seconds. Once the desired height was attained, the transparency photomask was removed and additional layers were fabricated to seal the microcontainer from the top. Following a thorough rinse of the fabrication solution, the microcontainer design can be evaluated by introduction of motile cells (e.g., *E. coli*). If chamber parameters require additional optimization, the entire process, from mask re-design and printing through structure evaluation, can be iterated in ca. 10 to 30 minutes.
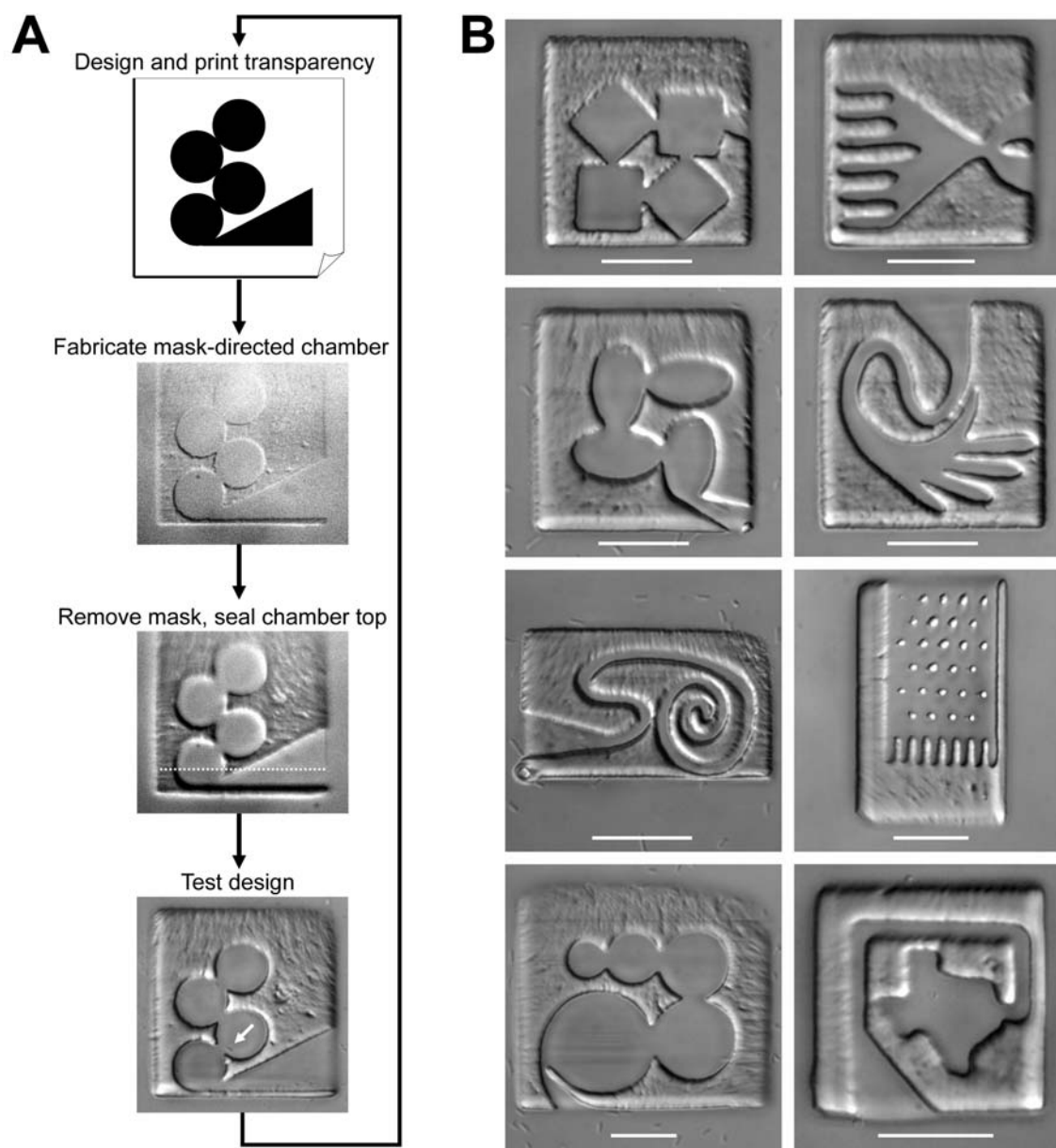
Figure 3.7:   Rapid prototyping using MDML. (A) A scheme for the rapid prototyping of a microchamber for the directed motility of motile bacteria. (B) This approach allows rapid iteration and fabrication of arbitrary microchamber geometries. Microchamber tops are sealed by scanning the laser beam without a photomask in place. Scale bars, 15 μm.

In comparison to conventional lithography, where specialized masters (e.g., using chrome masks, electron-beam or laser-beam lithographies) can take days to weeks to produce, soft lithography using transparency-based photomasks is a more rapid process [5]. However the layering and exposure of photoresist, development of the master and curing times for the elastomeric molds can result in prototyping times (for a single device) of ~1 to 3 days. Since MDML described here is a direct-write, aqueous-based process, there are no development or curing steps. The rate-limiting step is generally the time for mask (re)design. This flexible and rapid process should prove valuable for the development of bio-MEMs and biohybrid devices (discussed in Chapter 5).

More complex 3D microstructures employing multiple levels were created using this approach. Figure 3.8 shows a two-level microcontainer for entrapment of motile *E. coli* fabricated from sequential masks. After fabricating the substrate-bound passageway to a height of ~5 μm, the 'ground floor' mask was removed and the 'second floor' mask was aligned to insure proper overlap. This procedure allowed directed access into the top chamber while sealing the ground floor passageways in a single step. Upon completing the second floor (~4 μm in height) the mask was removed and the top sealed by fabrication additional horizontal planes (~1 μm thick). In this device, smooth-swimming *E. coli* enter the container through an aperture (Figure 3.8B–C), and swim through a passageway to the overlap region of the two stories. Here, the bacteria are shunted vertically into the top chamber. Ultimately, cells accumulate to a point that the chamber becomes tightly packed, preventing entry of additional cells (inset).
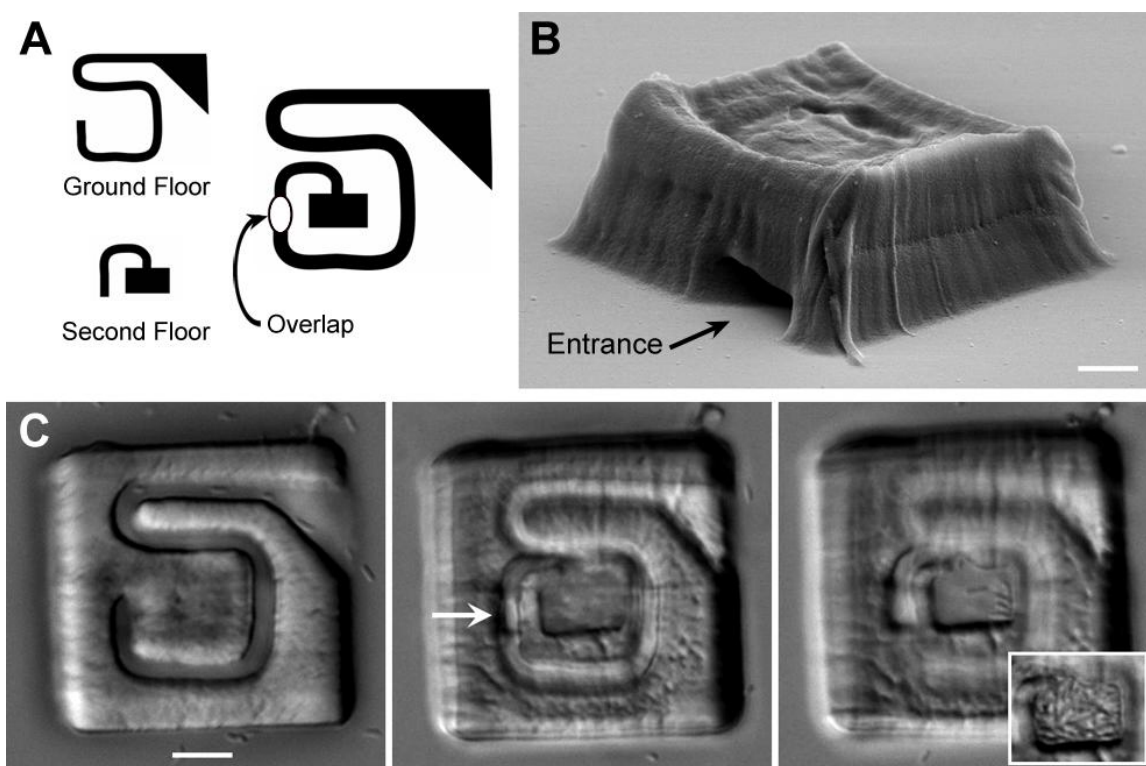
Figure 3.8: A two-story BSA microstructure fabricated using ground floor and second floor masks sequentially (A). The overlap region shunts bacteria from the ground floor to the second floor loft. (B) SEM of the resultant two-story BSA microstructure. (C) DIC images showing *E. coli* cells (RP9535) entering and transiting the ground floor passage (left panel) to the overlap region (arrow, middle panel) and up to the loft (right panel), which ultimately becomes filled (inset). Scale bars (B, C), 5 μm.

This demonstration shows the unique capabilities of 3D layering of complex and functional microcontainers composed of biomaterials using MDML. However, fabrication of this structure required significant trial and error for proper alignment of sequential masks. Mask alignment was achieved by outlining the ground floor dimensions post-fabrication using the drawing tools of an image acquisition program. This provided the critical alignment parameters, similar to using alignment marks in microelectronic fabrication [11], which could be superimposed while the second mask was adjusted in the mask plane. This strategy was far from optimal and a functional

70

structure was attained only after a number of attempts. Also, when microstructure fabrication required focusing vertically through a significant thickness of previously photocrosslinked protein (as was the case here) resolution of higher z-plane features was typically diminished.

Mask alignment is a crucial step in microelectronics fabrication and as such highly specialized mask alignment systems have been developed for accurate alignment of planar components with nanometer-scale features [11]. There are a number of sources of alignment errors — including aberrations from optical components and calibration of mechanical steppers — that must be minimized to insure alignment of the sequential masks required to integrate the micro/nanoscale components of microelectronics and MEMs devices [11]. These difficulties are potentially circumvented if photomasks could be generated on a single display component, since once fixed into place it would not require realignment. Proposals for 'maskless' or 'dynamic mask' systems have including using automated spatial light modulators such as liquid crystal displays (LCD) and digital micromirror devices (DMD) in place of photomasks [22-24]. DMDs are the digital image generation component in Digital Light Projection technology (DLP®; [7]), now pervasive in the digital projector and high definition television set markets. The low cost of DMDs as a mass produced item in commercial products, and the ability to withstand realatively high irradiation intensities, presented an attractive opportunity for evaluation of an automated mask element.

3.3.3 DMD-Directed Multiphoton Lithography (DMD-DML)

The digital micromirror device (DMD) was invented in 1987 by engineers at Texas Instruments. It consists of an array of several hundred thousand micromirrors that can be individually angled to $\pm$ 10° corresponding to 'on' and 'off' states (Figure 3.9). Pixel resolution corresponds to the number of mirrors in the array (for instance, 600 x

800, 1920 x 1080, etc.). In comparison to transmission-based LCD technology, where the low optical density of 'off' pixels can hinder the contrast of transferred patterns, the reflective character of the DMD improves both contrast and pixel switching times (LCD ~20 ms; DMD, ~16 µs) and thus has garnered much recent attention for applications requiring micro-stereolithography [23, 24].
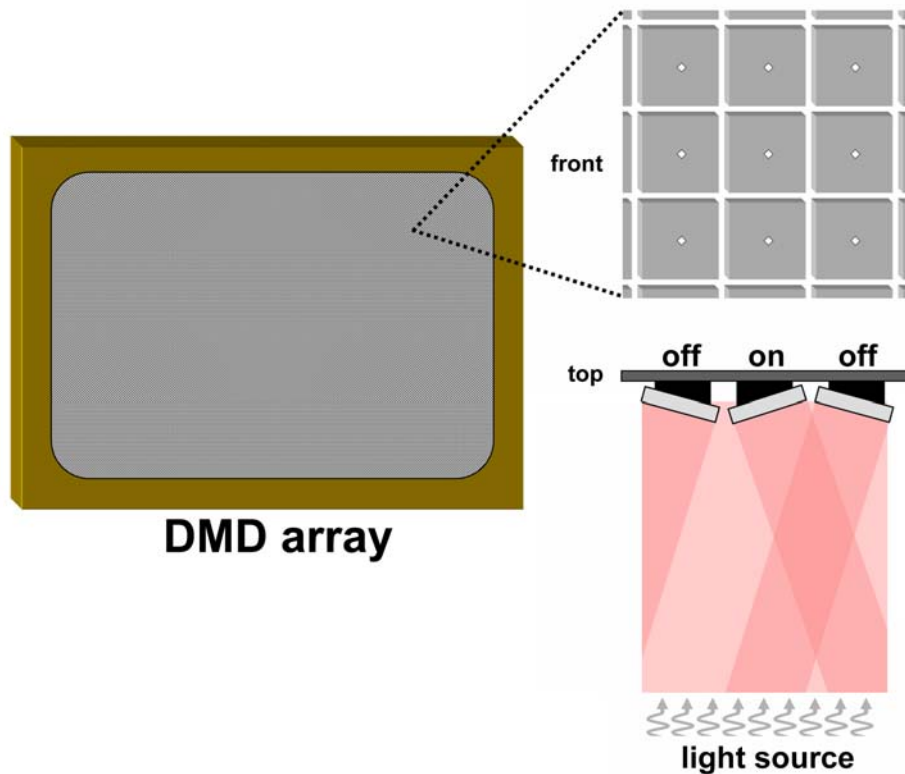
Figure 3.9:   Simplified schematic of a DMD array. Micromirrors are typically 16 x 16 µm and can be individually angled ± 10° corresponding to 'on' and 'off' states which direct the reflection of a light source.

Figure 3.10 shows a schematic with a DMD incorporated into a scanning laser system. Ti:S laser light is raster scanned in a rectangular pattern across the face of a DMD positioned in a focal plane conjugate with the front focal plane of a microscope objective. The DMD used for these studies was a component of a partially dismantled

digital projector. The DMD was exposed by removing its optics, optics housing and light source. By retaining the projector electronics, the output from a desktop computer (paralleling the monitor display) controlled the reflective pattern generated on the DMD. A white screen (all mirrors in the ON position) was used for alignment. A rectangular ordered diffractive pattern of light could be observed after the beam reflected off of the chip. Aligning the laser beam orthogonal to the chip face allowed ~40% of the incident power to be collected from the zero order reflection. By scanning over an area on the DMD roughly corresponding to approximately a quarter of the active micromirrors, rectangular protein structures (~60 x 40 µm) were fabricated at the sample plane. As with all laser scanning microscope systems, alignment required coordination of optical focal planes (for instance across the face of the DMD) with beam translational pivot points. Once these positions were stabilized, only occasional and minor adjustments in alignment were needed.
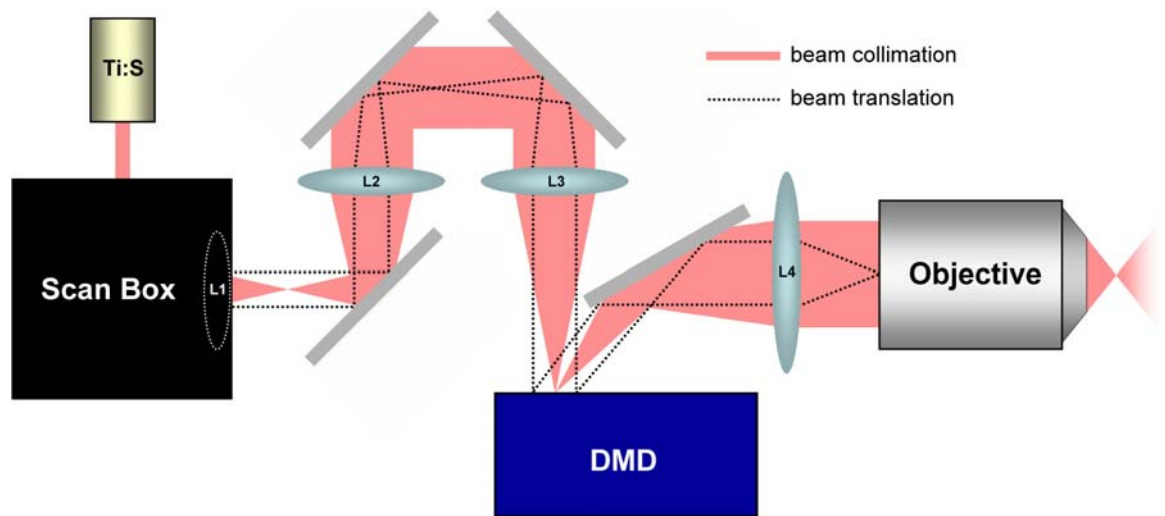
Figure 3.10: Schematic for DMD-directed multiphoton lithography. Dotted lines ("beam translation") denote the limits of the scan position of the beam axis. L1-4 designates the position of lenses.

In combination with the intrinsic 3D resolution of multiphoton lithography, this approach allowed sequential horizontal fabrication planes of arbitrary complexity to be stacked without adjusting alignment. Sequential masks used to direct the fabrication of a complex microstructure could be readily changed on a computer monitor. Figure 3.10A shows fabrication of a BSA, gear-like microstructure using two sequential masks. Indeed, with this approach little additional effort was required to fabricate microstructures from longer sequences of masks. Therefore, this strategy appeared well-suited to direct the replication of biological tissue encoded by 3D imaging technologies (e.g., computed tomography, magnetic resonance imaging, confocal and multiphoton microscopy), which generate data that can be analyzed as stacks of sequential images (Figure 3.10B).
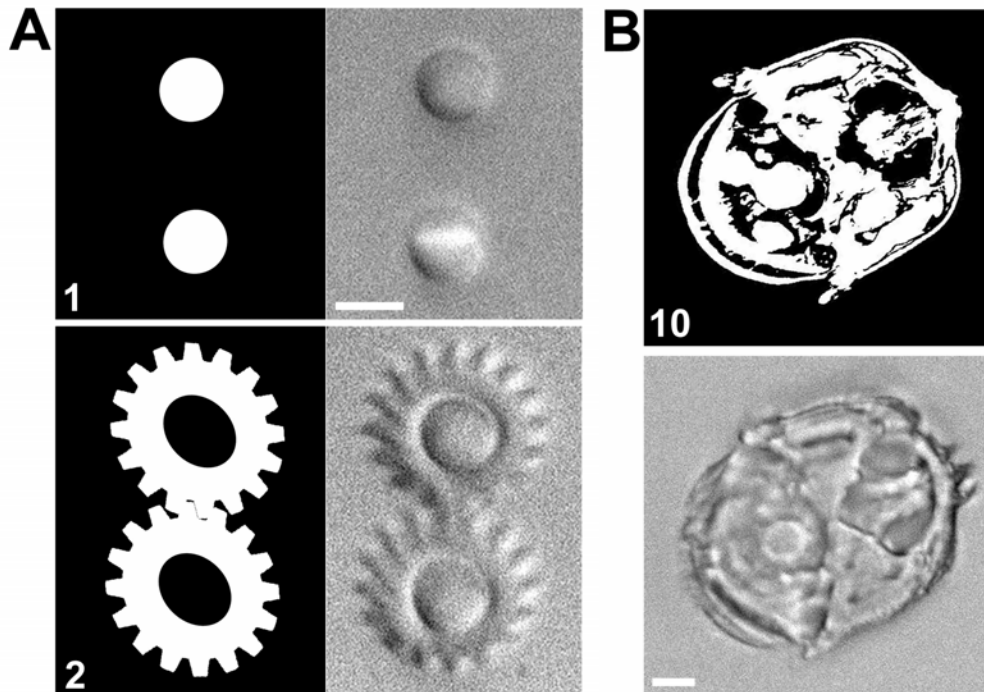
Figure 3.11: DMD-directed MDML allows facile fabrication of multiple horizontal planes. (A) A BSA gear set is fabricated using two sequential masks. In this instance, a 10° skew is applied to the gear mask to fabricate circular gears. (B) An image stack comprised of horizontal planes from an MRI scan directs fabrication of an acrylate microreplica. Numbers denote the position of the mask in the total sequence of masks used to direct fabrication (total = 2 for A; 150 for B). Scale bars, 5 μm.

To investigate the capabilities of this approach for tissue microreplication, tomographic data of biological specimens was attained from the Digital Morphology library (digimorph.com). Figure 3.12 shows scanning electron micrographs of tissue replicas composed of crosslinked BSA and defined by image stacks encoding high resolution X-ray computed tomographic data. Input data from 60 – 120 CT image planes directed fabrication of microstructures on glass substrates using step sizes of between 0.1 and 0.5 μm/z–step with fabrication times between < 4 min/structure. Truncation of whole image stacks or sequences produced sectioned microstructures with high 3D fidelity in both coronal (Figure 3.13, top panel) and horizontal (Figure 3.13, lower panel) planes.
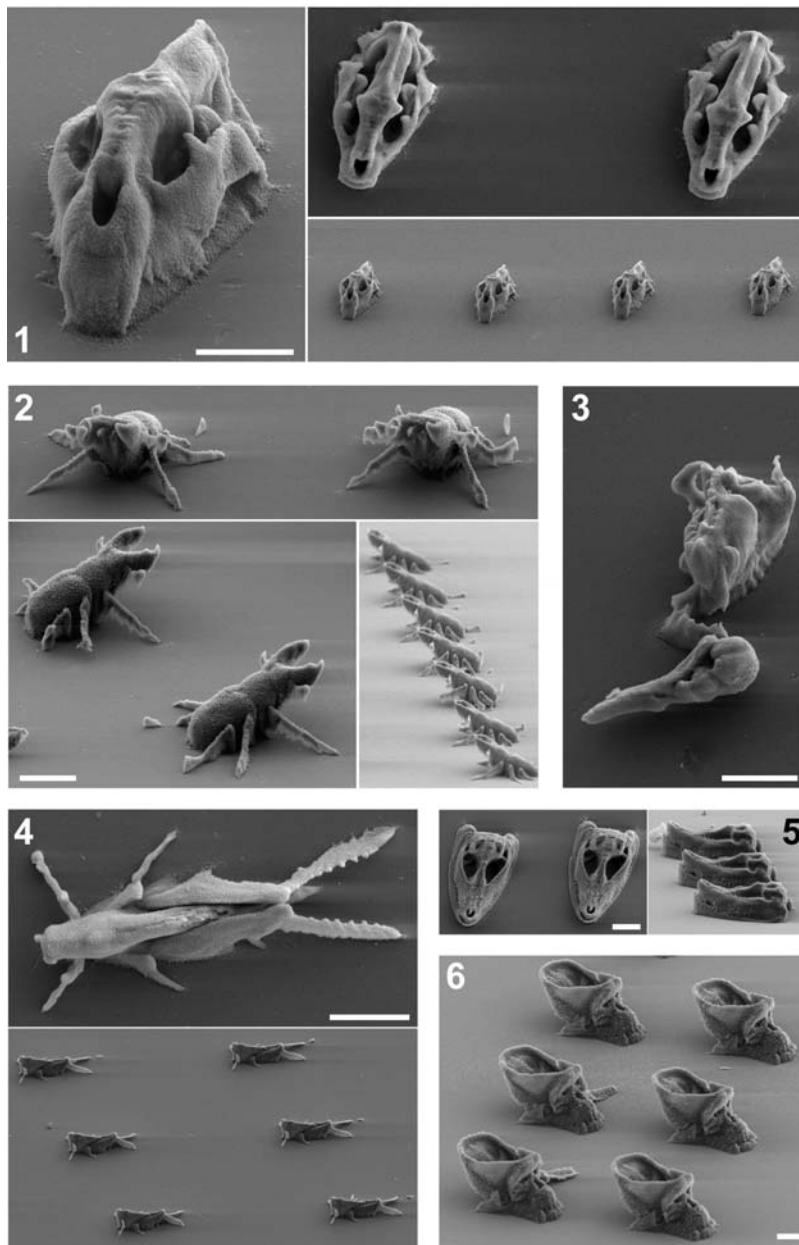
Figure 3.12: Microreplication of biological organisms. Synchronization of DMD image sequences (high resolution X-ray CT data) with vertical sample plane steps enables animal replicas to be fabricated rapidly ($1 - 2$ s plane^{-1}). SEMs of organisms: **1**, *Puma concolor* (puma); **2,** *Lucanus sp.* (staghorn beetle); **3,** *Alcedo cristata* (malachite kingfisher); **4**, *Schistocerca emarginata* (spotted bird grasshopper); **5,** *Alligator mississippiensis* (alligator); **6**, *Pan troglodytes* (common chimpanzee). Scale bars, 10 µm.
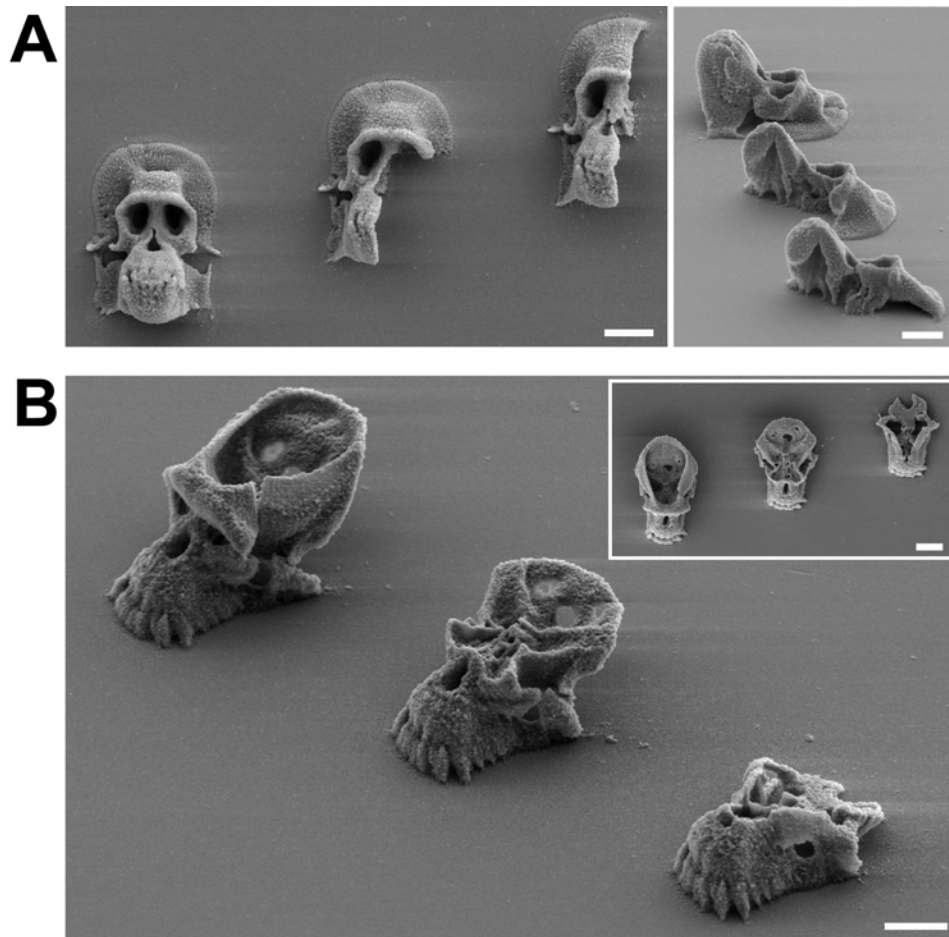
Figure 3.13: DMD-directed multiphoton lithography allows microstructure sectioning. (A) Truncation of DMD displayed images in a coronal stack produces saggital sectioning of chimpanzee skulls (left and right). (B) Subtracting sequential planes from the complete image sequence results in horizontally sectioned microstructures (inset shows top view). Scale bars, 10 μm.

In addition to studies using SEM, the accuracy of hydrated microreplicas was assessed using MPE fluorescence microscopy during and after the fabrication process. Figure 3.14 shows SEMs and MPE fluorescence images of pincushion protea microstructures. Panel B shows a side-view 3D reconstruction of the 110 images that provided plane data for the structure fabrication (B, top left) compared to a reconstruction of multiphoton-excited (MPE) fluorescence data acquired during fabrication of each

plane (B, top right). The BSA solution was spiked with BSA-FITC, and the MPE fluorescence emitted during fabrication of each plane was acquired using a CCD. The 3D reconstruction of the MPE fluorescence data was created using plane spacings defined by the distance of z steps (0.3 µm) used in fabrication. For the top view comparison (B, lower panels), a finished BSA-FITC structure was imaged using MPE fluorescence, and 6 consecutive x,y optical sections (acquired near the top of a protea replicate; sections spaced by 1 µm) were used to create an average-intensity projection (right). The resultant image can be compared to a maximum-intensity projection of the mask images (left) and show high fidelity replication for hydrated microstructures.

Some degree of distortion of microstructures was evident and could be partially attributed to the settling of minimally supported features that occurred during the preparation and dehydration process necessary for electron microscopy. Further, the MPE fabrication voxel has the shape of a prolate spheroid centered at the focus of the laser beam [25]. This voxel, which is elongated along the optical (z) axis, resulted in less resolution for fabricated structures in this dimension as compared to the x,y plane. Analysis of electron micrographs indicates that minimum feature sizes in the z axis are 3- to 4-fold larger than those in the x,y plane (~0.5 µm), which becomes apparent when fabrication is performed near the resolution limits of the optical system. It should be feasible to correct for this distortion by setting the minimum z-step distance to match the z-axis resolution and enlarging the horizontal planes (input masks) by a factor equivalent to the z-axis resolution. Unfortunately, this would significantly increase the overall size of microstructures (and decrease the minimum feature sizes).
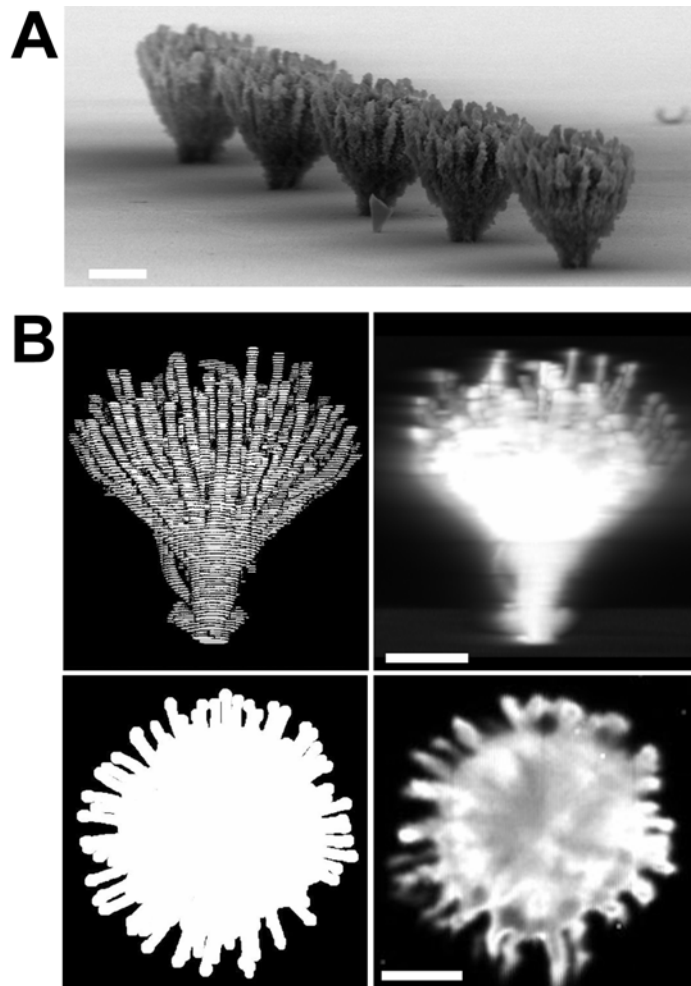
Figure 3.14: MPE fluorescence of *Leucospermum tottum* (pincushion protea) microreplicas. (A) SEM of a row of BSA protea microreplicas. (B) Predicted (left) and actual fluorescence images (right) of a protein protea acquired during fabrication (side view) and post-fabrication (top view). Scale bars, 10 μm.

In many instances, it could be useful to extend such microengineered materials over lateral dimensions larger than a single-scan plane. To achieve such capabilities automated procedures for coordinating x,y stage movements with sequential presentation of DMD masks were developed, enabling multiple horizontal scan planes to be 'quilted'

into larger integrated patterns. Using current scanning approaches, it may be feasible to fabricate materials over millimeter dimensions on a time-scale of tens of minutes.

Simple DMD mask sequences were designed for constructing complex 3D protein topographies. Braided filaments, for example, are microstructural motifs of particular relevance to a number of tissue engineering applications [26, 27]. To fabricate a triple braid, a DMD animation was created that displayed three circles translating through interwoven 'figure 8' patterns; by coordinating the mask sequence with precise steps of the focal plane along the optical axis, a protein microbraid was rapidly produced (Figure 3.15. In contrast to the significant computational encoding that would be needed to fabricate such structures using other direct-write procedures, with DMD-directed masking it is straightforward to modify or iterate rapidly basic parameters (e.g., size, shape, and overlap of geometric components), providing a facile approach for micro-material prototyping.
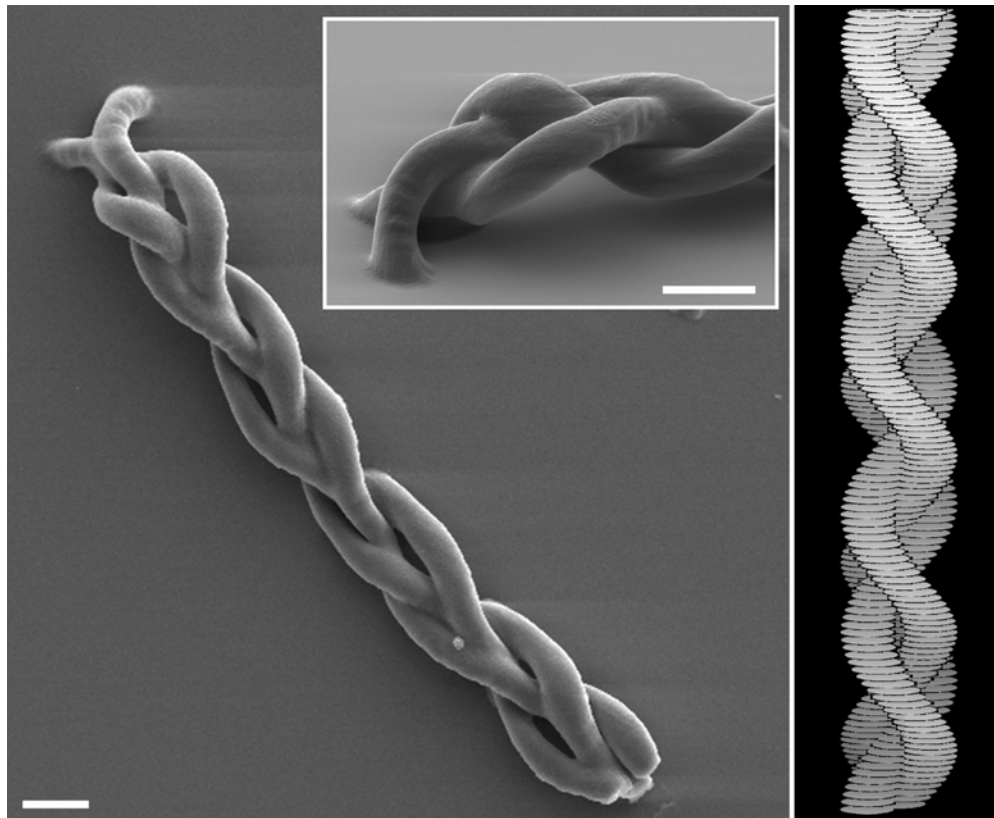
Figure 3.15: Using a mask animation to create a 3D object. (left panel and inset) A BSA microbraid fabricated using 150 sequential panes, each spaced by 1 μm. The mask data for each pane was an animation of three circles moving in interlocked 'figure 8' patterns. (right panel) Predicted 3D reconstruction based on mask images. Scale bars, 10 μm.

3.4 CONCLUSION

The capabilities of mask-directed multiphoton lithography are demonstrated for 3D rapid prototyping of complex microstructures and microgradients. These strategies could eliminate the minimum barrier height issue for neuronal guidance (discussed in Chapter 2) by allowing the facile fabrication of 'closed' guidance channels (i.e., channels

with sealed tops) with desired dimensions. Sealed microchambers may also be useful for the high resolution study of microorganism behavior — a topic discussed in Chapter 5.

Further, DMD-directed multiphoton lithography enables the fabrication of highly customized cellular microstructures. Image stacks encoding 3D cellular topography (using confocal, multiphoton or 3D deconvolution microscopy) could be used to direct the replication of the encoded cell using sequential negative masks or to fabricate a 3D 'mold' of the cell using positive masks. This should readily facilitate construction of highly resolved cellular microenvironments for directed cell guidance and development in 3D cultures.

Finally, this technology provides 3D tissue construct fabrication with micrometer resolution, and via extended scanning and patching, may provide a means to bridge the gap to conventional techniques used to create tissue implants/prostheses on longer (millimeter to centimeter) length scales. Production of complex tissue models, such as highly arborized networks (e.g., as found in bronchial and renal tissue) could potentially be accomplished using relevant biological polymers, allowing an unprecedented degree of flexibility and accuracy in the *ex vivo* study of biological processes.

3.5 REFERENCES

[1]   J. A. Lewis, "Direct ink writing of 3D functional materials," *Advanced Functional Materials*, vol. 16, pp. 2193-2204, 2006.

[2]   Y. N. Xia and G. M. Whitesides, "Soft lithography," *Angewandte Chemie-International Edition*, vol. 37, pp. 551-575, 1998.

[3]   D. G. Bucknall and Institute of Materials Minerals and Mining., *Nanolithography and patterning techniques in microelectonics*. Cambridge: CRC Press, 2005.

[4]   G. M. Whitesides, "The origins and the future of microfluidics," *Nature*, vol. 442, pp. 368-373, 2006.

[5]   H. B. Sun and S. Kawata, "Two-photon photopolymerization and 3D lithographic microfabrication," *Nmr - 3d Analysis - Photopolymerization*, vol. 170, pp. 169-273, 2004.

[6]   B. Kaehr, N. Ertas, R. Nielson, R. Allen, R. T. Hill, M. Plenert, and J. B. Shear, "Direct-write fabrication of functional protein matrixes using a low-cost Q-switched laser," *Anal Chem*, vol. 78, pp. 3198-202, 2006.

[7]   P. F. Van Kessel, L. J. Hornbeck, R. E. Meier, and M. R. Douglass, "MEMS-based projection display," *Proceedings of the Ieee*, vol. 86, pp. 1687-1704, 1998.

[8]   M. S. Hahn, J. S. Miller, and J. L. West, "Laser scanning lithography for surface micropatterning on hydrogels," *Advanced Materials*, vol. 17, pp. 2939-+, 2005.

[9]   J. C. Love, D. B. Wolfe, H. O. Jacobs, and G. M. Whitesides, "Microscope projection photolithography for rapid prototyping of masters with micron-scale features for use in soft lithography," *Langmuir*, vol. 17, pp. 6005-6012, 2001.

[10]   J. El-Ali, P. K. Sorger, and K. F. Jensen, "Cells on chips," *Nature*, vol. 442, pp. 403-11, 2006.

[11]   H. J. Levinson, *Principles of lithography*, 2nd ed. Bellingham, WA: SPIE Press, 2005.

[12]   M. C. Cushing and K. S. Anseth, "Hydrogel cell cultures," *Science*, vol. 316, pp. 1133-1134, 2007.

[13]   B. Alberts, *Essential cell biology*, 2nd ed. New York, NY: Garland Science Pub., 2004.

[14]   E. R. Kandel, J. H. Schwartz, and T. M. Jessell, *Principles of neural science*, 4th ed. New York: McGraw-Hill Health Professions Division, 2000.

[15]   J. Q. Zheng, M. Felder, J. A. Connor, and M. M. Poo, "Turning of Nerve Growth Cones Induced by Neurotransmitters," *Nature*, vol. 368, pp. 140-144, 1994.

[16]   N. L. Jeon, S. K. W. Dertinger, D. T. Chiu, I. S. Choi, A. D. Stroock, and G. M. Whitesides, "Generation of solution and surface gradients using microfluidic systems," *Langmuir*, vol. 16, pp. 8311-8316, 2000.

[17]   R. Allen, R. Nielson, D. D. Wise, and J. B. Shear, "Catalytic three-dimensional protein architectures," *Anal Chem*, vol. 77, pp. 5089-95, 2005.

[18]   R. T. Hill and J. B. Shear, "Enzyme-nanoparticle functionalization of three-dimensional protein scaffolds," *Anal Chem*, vol. 78, pp. 7022-6, 2006.

[19]   S. K. W. Dertinger, X. Y. Jiang, Z. Y. Li, V. N. Murthy, and G. M. Whitesides, "Gradients of substrate-bound laminin orient axonal specification of neurons," *Proceedings of the National Academy of Sciences of the United States of America*, vol. 99, pp. 12542-12547, 2002.

[20]   X. Y. Jiang, Q. B. Xu, S. K. W. Dertinger, A. D. Stroock, T. M. Fu, and G. M. Whitesides, "A general method for patterning gradients of biomolecules on surfaces using microfluidic networks," *Analytical Chemistry*, vol. 77, pp. 2338-2347, 2005.

[21]   N. Zaari, P. Rajagopalan, S. K. Kim, A. J. Engler, and J. Y. Wong, "Photopolymerization in microfluidic gradient generators: Microscale control of substrate compliance to manipulate cell response," *Advanced Materials (Weinheim, Germany)*, vol. 16, pp. 2133-2137, 2004.

[22]   A. Bertsch, J. Y. Jezequel, and J. C. Andre, "Study of the spatial resolution of a new 3D microfabrication process: the microstereophotolithog. using a dynamic mask-generator technique," *Journal of Photochemistry and Photobiology, A: Chemistry*, vol. 107, pp. 275-281, 1997.

[23]   C. Sun, N. Fang, D. M. Wu, and X. Zhang, "Projection micro-stereolithography using digital micromirror dynamic mask," *Sensors and Actuators, A: Physical*, vol. A121, pp. 113-120, 2005.

[24]   Y. Lu, G. Mapili, G. Suhali, S. Chen, and K. Roy, "A digital micro-mirror device-based system for the microfabrication of complex, spatially patterned tissue engineering scaffolds," *Journal of Biomedical Materials Research, Part A*, vol. 77A, pp. 396-405, 2006.

[25]   H. B. Sun, T. Tanaka, and S. Kawata, "Three-dimensional focal spots related to two-photon excitation," *Applied Physics Letters*, vol. 80, pp. 3673-3675, 2002.

[26]   J. W. Freeman, M. D. Woods, and C. T. Laurencin, "Tissue engineering of the anterior cruciate ligament using a braid-twist scaffold design," *J Biomech*, vol. 40, pp. 2029-36, 2007.

[27]   H. H. Lu, J. A. Cooper, Jr., S. Manuel, J. W. Freeman, M. A. Attawia, F. K. Ko, and C. T. Laurencin, "Anterior cruciate ligament regeneration using braided biodegradable scaffolds: in vitro optimization studies," *Biomaterials*, vol. 26, pp. 4805-16, 2005.

Chapter 4: Stimuli-Responsive Behavior of Protein Matrices

To characterize the chemical functionality or ligand binding properties of MPE photocrosslinked microstructures, matrices comprised of different proteins (e.g., 'experimental' and 'control' structures) were routinely interrogated side by side. During one such experiment, matrices comprised of BSA and avidin were rinsed with a chemical solution (containing phosphoserine) that dropped the solution pH from 7 to ~5. Avidin matrices were observed to swell rapidly (within seconds) while matrices comprised of BSA experienced little volume change. This surprising result provided the impetus to begin to study the hydrogel or 'stimuli-responsive' properties of protein matrices. Combined with the microfabrication techniques described thus far, this further provided a foundation to begin to develop unique, responsive materials for 3D micromechanical actuation.

4.1 INTRODUCTION

The past 20 years has seen an enormous increase in the interest and design of stimuli-responsive materials. Materials deemed 'intelligent' or 'smart' polymers/hydrogels, shape-memory or self-folding materials can exhibit abrupt physical or chemical changes (e.g., volume, shape, activity) following an environmental cue [1, 2]. Materials responsive to temperature [3], pH [4], ionic strength [5], light [6], and electric fields [7] have been developed with potential applications ranging from targeted delivery, artificial tissues, sensors, actuators, and valves.

Hydrogels are a class of stimuli-responsive polymers with hydration properties and elasticity similar to biological tissues [8]. Gels can be functionalized with chemistries that mimic, for instance, the extracellular matrix. Thus, use of these materials as scaffolding for cell cultures has been heavily explored [9-11]. Further, hydrogels can be

engineered to cycle between swollen and condensed states through interaction with the physical or chemical environment. One of the most studied responsive hydrogels, the temperature sensitive poly(N-isopropylacrylamide) (PNIPAm) undergoes a sharp transition between hydrophilic (swollen polymer) and hydrophobic states (contracted polymer) at 32°C [3]. This 'smart' behavior results from the thermodynamic competition between the enthalpic contribution of water, hydrogen bonded to isopropyl moieties, versus the entropic gain of releasing water to bulk solution (Figure 4.1) and thus dehydrating the polymer at temperatures > 32°C. The sharp phase transition of PNIPAm and its derivatives have been exploited for a variety of unique and interesting applications including nanoscale delivery devices [12] and adaptable microlenses [13].
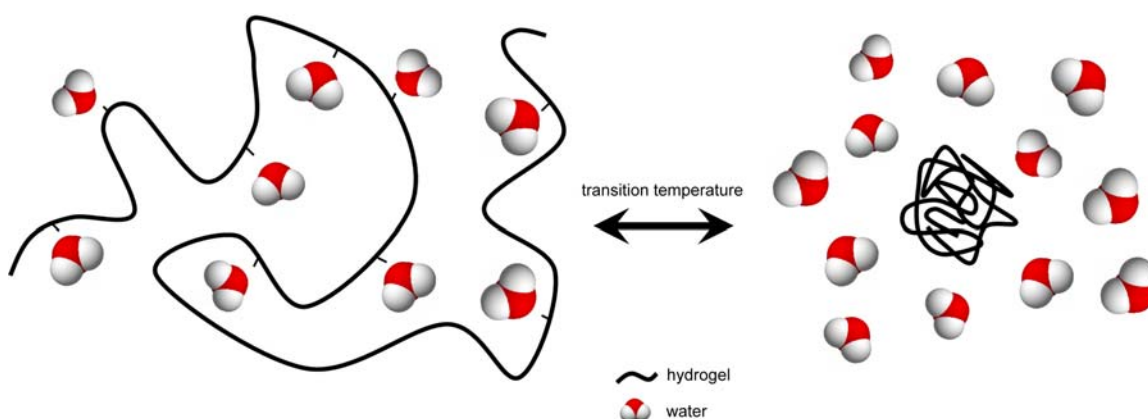
Figure 4.1: Schematic of a temperature sensitive hydrogel.

Hydrogels that respond to pH contain weak acid or base pendant groups and thus pH-mediated responses are largely driven by electrostatic interactions between polymer chains [2]. pH and temperature sensitive hydrogels have been extensively characterized as components in controlled release devices for theraputics with current research directed

at providing precise targeting or 'molecular imprinting' of material responsiveness [14]. Accordingly, responsive hydrogels are increasingly coupled to molecular recognition components, allowing the intended response to occur only in the presence of a target molecule. One approach to accomplish this goal has been to develop hybrid gels that contain, for instance, functional proteins that modulate gel behavior via ligand binding [15, 16].

Peptides and proteins naturally contain ionizable and hydrogen bonding moieties; the interactions of which define the structure, hydration, and function of the protein. Perturbation of these interactions by changes in solvent temperature or pH can result in deformation or unfolding of the native structure [17, 18]. Additionally these interactions can be engineered to provide alternative stability and function [19]. In essence, a protein molecule in solution behaves much like a responsive polymer in that both its confirmation and hydration are directly coupled to the surrounding milieu.

Further, many proteins undergo large structural changes upon ligand binding. As an example, calmodulin (CaM), a ubiquitous calcium binding protein, exists in distinct and drastically different structural states depending on the presence or absence of bound ligands. This property has made CaM an attractive molecule for incorporation in hydrogels, and has been used to generate ligand-induced swelling responses [15, 16].

Self-actuating materials that do not require external power sources hold obvious advantages as mechanical components for microscale platforms such as microfluidic devices. Though microfluidic chips may one day come to revolutionize chemical analysis and perhaps even synthesis, the technology has yet to fully emerge out from the academic research laboratory. This is in part because current operation of microfluidic chips

requires addressment by external, specialized equipment (e.g., external pumping and gating mechanisms, high resolution optics) — hindering the dissemination of the technology into, for instance, a (remote or field) clinical setting. Stimuli-responsive materials such as hydrogels could potentially fulfill both capacities, as both micromechanical and analysis components, enabling a microfluidic chip to be all inclusive [4]. The possibility for exploiting hydrogels in microscale devices has fueled interest in developing microfabrication strategies that offer true 3D control over hydrogel topography.

This chapter examines the stimuli-responsive properties of protein matrices. Hydrogel swelling properties of matrices composed of a number of proteins and protein mixtures are investigated under a range of environmental conditions. The mechanical properties of protein matrices for prescribed 3D microactuation and microparticle translocation using material gradients are evaluated.

4.2 EXPERIMENTAL METHODS

4.2.1 Materials, hydrogel fabrication and characterization

Bovine serum albumin (BAH64-0100) was supplied by Equitech-Bio (Kerrville, TX). Avidin (A-887) was supplied by Molecular Probes (Eugene, OR). Lysozyme (L6876), methylene blue (M-4159), and flavin adenine dinucleotide (F-6625) were supplied by Sigma-Aldrich (St. Louis, MO). PMMA microparticles (19130) were supplied by Polysciences.

Hydrogels composed of photo-crosslinked protein were fabricated onto untreated #1 microscope cover glass using the output of a mode-locked titanium:sapphire (Ti:S) laser (Tsunami; Spectra Physics) operating at 730 to 740 nm. Translation of the focal

point through a solution of concentrated protein was performed using a scanning stage (prior) as well as a confocal scanner (BioRad MRC600). Structures could be further defined using transparency based photomasks or DMD masking a technique described in Chapter 3. The laser output was adjusted to approximately fill the back aperture of an oil-immersion objective (Zeiss 100x Fluar, 1.3 numerical aperture) situated on a Zeiss Axiovert inverted microscope system. Desired powers were obtained by attenuating the laser beam using a half-wave plate/polarizing beam splitter pair. To extend structures along the z dimension (i.e., along the optical axis), the position of the laser focus was translated manually within fabrication solutions using the microscope fine focus adjustment.

Microstructures composed of photo-cross-linked protein were fabricated from solutions containing protein at $320 - 400$ mg mL^{-1} unless otherwise specified and either $1.2 - 3$ mM methylene blue or 5 mM FAD as a photosensitizer. At protein concentrations $\sim 40\%$, swelling was generally noticable after rinsing away the fabrication solution with neutral buffer. Equilibrium swelling data depicted in Figure 4.4B was acquired by 3 minute exposure of microstructures in phosphate (0.5 mM) buffered solutions of pH 2.02, 2.63, 3.26, 3.78, 4.48, 5.17, 5.76, 6.30, 7.00, 7.66, 8.19, 8.90, 9.41, 10.06, 10.73, 11.33 and 12.00. Measurement (unless otherwise noted) of rectangular areas (A) were obtained ~ 3 μm above the surface and all equilibrium swelling ratios were calculated by the ratio A/A° where $A^{\circ} =$ area before treatment.

Unless otherwise noted, microstructures were imaged and analyzed using DIC, fluorescence, and scanning electron microscopy methods previously discussed in detail in Chapters 2 and 3.

4.3 RESULTS

4.3.1 Photocrosslinked protein matrices as responsive polymers

As shown in Chapters 2 and 3, multiphoton fabricated matrices can retain similar ligand-binding and catalytic functionality of their component proteins, implying that native electrostatic and hydrophobic interactions governing stable protein conformation remain significantly intact within microstructures. As 'monomers' crosslinked into a polymeric microstructure, native protein confirmation would be vulnerable to environmental changes — particularly those known to perturb native structure such as pH extremes (e.g., < 2 and > 12), providing a swelling mechanism by altering hydrogen bonding networks and salt bridges to ultimately increase the solvent space within the microstructure matrix (Figure 5.2).
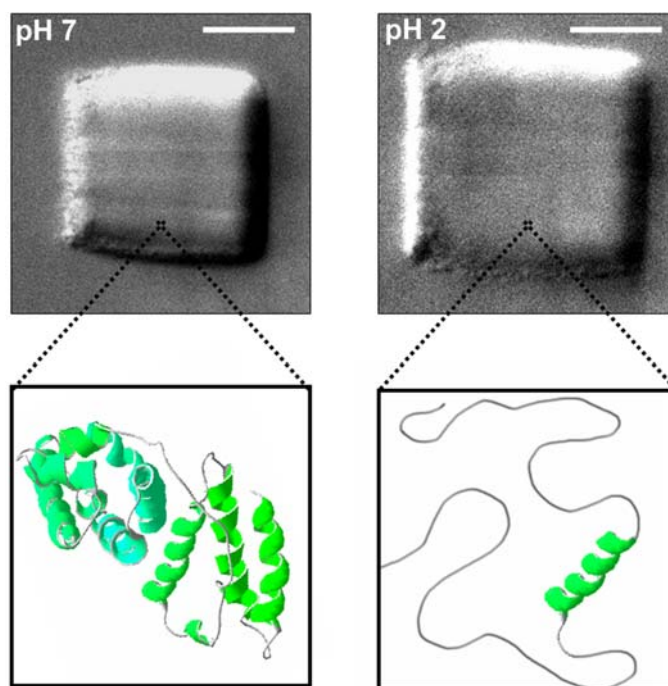
Figure 4.2:   Photocrosslinked protein matrices as responsive hydrogels. Top panels show a BSA protein matrix at neutral and acidic pH. Exposure to acidic pH likely involves some degree of unfolding of matrix incorporated proteins (lower panels). Scale bars, 10 μm.

This program of research began following the qualitative observation that when exposed to acidic conditions, microstructures composed of avidin and BSA swell differentially. The ability to direct-write potentially 'smart materials' with high 3D resolution provided the motivation to further examine and explore protein matrix responsivity. For instance, using a mask-directed (MDML) approach as outlined in Chapter 3, complex microstructures such as 'microhands' could be readily fabricated in positions to allow prescribed interactions upon swelling (Figure 4.3). Other microfabrication methods have been explored to create hydrogels with micro- to nano-scale resolution [20, 21] but lack the free-form 3D capabilities of multiphoton lithography. A two-photon fabricated hydrogel responsive to UV illumination has been

reported [22] but the response to light was not reversible and the researchers did not take advantage of the sub-micron resolution capabilities of multiphoton lithography.
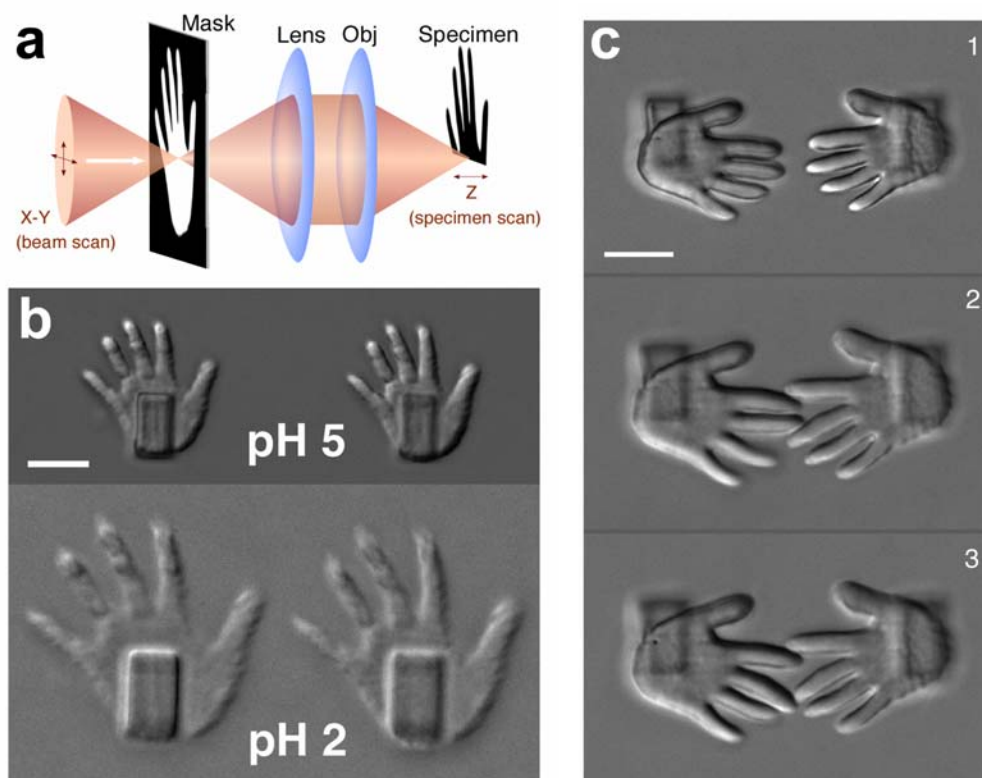
Figure 4.3: Hydrogels of arbitrary 3D geometries can be created using MDML (Chapter 3) in which a negative photomask placed in a conjugate focal plane directs the fabrication of the positive microstructure (a, for simplification the orientation of the mask and specimen are the same). BSA microhands resting atop ~ 3 micron tall BSA pillars (b, top panel) swell following a decrease in bath pH (b, bottom panel) — a process that is reversible. Direct-write fabrication of hydrogel matrices enables structures to be positioned arbitrarily (c, panel 1) allowing precise interactions between swelled states (c, panels 2 and 3; variable interdigitation is achieved by cycling between pH 5 and pH 3). Scale bars, 10 μm.

The vast range of proteins that potentially can be used to fabricate microstructures provides a naturally diverse set of building blocks for engineering hydrogel responsivity. To characterize differences in swelling behaviors of protein hydrogels, test structures (vertical arches, 3D rectangular matrices; Figure 4.4a) comprised of BSA, avidin, and lysozyme were fabricated. Swelling measurements of highly reproducible rectangular structures were used to determine pH dependent swelling profiles of the three proteins. Hydrogels comprised of these proteins exhibited distinct equilibrium swelling profiles (transition pH values, swelling ratios) over a broad pH range (Figure 4.4b). In each case, hydrogels reached a minimum size at pH values similar to isoelectric points of the component proteins ($pI_{avidin} \approx$ 10-10.5; $pI_{BSA} \approx$ 4.7-4.9; $pI_{lysozyme} \approx$ 11-11.3), a finding consistent with the pH-dependence of protein solubility and hydration [17,18]. Further, the swelling data indicated pH ranges in which microstructures fabricated from, for instance, BSA and avidin would actuate both independently and in concert. The arch structures shown in Figure 4.4b were fabricated stepwise from solutions of avidin followed by BSA and then subjected to directed flow of abrupt pH changes. From pH 7 $\rightarrow$ 5 and 7 $\rightarrow$ 10, arches swell and subsequently bend independently toward the direction of flow. At pH 2, both BSA and avidin arches bend in unison. These results demonstrate the unique possibilities for autonomous response using pure protein matrices with distinct swelling profiles. Independent actuation of hydrogel response has been demonstrated using 2D hydrogels composed of acrylate-based materials polymerized in microchannels [4]. Nevertheless, the results demonstrated here using aqueous-based and potentially biocompatible chemistries with strict control over 3D microarchitecture should enable a wider range of materials and applications to be explored where microscale actuation is desired.
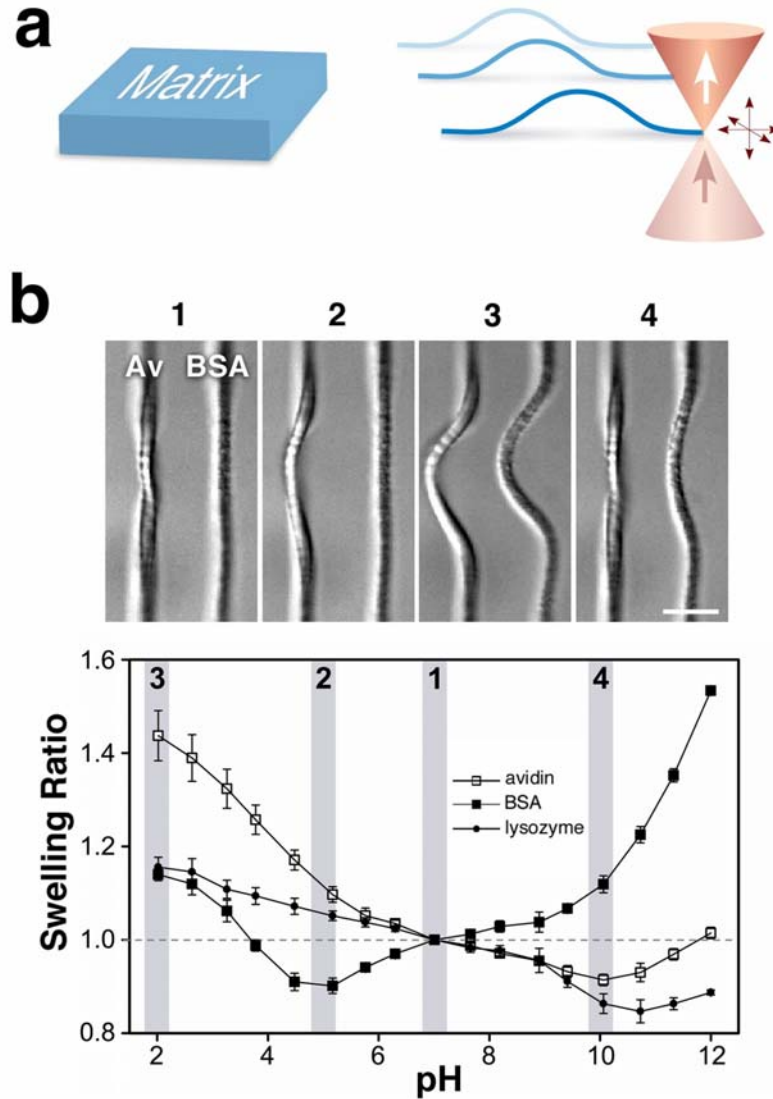
Figure 4.4: pH dependent hydrogel behavior depends on the identity of protein incorporated into the matrix. (a) Test structures (3D rectangular matrices and arches) were fabricated from solutions of avidin, BSA and lysozyme (b, scale bar, 5 µm). Protein arches comprised of avidin and BSA were subjected to directed flow (0.13 ml/sec from right to left) of abrupt pH steps (numbers correspond to the pH values for the plot in b) and could be actuated individually (panels 2, 4) or in concert (panel 3) depending on the pH (see supplemental movie). Equilibrium swelling of rectangular matrices composed of avidin, BSA and lysozyme show distinct swelling profiles. Minimum sizes were observed at or near the isoelectric point of the incorporated protein. Error represents the standard deviation (n = 4 structures).

94

The equilibrium swelling profiles shown in Figure 4.4 predict that matrices fabricated from a combination of proteins should exhibit a pH response that is intermediate to that of 'pure' matrices. This is demonstrated in Figure 4.5. By fabricating matrices from a combination of BSA and lysozyme, microstructures could be tuned to expand or contract to varying degrees upon stepping solution pH from 7 to 11.9. These combined results (Figures 4.4b, 4.5) imply that a broad range of hydrogel swelling profiles should be possible simply through judicious selection of protein building blocks. Moreover, by engineering proteins that, for example, unfold under milder conditions as has been demonstrated using engineered avidin [19], even greater versatility should be possible.
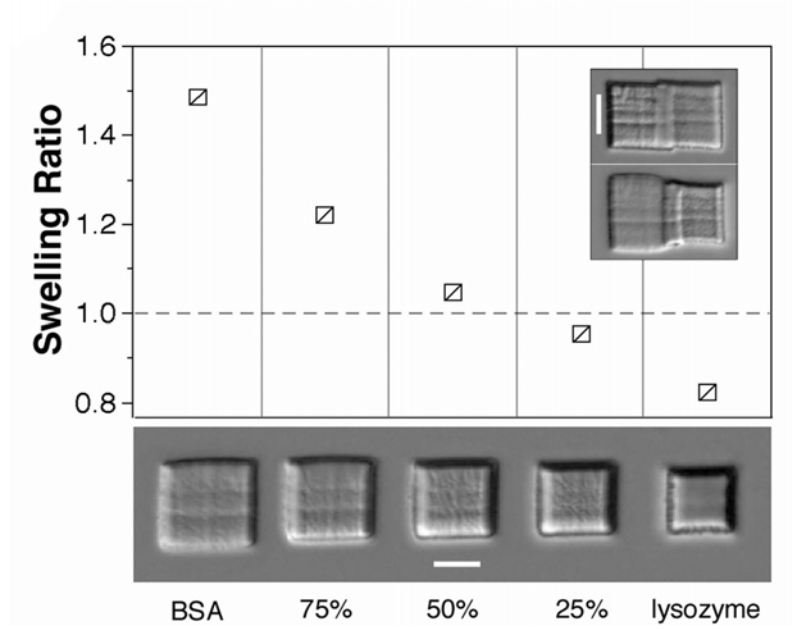
Figure 4.5: Structures fabricated from a mixture of BSA and lysozyme (percentages represent wt BSA/wt total protein content) show intermediate swelling at pH 11.9 compared to 'pure' BSA and lysozyme structures. The inset shows conjoined matrices (BSA, left; lysozyme, right) at pH 7 (top panel) and pH 11.9 (bottom panel). Scale bars, 10 µm.

Hydrogels that respond to pH are inherently sensitive to changes in ionic strength [23]. During experiments to establish pH dependent equilibrium swelling profiles, matrices, especially in a swollen state, were observed to be highly sensitive to fluctuations in ionic strength. To begin to quantify ionic strength sensitivity, the effects of non-chaotropic salts (those that do not act directly upon proteins), NaCl, Na_2SO_4 and Na_2PO_4 on swollen BSA microstructures was investigated (Figure 4.6). Under basic conditions (pH 11.9, NaOH), introduction of high concentrations of these salts (> 0.5 M) resulted in microstructure collapse. In acidic solutions (pH 2.2 HCl), contraction occurred at much lower concentrations. Sulfate was particularly effective at contracting swollen microstructures at relatively low concentrations (~1 – 50 mM), a result in agreement with the efficient "salting out" activity of sulfate on BSA dissolved in low pH solutions [24]. Proteins can precipitate out of solution with an increase in ionic strength (i.e., 'salt out'), an effect often used for protein purification. Generally, salting out is most effective at a pH near the isoelectric point of the protein as this is where the entropic gain resulting from dehydrating hydrophobic regions on proteins is greatest. At pH < 3, serum albumin is essentially fully uncoiled under the limits of disulfide bonds and thus further hydrophobic surfaces involved in tertiary structure stability are exposed to solvent [25]. Avidin structures showed similar acid-swelled contraction behavior following addition of Na_2PO_4 and Na_2SO_4, but these effects were not quantified as extensively as for BSA matrices. Further, BSA is one of the most ubiquitous (and inexpensive) proteins in the biochemical laboratory and was therefore adopted as the primary matrix component for many initial studies to design structures for micromechanical manipulations.

96
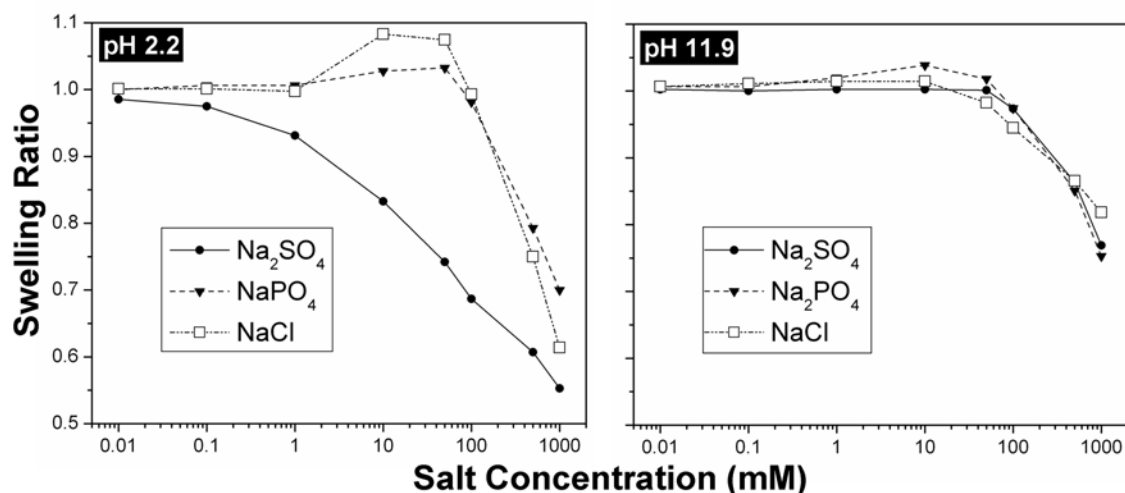
Figure 4.6:   Protein microstructure equilibrium response to ionic strength. BSA rectangular microstructures were swelled in either acidic (pH 2.2 HCl) or basic (pH 11.9, NaOH) conditions and swelling ratios ($A/A^°$ where $A^°$ = area before introduction of salts) were determined for a number of salts. Under acid conditions, significant contraction of microstructures was observed at low concentrations of Na_2SO_4 compared to $NaPO_4$ and NaCl.

The effects of matrix exposure to the denaturants urea and guanidium hydrochloride (GuHCl) were also investigated using avidin and BSA matrices. Introduction of these reagents led to noticeable swelling (5 – 50 % increase in area measurements of rectangular matrices) beginning at ~100 mM and independent of pH. This further suggests that swelling likely involves some degree of denaturation of matrix incorporated proteins. Matrices, could tolerate extended periods of incubation in denaturant concentrations as high as 10 M urea for > 48 hours though usually some degradation was observed following removal of denaturants. Interestingly, denaturant induced swelling of avidin microstructures appeared to attenuate in the presence of biotin — a result discussed in the following section.

The ability to modulate the swelling response of a hydrogel with ligand interactions is an exciting area of research in hydrogel design and synthesis. Gels have been synthesized that incorporate (usually covalently) antibodies [26], lectins [27], and the calcium binding protein calmodulin (CaM) [15, 16] into polymeric networks, providing polymer swelling responses mediated by ligand binding events. Though triggered by ligand binding, the swelling mechanism of these materials is generated primarily through changes in crosslinking density of the polymer network (though there are some recent exceptions; [16]). CaM is a particularly attractive candidate for matrix incorporation as contraction of the 'extended', calcium bound confirmation brings the separation distance between the ends of the molecule from ~50 Å to 15 Å upon ligand binding (such as the drug trifluoperazine) [28, 29]. This is just one example of the more than 200 characterized protein motions [30]. Ligand-induced actuation would greatly extend the utility of 3D protein matrices — potentially obviating the need for harsh conditions to generate responses (e.g., pH extremes) and would provide greater flexibility for cell culture and sensing applications. Though conditions to incorporate CaM into photocrosslinked protein matrices have not (currently) been determined, ligand-induced hydrogel response was assessed using the avidin-biotin system.

The avidin-biotin complex is exceptionally stable with a dissociation constant (K_d) of ~10^{-15} M. Furthermore, the denaturation temperature of avidin increases from 84°C, in the free state, to 117°C in the biotin-bound state [31]. Avidin is a tetrameric protein consisting of four interlocking β-barrels and has been engineered to be monomeric by substitution of tryptophan residues important for subunit stabilization. In this work, addition of biotin to monomeric avidin at pH values close to 7 resulted in tetramerization. As stated, microstructure swelling at pH extremes likely involves

denaturation. In the case of avidin, unfolding is preceded by subunit dissociation — a condition met only beyond pH < 2 or > 3 M GuHCl [32]. Thus, a microstructure comprised of avidin, swollen in conditions in which subunit dissociation/unfolding occurred (e.g., acid or denaturants), was hypothesized to contract with the addition of biotin. Unfortunately, biotin-induced contraction under acid-swelled conditions proved difficult to distinguish from ionic-strength contraction (in part due to the low solubility of biotin in acid solutions). However, when avidin microstructures were first rinsed with biotin, swelling was greatly attenuated following exposure to denaturants when compared to structures not exposed to biotin (Figure 4.7). This result indicates that ligand-induced responses of avidin matrices by biotin should be feasible, although the extreme sensitivity of protein matrices to non-specific ionic changes must be controlled.
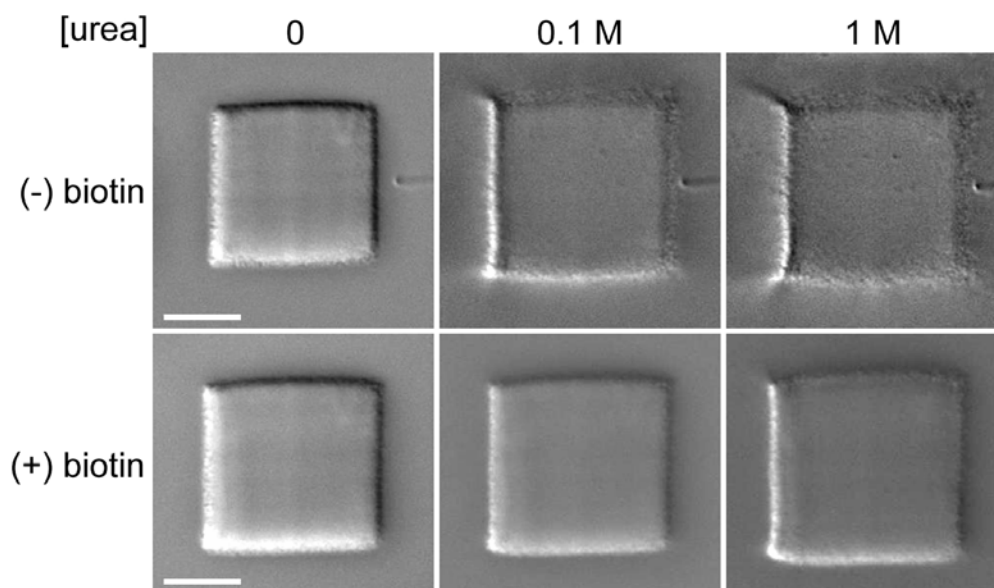
Figure 4.7:   Biotin binding to avidin microstructures attenuates swelling response in the presence of urea. Matrices composed of crosslinked avidin were treated with biotin (5 μM, 5 min) and then exposed to urea (bottom panels). Structures fabricated under identical conditions but without biotin treatment swelled significantly more (> 65%, top panels) at high concentrations of urea (up to 10 M). The result suggests biotin binding can stabilize microstructures composed of avidin in a manner similar to (biotin-bound) avidin stabilization observed in free solution [32].

4.3.2 Protein Microactuators

The ability to rapidly and precisely manipulate microscale objects has important applications in various fields of applied science and engineering, motivating the development of translocation strategies based on mechanical, fluidic, and optical mechanisms [33-36]. Stimuli-sensitive hydrogels could offer an alternative means to effect precise motions on the microscale, potentially through the action of multiple, independent components functioning in concert and without the need for an external power source. For instance, it is straightforward to fabricate a protein line beginning from the substrate and into contact with a micro-object such as a microsphere to form a tether.

Rex Nielson in our laboratory has used this approach to tether microparticles of various composition (including, latex, PMMA, iron oxide, and glass) with diameters as large as 60 μm and has subjected tethers particles to forces exceeding 500 μN (by directed flow) without dislocation of the particle or substrate/tether interface. Given the hydrogel properties of a protein tether, microparticle translocation strategies using the mechanisms of hydrogel swelling and collapse were explored.

Figure 4.8 shows two experiments in which PMMA microspheres were tethered to a surface by protein cables composed of BSA. Swelling conditions (i.e., pH 3) resulted in translocation of the microparticles which could be returned to their positions following initial fabrication with an increase in bath ionic strength. The kinetics of actuation could be attenuated by decreasing the concentration of the ion, in this case sulfate, introduced into solution (although more precise quantification of this observation was not performed on high aspect ratio tethers shown in Figure 4.8 largely due to the subsequent development of more robust and predictable, gradient tethers).
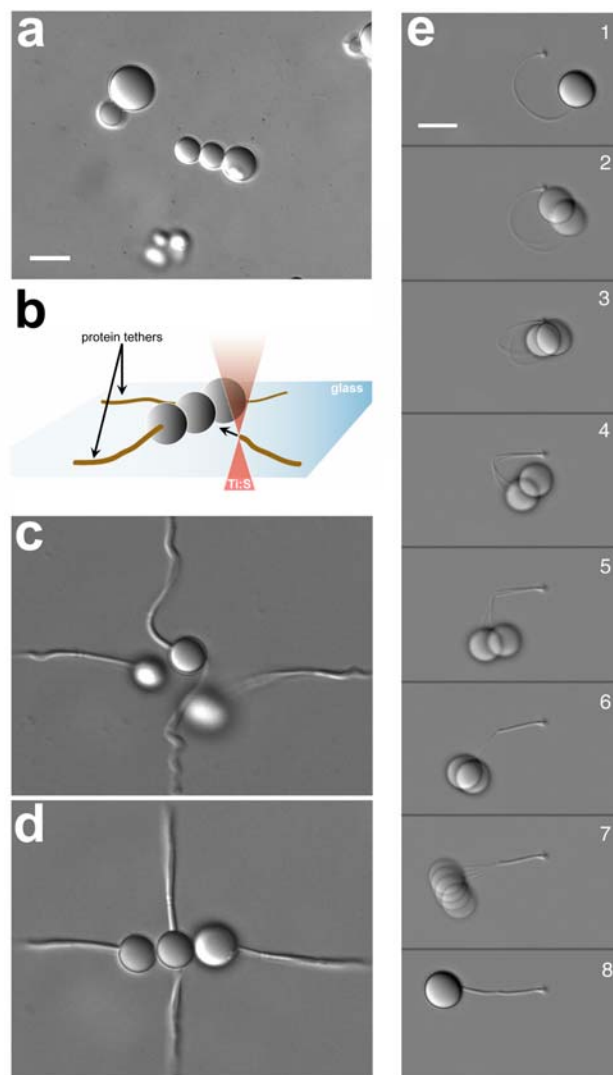
Figure 4.8: Tethering and translocation of microspheres with hydrogel cables. (a) PMMA microspheres in a BSA fabrication solution (a) are tethered to the glass substrate by translating the laser focal point from the glass and into direct contact with the microsphere (b). Changing the solution pH from 7 to 2.2 resulted in 3D dislocation of microspheres (c) which were reoriented to their initial contacts with the addition of Na_2SO_4 (to a final concentration of 1 mM). A single microsphere tethered to the substrate with a BSA cable (e, panel 1) was translocated (e, panels 2-8; total duration of movement, ~3 sec) by addition of Na_2SO_4 (to a final concentration of 0.5 mM), contracting the cable length by ~ 35% and returning the microsphere to the position it occupied immediately after initial fabrication. Scale bars, 10 μm.

Figure 4.8e shows the time-lapse response of a BSA cable contraction resulting in translocation of a microsphere and decreasing the length of the cable by ~ 35%. Interestingly, this motion involved a noticeable bend modulated by the 'joint' or 'kink' near the middle of the cable that produced an 'arm-like' actuation. In this case, the kink was an artifactual result of the mechanical actuators in the motorized scanning stage used to translate the x,y position of the beam focus. However, similar kinks could be produced by shuttering (for ~1 sec) the beam during fabrication under similar conditions (e.g., fabrication solutions and stage scanning speed; 5 μm sec^{-1}). The result suggested that 'programmed' heterogeneities could be effective towards tailoring more precise actuation. Similarly, the degree to which hydrogel microstructures swell was found to depend strongly on the density of the matrix (Figure 4.9) — a property that can be modulated both by protein concentration within the fabrication solution and laser exposure times [37-39]. With these principles in mind, a strategy was developed that enabled greater control of the bending properties of protein rods for use with more precise micromechanical actuation such as microparticle translocation.
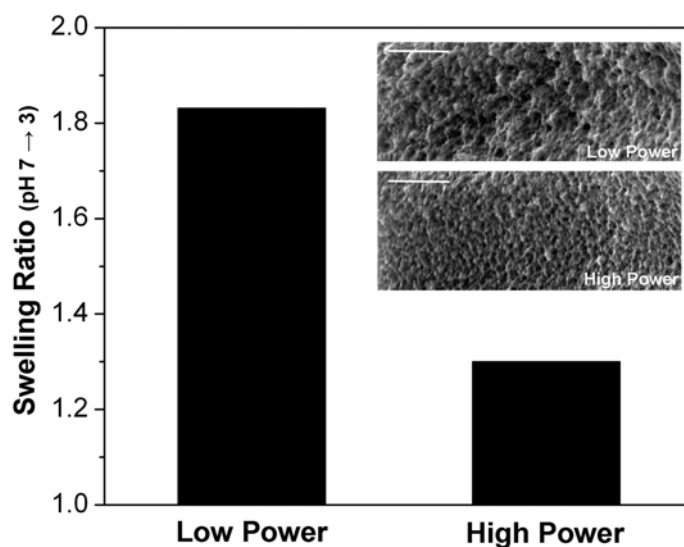
Figure 4.9: Hydrogel responsivity can be modulated by laser exposure. (a) Microstructures fabricated under low laser power (~ 9 mW before the back aperture of the objective) show increased pH-induced equilibrium swelling compared to structures fabricated with high power (~ 27 mW). Scanning electron micrographs (inset; scale bars, 2 μm) reveal differences in matrix porosity between low and high power structures.

Direct-write protein hydrogels offer the possibility for effecting novel 3D microactuation based on spatially defined gradients in matrix properties. By scanning the laser through protein solutions at different speeds, for example, matrices of varying density and thickness (and thus, capacity for expansion/contraction) could be fabricated. Using this design principal, protein rods were engineered to bend in predictable manners. Here, gradients of material across the width of a rod were created by raster scanning the laser focus in a transverse direction as the sample solution was translated longitudinally (i.e., along the rod axis; Figure 4.10). SEM and fluorescence studies of avidin rods were performed to characterize the material gradient. Fluorescence data of avidin gradient rods rinsed with biotin fluorescein showed a ratio of fluorescence signal of between 1.5 – 2.0 (edge/total width). SEMs revealed a gradient in thickness along the edge of a rod

extending ~0.34 – 0.37 μm above the height of the central matrix (measuring ~1.08 – 1.20 μm). Therefore the thickness gradient largely accounts for the ratio of fluorescent signal [considering (edge thickness + central thickness)/central thickness)].
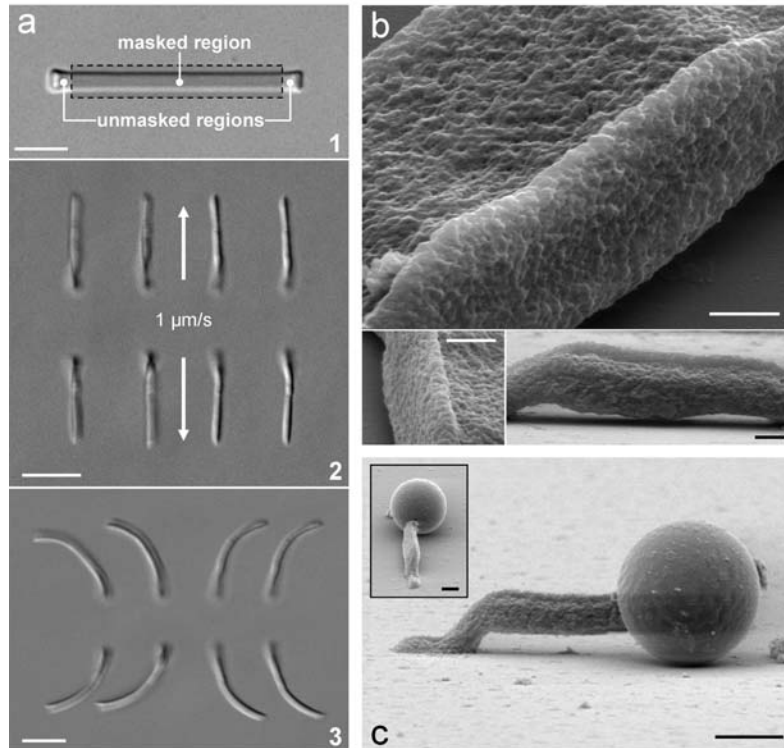
Figure 4.10: Fabrication of protein gradient rods using laser scanning. Laser scanning into concentrated fabrication solution produces a material gradient along structure edges. This "edge effect" is in large part due to longer dwell times at the edges occurring when galvanometer mirrors are driven by raster pattern waveforms. By using an opaque photomask to block out all but the raster scanned edges and translating the raster pattern longitudinally (along the rod axis) rods with predictable bending (when solution was changed pH was changed to allow swelling) were produced. (a, panel 1) A raster scanned microstructure produced using a confocal laser scanner with a horizontal scan frequency of ~500 Hz. 'Unmasked' left and right regions are translated at 1 μm/sec from the substrate into solution to produce tethered rods (panel 2). Panel 3 shows rod bending after pH 2.2 (HCl) rinse. (b) Scanning electron micrographs reveal a thickness gradient along the edge of a rod extending ~0.34 – 0.37 μm above the width (measuring ~1.08 - 1.20 μm) of the rod. (c) SEM of PMMA microparticle tethered to the substrate with a gradient rod. Scale bars for a and c, 3 μm; b, 1 μm.

The extent that rods bent in response to chemical exposure could be modulated by changing the overall matrix porosity, a function of the longitudinal scan speed (Figure 4.11a). By defining the bending capacity of microstructures with high spatial resolution, objects capable of sophisticated movements were constructed to perform complex micromechanical tasks. For example, it was possible to assemble fern-like rods — capable of unfurling themselves in response to chemical triggers — from linear sequences of distinct segments (Figure 4.11b); to create actuatable gates (Figure 4.11c); and to transport microscale objects across extended distances (> 40 μm, data not shown). Control over material gradients with this microscale, 3D resolution should greatly aid in both the prototyping and design of micromechanical actuators based on smart materials.
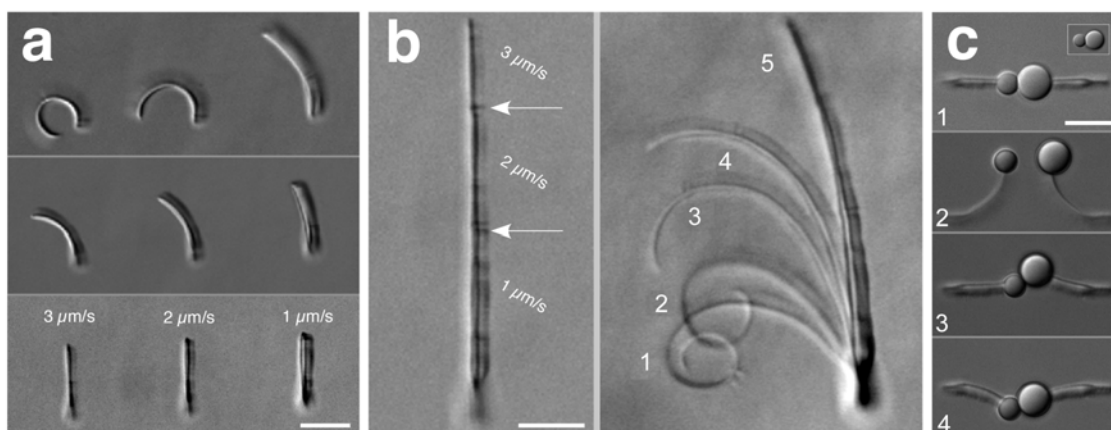
Figure 4.11: Predictable bending using gradient rods. (a) Protein rods incorporating a thickness gradient across the width of the rod were fabricated (40% protein solution wt/vol, pH ~ 7.5) and rinsed (pH 7, middle panel; pH 3, top panel). The degree of curvature varies according to the longitudinal scan speed used during fabrication. These components were incorporated into a single structure (b, left panel) and swelled at pH 3 (HCl). Abrupt change in ionic strength induces contraction of the multi-component rod (b, right panel). Numbers the sequence of positions as the rod unfurls. (c) Gradient rods tether microspheres to form a switchable gate (panel 1) that open at pH 3 (panel 2). Addition of 250 µM Na_2SO_4 causes gate closure (panel 3). Addition of 10 mM Na_2SO_4 further contracts gradient rods, repositioning the microspheres. Scale bars, 10 µm.

There has been much recent interest in understanding the physical mechanisms that lead to wrinkling and buckling of thin sheets of artificial and biological materials [40-42]. Natural structures such as leaves and flowers can adopt complex 3D conformations without apparent genetic programming [40]. It would be of interest to develop similar engineering principles for artificial materials. For instance, Klein *et al*. used a programmable mixer to control concentration gradients of hydrogel monomers across two dimensional disks (~ 1 cm diameter). Following polymerization, disks adopted complex 3D confirmations as a result of the gradient program [42]. The ability to program similar gradients on the microscale could have great utility towards the design of self (un)folding materials for medical implants and micro-delivery devices [43]. Here the

capabilities of DMD-directed multiphoton lithography to program hydrogel material density gradients using image gray-scaling were investigated. As a starting point, horizontal fabrication planes resembling the basic components of leaves and flowers (e.g., stems, petals) were prototyped and subjected to hydrogel swelling conditions.

As demonstrated in Chapter 3, DMD-directed multiphoton lithography enables automated alignment of sequential horizontal fabrication planes to create complex microstructures. Here, DMD generated patterns were employed to prototype horizontal (in plane) and vertical (out of plane) material microgradients composed of BSA matrix that would fold or bend predictably in response to environmental changes in pH and ionic strength. Unfortunately, the binary nature of the DMD system does not allow a simple means to provide continuous light attenuation (grayscale) using a scanning laser approach. In general, ripple patterns were observed resulting from periodic irradiation at the specimen plane due to the intermittent reflection by micromirrors of the scanning beam with each refresh cycle of the projector. Though in theory, this problem should be overcome by increasing either the DMD refresh cycle or the laser scanning speed (parameters that could not be readily adjusted with the current equipment), level power attenuation without noticeable ripple patterning (in comparison to 'all white' mask components) could be achieved using selected mask image colors (Figure 4.12a).

In contrast to gradient rods discussed in Figure 4.10 and 4.11, where the material is defined along the width of the rod from the image perspective, here vertical gradients were fabricated by stacking horizontal fabrication planes of differing material density. Therefore when the BSA planar components in Figure 4.12a (1, 2, 3) are assembled as shown, a cross-section down the center of the structure indicates the predicted bending transition on exposure to pH 2.2 (to a 'bowl' shape). Analysis of structures was attempted without the benefit of readily available 3D imaging. Nevertheless, 3D conformations

could be inferred by coordinating z-step measurements to in focus object features. Figure 4.12b shows the BSA microstructure diagrammed in panel 'a' immediately after post-fabrication (pH ~7.5, protein fabrication solution; left panel) and at pH 2.2. Here, the structure adopts a shallow bowl conformation of ~ 2-3 micron depth (inferred by measuring the distanced from the, in focus, stem 'trunk' to the 'tips'). Interestingly, the horizontal expansion of the circular component (defined by mask #2) appeared constricted by the 'stem' component (defined by mask #3), adopting a 'flower-like' shape. Using this approach, interactions between geometries of unequal matrix densities could be rapidly prototyped and evaluated in contracted and expanded states (Figure 4.12c). The ability to mimic natural biopolymers such as leaf and flower structures on the microscale is an exciting strategy for programming the 3D response of microscale materials for applications such as design of delivery devices that unfold in appropriate environments to release cargo.
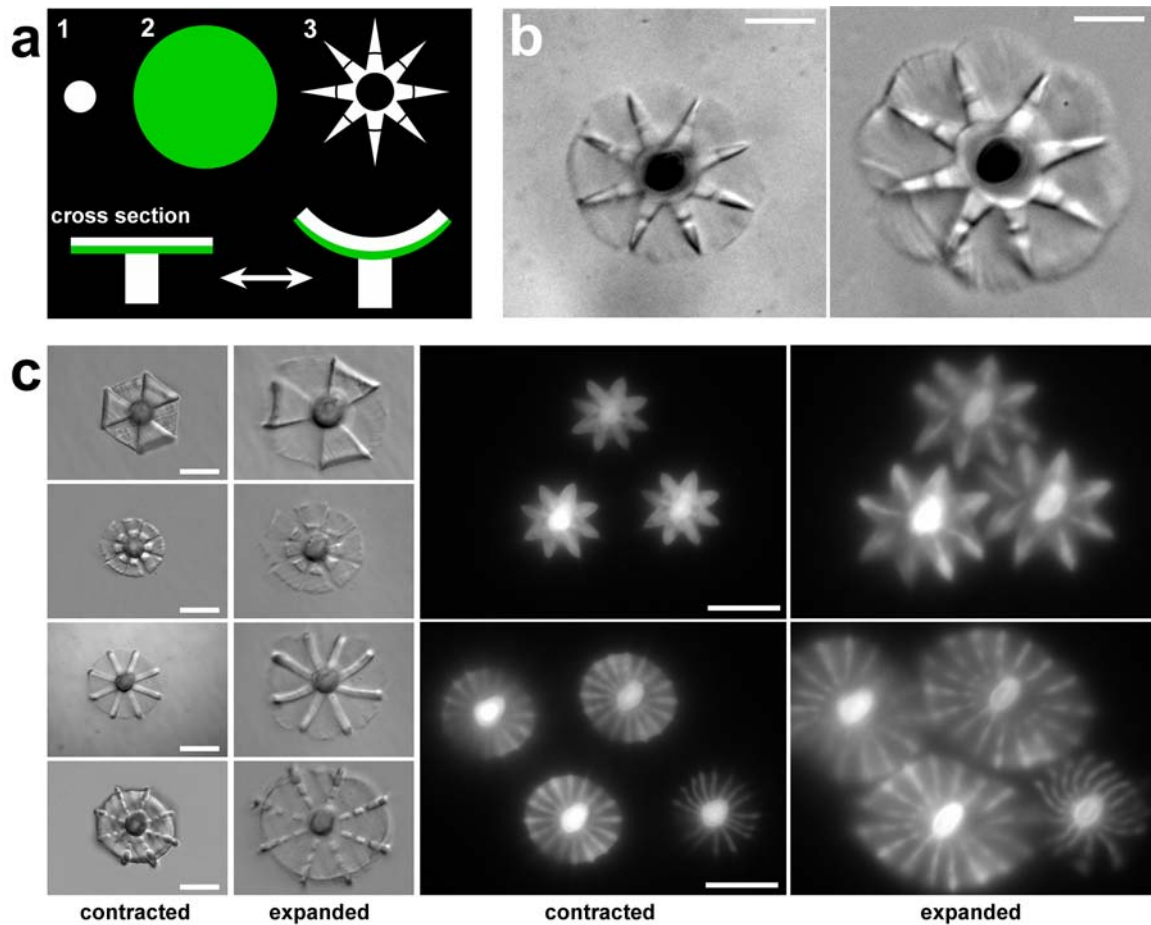
Figure 4.12: Prototyping of density gradients for 3D microactuation using DMD-MDML. (a) DMD 'masks' are used in sequence (1,2,3) while the horizontal laser scanning plane extends from the substrate (along the optical axis) to produce a flat disk on top of a pedestal of (structure height ~12 μm height). Cross-section of predicted contracted (a, left) and expanded (a, right) confirmations. (b) Structure produced using masks from (a), after fabrication (pH ~7.5, left panel) and at pH 2.2 (right panel). Restriction by 'stems' (dense material) induces a 'flower-like' conformation of the disk (defined by mask #2). Scale bar, 10 μm. (c) DIC and wide-field fluorescence images of 'flower' prototypes in contracted (pH 7) and expanded (pH 2.2) states. Scale bars, 10 μm.

4.4 CONCLUSION

These studies demonstrate the unique mechanical properties of hydrogels composed of MPE photocrosslinked proteins and provide a foundation for achieving more specific microactuation based on fabrication using different protein building blocks — in particular those that undergo significant conformational changes induced by ligand binding and release. Moreover, the ability to precisely define both the overall 3D micro-architecture of hydrogels in parallel to prescribing internal density gradients offers unique opportunities for the design of intelligent materials. Finally, the 3D microfabrication of responsive materials demonstrated here can perhaps be extended to non-proteinaceous materials; for instance, those that undergo light-induced volume changes (e.g., using the azobenzene photoisomerization mechanism).

4.4 REFERENCES

[1]   S. Minko, *Responsive polymer materials : design and applications*, 1st ed. Ames, Iowa: Blackwell Pub., 2006.

[2]   E. S. Gil and S. M. Hudson, "Stimuli-responsive polymers and their bioconjugates," *Progress in Polymer Science*, vol. 29, pp. 1173-1222, 2004.

[3]   H. G. Schild, "Poly (N-Isopropylacrylamide) - Experiment, Theory and Application," *Progress in Polymer Science*, vol. 17, pp. 163-249, 1992.

[4]   D. J. Beebe, J. S. Moore, J. M. Bauer, Q. Yu, R. H. Liu, C. Devadoss, and B. H. Jo, "Functional hydrogel structures for autonomous flow control inside microfluidic channels," *Nature*, vol. 404, pp. 588-90, 2000.

[5]   B. Zhao and J. S. Moore, "Fast pH- and Ionic Strength-Responsive Hydrogels in Microchannels," *Langmuir*, vol. 17, pp. 4758-4763, 2001.

[6]   A. Lendlein, H. Jiang, O. Junger, and R. Langer, "Light-induced shape-memory polymers," *Nature*, vol. 434, pp. 879-82, 2005.

[7]   Y. Osada, H. Okuzaki, and H. Hori, "A Polymer Gel with Electrically Driven Motility," *Nature*, vol. 355, pp. 242-244, 1992.

[8]   M. C. Cushing and K. S. Anseth, "Hydrogel cell cultures," *Science*, vol. 316, pp. 1133-1134, 2007.

[9]   M. J. Mahoney and K. S. Anseth, "Three-dimensional growth and function of neural tissue in degradable polyethylene glycol hydrogels," *Biomaterials*, vol. 27, pp. 2265-2274, 2006.

[10]   Y. Luo and M. S. Shoichet, "A photolabile hydrogel for guided three-dimensional cell growth and migration," *Nat Mater*, vol. 3, pp. 249-53, 2004.

[11]   C. N. Salinas, B. B. Cole, A. M. Kasko, and K. S. Anseth, "Chondrogenic Differentiation Potential of Human Mesenchymal Stem Cells Photoencapsulated within Poly(Ethylene Glycol)-Arginine-Glycine-Aspartic Acid-Serine Thiol-Methacrylate Mixed-Mode Networks," *Tissue Engineering*, vol. 13, pp. 1025-1034, 2007.

[12]   H. Weng, J. Zhou, L. Tang, and Z. Hu, "Tissue responses to thermally-responsive hydrogel nanoparticles," *Journal of Biomaterials Science, Polymer Edition*, vol. 15, pp. 1167-1180, 2004.

[13]   J. Kim, S. Nayak, and L. A. Lyon, "Bioresponsive hydrogel microlenses," *J Am Chem Soc*, vol. 127, pp. 9588-92, 2005.

[14]   M. E. Byrne, K. Park, and N. A. Peppas, "Molecular imprinting within hydrogels," *Advanced Drug Delivery Reviews*, vol. 54, pp. 149-161, 2002.

[15] J. D. Ehrick, S. K. Deo, T. W. Browning, L. G. Bachas, M. J. Madou, and S. Daunert, "Genetically engineered protein in hydrogels tailors stimuli-responsive characteristics," *Nat Mater*, vol. 4, pp. 298-302, 2005.

[16] W. L. Murphy, W. S. Dillmore, J. Modica, and M. Mrksich, "Dynamic Hydrogels: Translating a Protein Conformational Change into Macroscopic Motion," *Angew Chem Int Ed Engl*, vol. 46, pp. 3066-3069, 2007.

[17] J. B. Matthew and F. R. Gurd, "Stabilization and destabilization of protein structure by charge interactions," *Methods Enzymol*, vol. 130, pp. 437-53, 1986.

[18] R. K. Scopes, *Protein purification : principles and practice*, 3rd ed. New York: Springer-Verlag, 1994.

[19] O. H. Laitinen, V. P. Hytonen, H. R. Nordlund, and M. S. Kulomaa, "Genetically engineered avidins and streptavidins," *Cellular and Molecular Life Sciences*, vol. 63, pp. 2992-3017, 2006.

[20] M. Lei, Y. D. Gu, A. Baldi, R. A. Siegel, and B. Ziaie, "High-resolution technique for fabricating environmentally sensitive hydrogel microstructures," *Langmuir*, vol. 20, pp. 8947-8951, 2004.

[21] V. R. Tirumala, R. Divan, L. E. Ocola, and D. C. Mancini, "Direct-write e-beam patterning of stimuli-responsive hydrogel nanostructures," *Journal of Vacuum Science & Technology, B: Microelectronics and Nanometer Structures-- Processing, Measurement, and Phenomena*, vol. 23, pp. 3124-3128, 2005.

[22] T. Watanabe, M. Akiyama, K. Totani, S. M. Kuebler, F. Stellacci, W. Wenseleers, K. Braun, S. R. Marder, and J. W. Perry, "Photoresponsive hydrogel microstructure fabricated by two-photon initiated polymerization," *Advanced Functional Materials*, vol. 12, pp. 611-614, 2002.

[23] T. Tanaka, S. T. Sun, I. Nishio, G. Swislow, and A. Shah, "Phase-Transitions in Ionic Gels," *Ferroelectrics*, vol. 30, pp. 97-97, 1980.

[24] T. Arakawa and S. N. Timasheff, "Mechanism of protein salting in and salting out by divalent cation salts: balance between hydration and salt binding," *Biochemistry*, vol. 23, pp. 5912-23, 1984.

[25] D. C. Carter and J. X. Ho, "Structure of serum albumin," *Adv Protein Chem*, vol. 45, pp. 153-203, 1994.

[26] T. Miyata, N. Asami, and T. Uragami, "A reversibly antigen-responsive hydrogel," *Nature*, vol. 399, pp. 766-9, 1999.

[27] Y. Koshi, E. Nakata, H. Yamane, and I. Hamachi, "A fluorescent lectin array using supramolecular hydrogel for simple detection and pattern profiling for various glycoconjugates," *Journal of the American Chemical Society*, vol. 128, pp. 10413-10422, 2006.

[28] R. Chattopadhyaya, W. E. Meador, A. R. Means, and F. A. Quiocho, "Calmodulin Structure Refined at 1.7 Angstrom Resolution," *Journal of Molecular Biology*, vol. 228, pp. 1177-1192, 1992.

[29] W. J. Cook, L. J. Walter, and M. R. Walter, "Drug-Binding by Calmodulin - Crystal-Structure of a Calmodulin Trifluoperazine Complex," *Biochemistry*, vol. 33, pp. 15259-15265, 1994.

[30] H. M. Berman, J. Westbrook, Z. Feng, G. Gilliland, T. N. Bhat, H. Weissig, I. N. Shindyalov, and P. E. Bourne, "The Protein Data Bank," *Nucleic Acids Research*, vol. 28, pp. 235-242, 2000.

[31] M. Gonzalez, C. E. Argarana, and G. D. Fidelio, "Extremely high thermal stability of streptavidin and avidin upon biotin binding," *Biomol Eng*, vol. 16, pp. 67-72, 1999.

[32] N. M. Green, "Avidin," *Adv Protein Chem*, vol. 29, pp. 85-133, 1975.

[33] E. W. Jager, E. Smela, and O. Inganas, "Microfabricating conjugated polymer actuators," *Science*, vol. 290, pp. 1540-5, 2000.

[34] D. G. Grier, "A revolution in optical manipulation," *Nature*, vol. 424, pp. 810-6, 2003.

[35] S. T. Chang, V. N. Paunov, D. N. Petsev, and O. D. Velev, "Remotely powered self-propelling particles and micropumps based on miniature diodes," *Nat Mater*, vol. 6, pp. 235-40, 2007.

[36] A. Terray, J. Oakey, and D. W. Marr, "Microfluidic control using colloidal devices," *Science*, vol. 296, pp. 1841-4, 2002.

[37] S. Basu, C. W. Wolgemuth, and P. J. Campagnola, "Measurement of norma and anomalous diffusion of dyes within protein structures fabricated via muftiphoton excited cross-linking," *Biomacromolecules*, vol. 5, pp. 2347-2357, 2004.

[38] B. Kaehr, N. Ertas, R. Nielson, R. Allen, R. T. Hill, M. Plenert, and J. B. Shear, "Direct-write fabrication of functional protein matrixes using a low-cost Q-switched laser," *Anal Chem*, vol. 78, pp. 3198-202, 2006.

[39] B. Kaehr and J. B. Shear, "Mask-directed multiphoton lithography," *J Am Chem Soc*, vol. 129, pp. 1904-5, 2007.

[40] E. Sharon, B. Roman, M. Marder, G. S. Shin, and H. L. Swinney, "Mechanics: Buckling cascades in free sheets - Wavy leaves may not depend only on their genes to make their edges crinkle.," *Nature*, vol. 419, pp. 579-579, 2002.

[41] T. Mora and A. Boudaoud, "Buckling of swelling gels," *European Physical Journal E*, vol. 20, pp. 119-124, 2006.

[42] Y. Klein, E. Efrati, and E. Sharon, "Shaping of elastic sheets by prescription of non-Euclidean metrics," *Science*, vol. 315, pp. 1116-20, 2007.

[43] C. Alexander and K. M. Shakesheff, "Responsive polymers at the biology/materials science interface," *Advanced Materials*, vol. 18, pp. 3321-3328, 2006.

Chapter 5: Microarchitectures for Behavioral Microbiology

5.1 INTRODUCTION

The study of microorganisms spans many diverse areas of biological research and is critical for human health and disease. Microorganisms are an important and accessible window into the biochemical dynamics of cellular metabolism, signal transduction, transcription and translation, evolution and environmental adaptation. Microbiology has played a key role in enabling the genetic and genomic scientific revolutions to occur and microorganisms provide a set of common laboratory tools for genetic engineering and biochemistry.

Today the field of microbiology is as exciting as ever, as microorganisms gain increasing attention from scientists in diverse fields. Bacterial physiology and motility provide applied physicists and engineers a framework to begin to understand, model and mimic mechanical engineering at the molecular and nanoscale [1]. Mathematical biologists rely on the empirical observations of microbial communities to refine models of population and evolutionary dynamics [2, 3], and microbiology potentially offers a means to qualitatively study highly complex and emerging biological systems and ecologies [4].

However the techniques used to culture and study microorganisms have changed little since developed over 100 years ago. The number of bacterial species is vast (~ 10^9; [5]), and traditional pure liquid and agar culture methods are compatible with only a tiny fraction of microorganisms [6]. Though bacteria are generally studied as a population, the genetic variation among individual cells — giving rise to phenotypic variations in persistence, pathogenicity, viability, motility, etc. — can differ significantly even within clonal populations [7, 8]. For microbiology to move forward, new techniques must be

developed that allow greater resolution of individual cellular behavior and population dynamics over time.

The microfabrication techniques presented thus far are perfectly suited to the size and scale of microorganisms such as *E. coli*. In this chapter, mask-directed multiphoton lithography (MDML) is used for the prototyping and fabrication of microchambers and microdevices that provide a novel platform for the study of microorganisms under controlled and environmentally flexible conditions and may offer insight into microgeometries that allow the mechanical energy of motile cells to be harnessed. Figure 5.1 shows a basic bacterial microchamber created using MDML. Chambers composed of crosslinked proteins can be fabricated with well defined internal and external dimensions to suit applications of interest. Chambers are fabricated plane-by-plane, rising from a glass substrate to a desired height and sealed from the top to allow unobtrusive visual access using standard DIC (inverted) microscopy.

The ability to fabricate microstructures in the presence of cells (Chapter 2) in addition to the mechanical responsivity of protein matrices (Chapter 4) provides additional control over experimental parameters. Further, the porosity and diffusion characteristics of photocrosslinked protein matrices [9] should allow exchange of nutrients and waste into and out of chambers via diffusion, obviating the need for forced solution flow. This material characteristic stands in contrast to other microfabrication techniques for cell culture that rely on the elastomeric materials of soft lithography (e.g., PDMS). In cases where PDMS microchambers have been proposed for small population studies of cells, chambers must be individually addressed with inlet/outlet channels or valves that provide the necessary plumbing for a chemostatic environment [8, 10, 11]. By using porous proteinaceous materials for microenclosures, additional microfluidic interfacing is not needed. Once the desired cells are in place, the platform could be

117

submersed in potentially any medium (e.g., nutrient broth, ocean water, etc.) and under a variety of physical conditions (e.g., different temperatures and flow conditions).
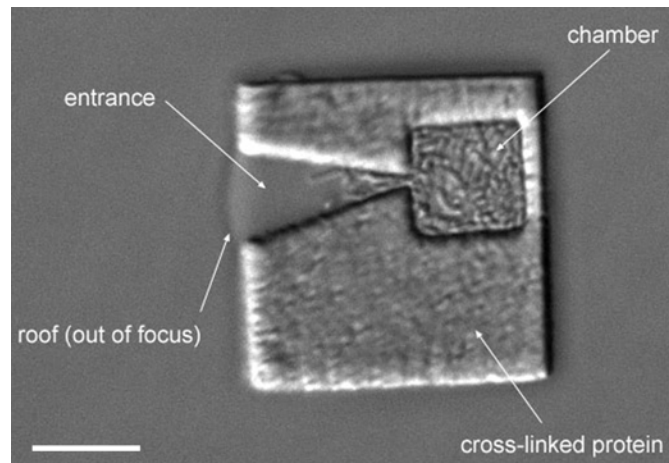
Figure 5.1:   A microculture platform for microbiological studies. The height of the roof is approximately 5 µm above the coverslip surface. Scale bar, 5 µm.

With these fabrication abilities, questions regarding bacterial communication and environmental interaction can be addressed. For instance, the precise mechanisms and necessary conditions by which microorganisms coordinate gene expression and behavior in high population density environments — the quorum sensing paradigm [12] — is unclear. Quorum sensing behavior relies on the production and secretion of diffusible molecules by cell populations. When these molecules reach a critical concentration level in cell cultures, gene expression is altered leading to coordinated population behaviors such as production of virulence factors and biofilm formation [12]. Recently, ecologists have challenged the quorum sensing paradigm; noting that the quorum sensing response could be initiated by a single cell in a cloistered environment of little mass transfer [13]. Techniques proposed here may be capable of addressing these questions and provide the means to mimic and interrogate more complex ecologies, such as the pulmonary microenvironment — a locus of infection for cystic fibrosis patients [14].

Additionally, the ability to readily define chamber geometries provides a means to spatially organize or direct the motility of cells. The study of motility in microorganisms offers fertile ground for the field of nanobiotechnology with an interest in harnessing micro and nanomechanical work [1]. The highly efficient fluid propulsion generated by bacterial and eukaryotic flagella [15] is a remarkable example of nanomechanical engineering, but technologies to reassemble or otherwise duplicate these structures as stand alone components do not yet exist. Thus, recent interest has turned toward developing biohybrid devices powered by whole cells. Motile microorganisms have been employed to mix fluids in microfluidic environments [16], shuttle microparticles [17], and rotate microrotors [18]. In these examples, cells were chemically attached or otherwise 'glued' to device materials, drastically limiting the lifetime of the proposed device. In contrast, the rapid prototyping capabilities of MDML provides the means to derive useful engineering solutions for cell-powered microdevice geometries and may enable longer lifetime devices (mixers, pumps) through the design of inherent turnover mechanisms of the functional units (i.e., motile cells).

5.2 EXPERIMENTAL METHODS

5.2.1 Materials and Cell Culture

Bovine serum albumin (BSA, BAH64-0100) was supplied by Equitech-Bio. Avidin (A-887) and fluorescein biotin (B-1370) were supplied by Molecular Probes. PMMA microparticles (19130) were purchased by Polysciences. Methylene blue (M-4159) and flavin adenine dinucleotide (F-6625) were supplied by Sigma-Aldrich (St. Louis, MO).

E. coli strains were streaked on 1.5% agar (214050, Becton Dickinson) containing T-broth (1% Tryptone [211705, Becton Dickinson], 0.5% NaCl) and grown at 35°C. Single-colony isolates was used to inoculate 2 ml of T-broth which were grown to saturation on a rotary shaker (200 rpm) at 32°C. An aliquot was diluted 1:100 into another 2 ml of T-broth and grown ~4.5 h to mid-exponential phase. Bacteria solutions were diluted for experiments 1:10-100 in either motility buffer (0.01 M KPO_4, 0.067 M NaCl, 10^{-4} M EDTA, 10^{-2} M sodium lactate, pH 7.0) or PBS (10^{-2} M potassium phosphate, pH 7.0).

5.2.2 Strains

E. coli strains RP437 (wt) and RP9535 (ΔcheA) — kindly provided by John S. Parkinson (Department of Biology, University of Utah) — display distinct motility phenotypes and were the predominant microorganisms used in this work. Individual *E. coli* use ~ 5-8 peritrichous flagella actuated by a rotary motor for motility. When the rotary motor (powered by a proton gradient) spins counter-clockwise, the flagella form a unified helical bundle resulting in forward movement termed a 'run' (Figure 5.2) the average duration of which persists (in wt cells) for ~ 1 second. Clockwise rotation of the rotary motor uncoils the flagellar bundle resulting in a 'tumble' persisting, on average, for ~ 0.1 seconds (orienting the following run in a random direction). In this way the cell is able to sample the environment (termed 'random walk'; [19]). In the presence of a gradient of chemoattractant or repellent, the random walk becomes biased to or away from the gradient by simply increasing the run/tumble ratio and producing overall movement that is biased toward or against the chemical source. RP437 is wild type for this behavior. RP9535 is mutant (ΔcheA) for a histidine kinase — the activity of which is required for clockwise rotation of the rotary motor. Consequently the movement of

RP9535 consists almost entirely of runs, and it is thus referred to as a 'smooth-swimming'.
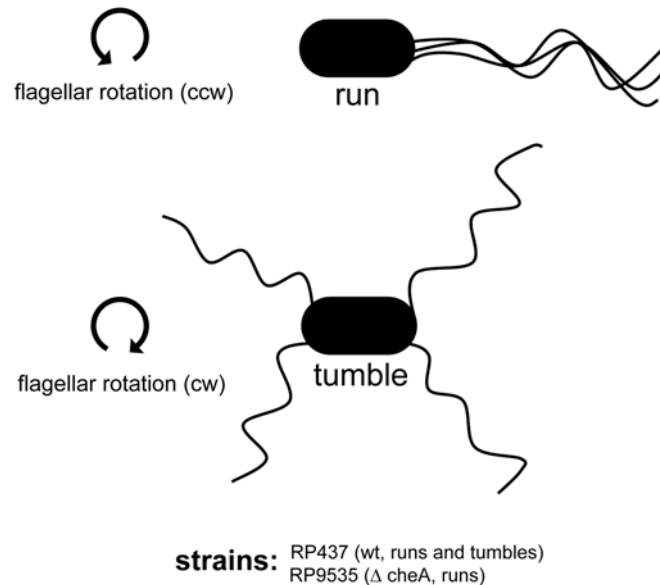
Figure 5.2:   Bacterial taxis is a result of runs and tumbles.

5.2.3 Matrix Fabrication

Microchambers composed of photo-crosslinked protein were fabricated onto untreated #1 microscope cover glass using the output of a mode-locked titanium:sapphire laser (Tsunami; Spectra Physics) operating at 730 to 740 nm. Laser output was adjusted to approximately fill the back aperture of an oil-immersion objective (Zeiss 100x Fluar, 1.3 numerical aperture) situated on a Zeiss Axiovert inverted microscope system. Desired powers were obtained by attenuating the laser beam using a half-wave plate/polarizing beam splitter pair. The internal and external geometries of microchambers were defined using mask-directed multiphoton lithography (MDML) described in detail in Chapter 3.

Microchambers composed of photo-cross-linked protein were fabricated from solutions containing protein at 400 mg mL^{-1} unless otherwise specified and either 3-5 mM methylene blue or 5 mM FAD as a photosensitizer. Chambers were imaged on the Axiovert microscope using a 12-bit 1392 x 1040 element CCD (Cool Snap HQ; Photometrics).

5.3 RESULTS

5.3.1 Cell Trapping and Incubation

By scaling cell culture enclosures down to the volume of individual or small numbers of cells, behaviors that would otherwise be averaged in population studies in liquid or agar culture can be resolved [8]. Figure 5.3 shows a microstructure comprised of crosslinked BSA designed to trap motile *E. coli*. Here a large aperture entrance directs cells from the surrounding media into a passage that leads to a smaller aperture (of a diameter near the width of a single cell, ~ 1 μm) directing cells into the cubical chamber. In this way, the chamber is filled passively; cells are directed into the structure by their motion trajectories in the surrounding media. In this example, complete chamber packing was rapid (~ 20 min) — coinciding with markedly decreased cell movement. The phenotypic change from motile to immotile is crucial for the life cycle of pathogenic and biofilm forming microorganisms. In native environments, the precise mechanisms are not fully understood, though it is known that the change can be initiated by geometric constraints (that influence the mass transfer of nutrients and wastes) and cell-substrate interactions [14, 20]. Micro-enclosures composed of (or containing) biologically relevant substrates (e.g., mucin) may provide a means to better elucidate these mechanisms in constrained geometries.

The filled chamber shown in Figure 5.3 was rinsed and incubated in T-broth for 12 hours after initial filling with bacteria. Cells in the chamber continued to divide, resulting in slight bulging of the vertical internal walls (Figure 5.3C) and considerable expansion of the top of the chamber. Remarkably, the crosslinked top sheet of BSA (~ 1 μm width before expansion) remained intact. Scanning electron micrographs (SEMs) revealed the extent of expansion (Figure 5.3E), where outlines of individual bacterial cells can be seen from their invagination imprint upon the expanded protein sheet (Figure 5.3E). In some cases expansion exceeded the structure height by > 3 times (Figure 5.3F). Occasionally, small tears developed along the edges of the cell domes — likely during the dehydration process required for SEM — revealing the cells inside (F, lower panel).

The surprising flexibility of the protein sheet can in part be explained by the conformational flexibility of crosslinked BSA described in Chapter 4, allowing expansion of crosslinked matrices by the hydrogel nature of incorporated proteins and further enabled by the slow kinetics of expansion (~ 12 hours). However, it is currently unknown whether specific cell-substrate interactions contribute to maintaining the integrity of the structure (as has been proposed for some types of pathogenic biofilms [14]). Disruption of known cell-substrate interactions of biofilm forming bacteria — such as the *P. aeruginosa* / mucin interaction involved in cystic fibrosis infection — at various time points during cell division may shed light on this interaction.
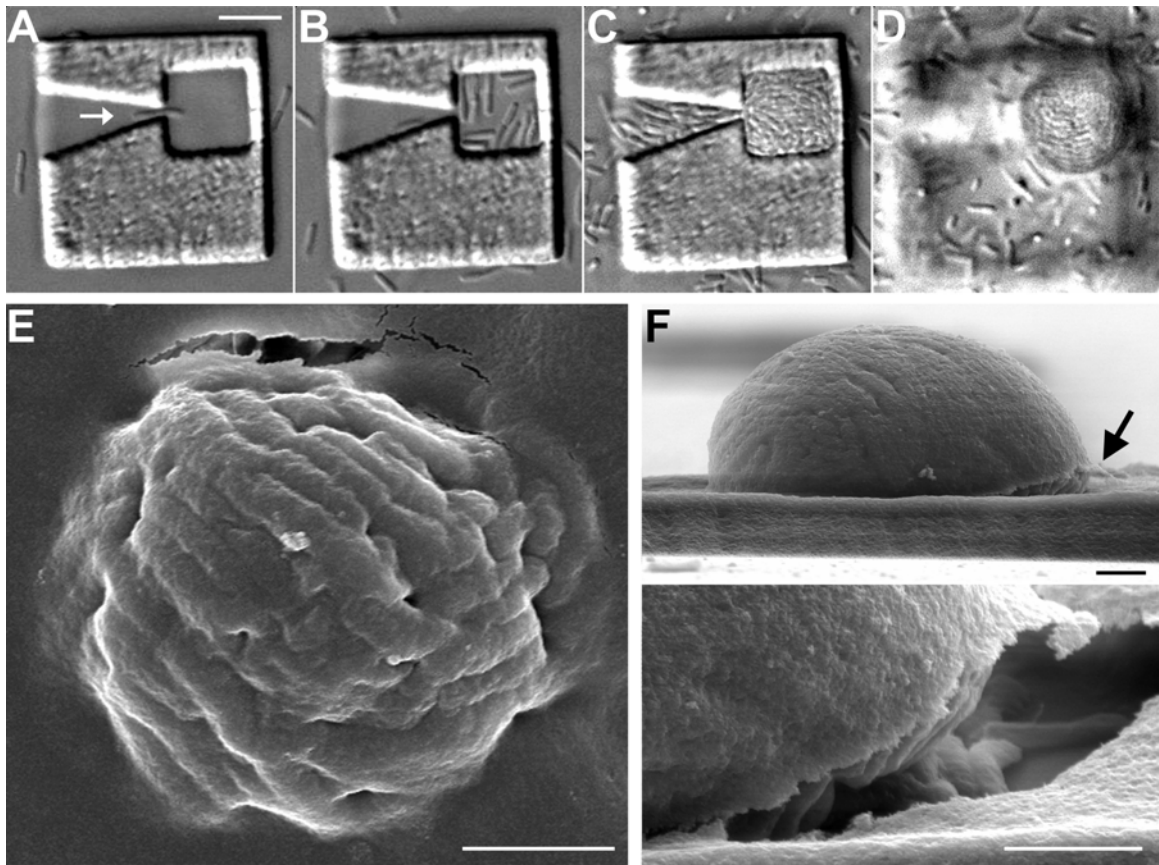
Figure 5.3: A microchamber composed of crosslinked BSA for the trapping and incubation of bacteria. (A; scale bar, 5 μm) The design enables passive loading of a motile cell (arrow) directed into the internal chamber through an aperture roughly the diameter of a bacterium. (B) Approximately 1 min after the first cell entered, the entry of additional cells induces transient organization of cell bodies along the walls. (C) 12 hours after incubation in nutrient rich media, cells continue to divide which (D) expands the top sheet of crosslinked BSA. SEM images reveal 3D expansion of chamber tops, resulting in invaginated protein matrix by imprinting of underlying cell bodies (E, left panel) and significant vertical expansion (F, top panel; arrow indicates view of the bottom panel). Scale bars for E and F, 2 μm.

This experiment could be readily repeated using more elaborate microchamber geometries. Structures shown in Figure 5.4 were fabricated using transparency mask-based MDML which is limited, in a practical sense, to the creation of vertical walls.

Much greater control of the 3D internal chamber geometries could be achieved using DMD-directed multiphoton lithography — efforts currently being pursued.

These high density cell cultures (estimated at ~10^{11} - 10^{12} cells cm^{-3}) combined with genetic labeling provide a means to quantitatively address questions regarding the quorum-sensing paradigm and determine the minimum number of cells needed for quorum-sensing responses. Future work using matrix materials and/or microstructure geometries that enable asymmetric diffusion [21] to concentrate quorum signaling molecules while retaining chemostatic conditions may provide a route to directly measure the contribution of the effects of mass transfer on the quorum-sensing response [13]. Further, using this approach, the complex 3D topologies of tissue structures prone to infection can be mimicked and evaluated under well controlled settings. Finally, the ability to mold colonies into arbitrary 3D shapes may provide a useful means for therapeutic delivery — where an injectable, geometric bolus of cells is required [22, 23].
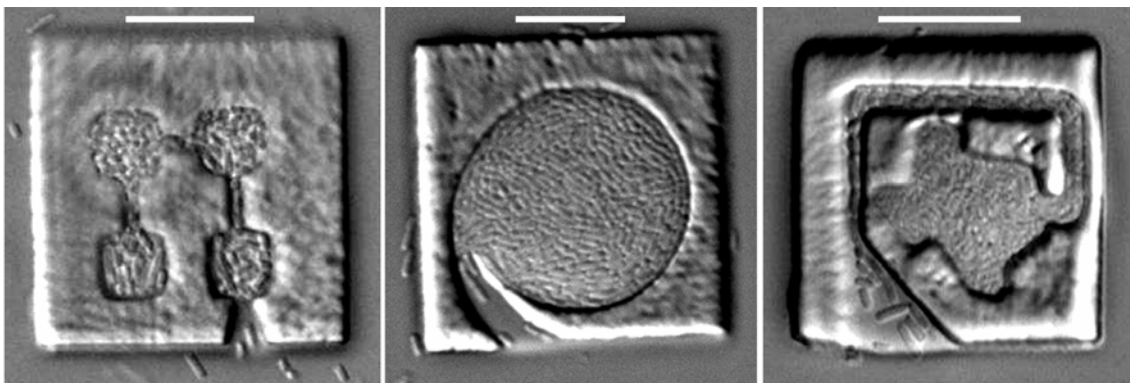

Figure 5.4: Microchambers of arbitrary internal dimensions can be used to grow high density molded cell cultures. Scale bars, 10μm.

Microchambers capable of trapping and incubating single cells allow the observation of cellular behaviors lost in studies of cell populations. In addition to structural and behavioral differences, genetic variations such as spontaneous mutation,

gene expression 'noise', and the mechanisms of horizontal gene transfer must be studied in single or small populations of cells [8, 24]. A biocompatible microfabrication system potentially enables both passive and active means to trap and incubate single cells. Here the term 'active' would describe the *in situ* fabrication of a chamber over a target cell. In this scenario, cells could be selected via phenotypic criteria (e.g., speed, size, chemotaxic behavior). Currently this proposal faces challenges. The average swimming speed of *E. coli* cells is ~ 20 μm sec^{-1}. Therefore fabrication of a trap must be rapid, well-placed and large enough to contain the cell (as it continues to swim) for the duration of fabrication. Using fabrication solutions with high concentrations of protein (~ 400 mg ml^{-1}) greatly increases the viscosity of solution [25], providing some means to attenuate the speed of cells. Unfortunately, cell viability using MDML fabrication has not yet been maintained with this approach. Currently, the high speed and large area coverage raster-scanning needed to use this approach can only be performed (reproducibly) with highly efficient photosensitizers (e.g., Rose Bengal and methylene blue) which can generate high local concentrations of phototoxic species. As a result, additional strategies (e.g., improved efficiency of relatively benign sensitizers via direct attachment to proteins) are needed to facilitate the biocompatibility of this process.

Figure 5.5 demonstrates an alternative approach for single-cell trapping and incubation. Here, a BSA chamber was fabricated with a narrow entrance aperture. Wild-type *E. coli* then was added to the fabrication solution (composed of BSA and the minimally toxic photosensitizer, flavin adenine dinucleotide, FAD). After a single bacterium entered the chamber, a BSA plug was rapidly crosslinked (within $\sim$2 sec) to seal the chamber and trap the cell. The cell was monitored and allowed to divide over

126

many hours, eventually filling the chamber with a clonal population. This approach decreased the time and overall area of *in situ* fabrication — conditions that were amenable for the less toxic FAD-generated photosensitization. However, the means by which a cell enters and is subsequently trapped using this configuration does not allow direct selection of specific phenotype (e.g., in a heterogeneous population of cells).
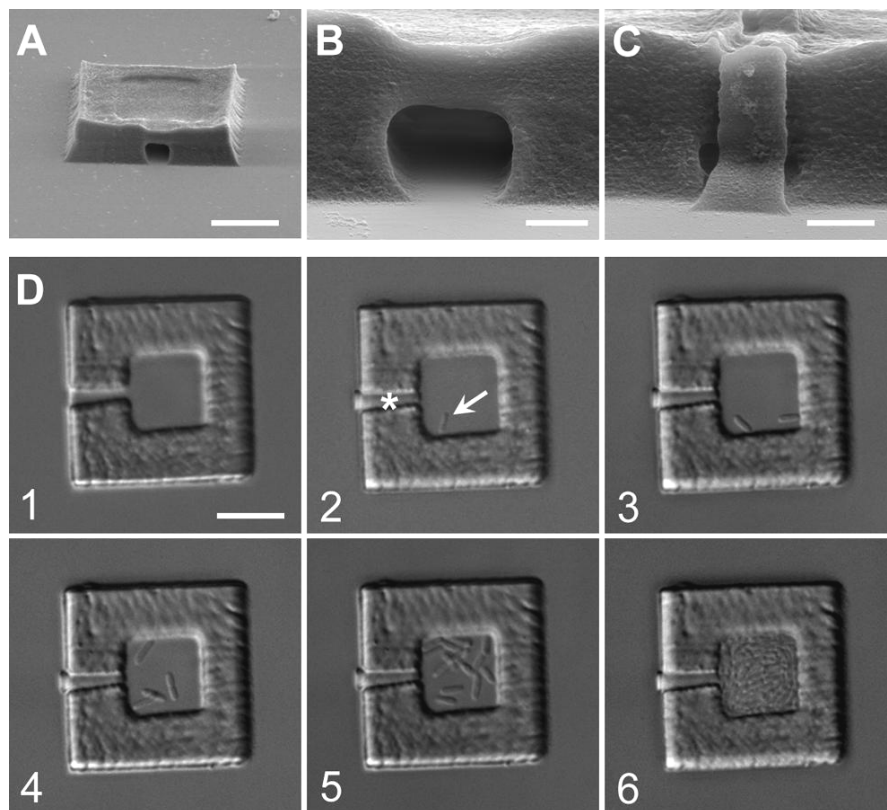
Figure 5.5: Biocompatible microfabrication allows trapping of a single bacterium. (A, B) SEM images of a BSA microcontainer similar to that shown in parts C and D. (C) SEM of a BSA container after the entrance was plugged with a bacterium inside. (D) Sequence showing a BSA container before (1) and immediately after (2) fabrication of a plug to trap a bacterium (arrow; scale bar, 10 μm.). Cell division eventually fills the trap with no loss of bacteria (3-6). Time points: (3) 172 min, (4) 360 min, (5) 590 mins, (6) 16 hrs. Scale bars: A/D, 10 μm; B/C, 2 μm.

The single-cell resolution of this approach in conjunction with the chamber porosity [9] provides a means to evaluate chemical treatments at any time point during the cell cycle. Figure 5.6 shows an initial demonstration of this capability. Here, smooth-swimming *E. coli* were allowed to enter a low-profile BSA microchamber (internal height ~2-3 microns). In this case, cells in the chamber quickly ceased moving, in part because of the restricted (lower profile) geometry and roughened matrix texture of the top protein sheet (which may increase the entanglement of flagellum). Cells were observed for ~1 hour then incubated in T-broth containing the antibiotic cephalexin — an inhibitor of septation. After incubation for 14 hours the cells observed in the chamber were highly elongated — the predicted phenotype of cephalexin treatment. Other researchers have used a similar treatment in PDMS-based microchambers to engineer the morphology of single cells [26]. In that study, cells were immobilized for the duration of treatment and then released upon removal of the PDMS mold. Protein-base microchambers (of sufficient internal height) allow the behavior of cells (e.g., motility) to be observed under selected treatments (e.g., antibiotics) at any stage in the growth cycle.

(+) cephalexin
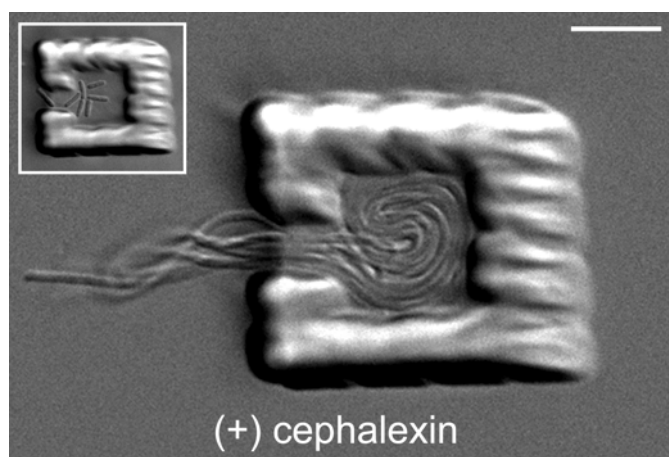
Figure 5.6: Protein microchamber incubators allow chemical treatment and observation at desired time points. Motile cells that enter the chamber are rapidly immobilized (inset, see text). Incubation in T-broth (14 hrs, 22 °C) containing the antibiotic cephalexin (75 μg ml^{-1}) results in cell elongation without cell division. Scale bar, 5 μm.

The hydrogel nature of MPE protein matrices, discussed in detail in Chapter 4, imparts further control and functionality to protein-based microchambers. By modulating the hydration of chamber walls, for example through a pH change, the volume of cell enclosures can be altered dynamically during division and growth; more extreme changes in chemical environment can be used to disrupt the integrity of the microchamber-substrate interface to achieve release of trapped cells (Figure 5.7) for further incubation and analysis. In this example, cell release is accomplished by brief exposure to a high pH solution (~12.2). In other experiments, smooth-swimming *E. coli* were incubated in pH 12 solutions for > 5 minutes, then returned to T-broth and incubated overnight. Though growth rates were not monitored, cells from overnight culture displayed the normal motile phenotype of RP9535.
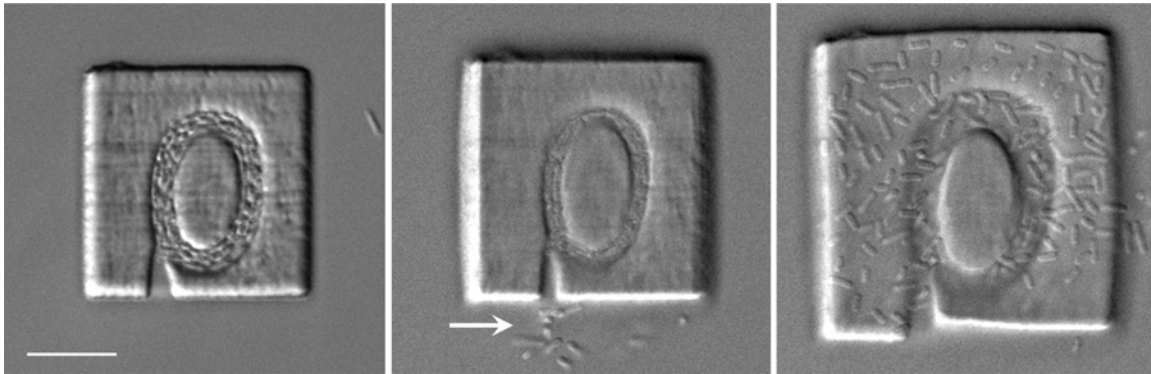
Figure 5.7: Releasing trapped cells through hydrogel response. Micro-enclosures comprised of protein matrices can be used to trap, incubate and release *E. coli* cells. Abrupt change in bath pH (7 to 12.2) causes temporary compression of the internal chamber, releasing a few cells (arrow, middle panel), and eventually disrupts the chamber-substrate interface (right panel; cells are seen here in between the glass substrate and the microchamber). Scale bar, 10 μm.

These initial studies demonstrating the basic properties and utility of 3D microchambers for bacterial microincubation provide the foundation for more complex experiments where prescribed chemical functionality of microstructures — using ligand binding proteins such as avidin — could enable heterogeneous populations to be sorted by specific, diffusible chemoattractants. Further, it should be possible to design geometries that enable more efficient release of cells, for instance using a combination of proteins of differing responsivity and under less harsh conditions — a necessary requirement for the release of more delicate cell types (e.g., neurons, stem cells).

5.3.2 Directed Motility

The ability to fabricate arbitrary entrances and internal chamber geometries of microstructures presents not only a means to prototype chambers that trap motile cells but also a way to direct their motion and positions over time. Here, the rapid prototyping capabilities of MDML were used to design microchambers for directed cell movement,

130

providing insight into engineering solutions for harnessing the mechanical energy of microorganisms.

Figure 5.8 demonstrates how the internal geometry of a microchamber can dictate the motion paths of smooth-swimming *E. coli*. Here, motile cells entering the circular microchamber are biased to swim clockwise or counter clockwise along the inner wall as prescribed by the circular geometry and asymmetry of chamber entrances. Cells that happen to reverse direction and swim counter to the intended direction can do so for < 1 revolution since the outcome of the counter-biased swim path along the chamber perimeter results in exit. As the number of cells that moved along the chamber perimeter increases, counter-biased movement was observed to decrease. The movement of cells along the chamber perimeter produces a microfluidic counter flow (Figure 5.8B). Here cells were allowed to accumulate in the chamber for ~ 2 hours after which two phenotypically diverse populations emerged: motile and non-motile cells. The fluidic force generated by motile cells that swim clockwise along the inner wall induces counter-clockwise rotation of non-motile cells in the center of the chamber. In this case, the rotational velocity of the central plug composed of non-motile cells was ~0.3 Hz (~17 rpm). This interesting and somewhat surprising result shows both the capabilities of (localized) phenotypic separation using cell motility-derived forces, and indicates the potential to rotate inanimate materials (e.g., a rotor) based on relatively simple geometric constraints of cell paths without requiring physical attachment of cells to the device.

Because the motility of wild-type cells (RP437) consists of both runs and tumbles, the rotation-bias imposed by the chamber geometries is, qualitatively speaking, not nearly as strict for RP437. The tumbling mechanism increases the probability that cell motion trajectories will not be as confined to the chamber perimeters, as is the case with smooth-swimming cells, but can often traverse across the circular chamber and increase the

131

chance of counter-bias movement. Consequently when wild-type cells were incubated with circular microchambers, the situation shown in Figure 5.8B (where the circular chamber is mostly filled with cells) has not been observed; as wild-type cells reorient their direction frequently, the probability of exit is greater than for smooth-swimming cells.
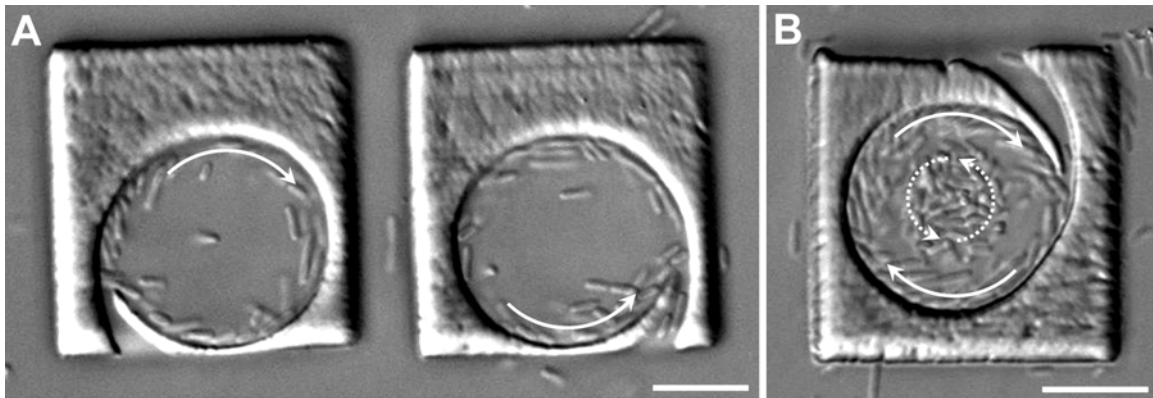
Figure 5.8: The internal geometry of microchambers dictates directionality of circular motion of smooth-swimming *E. coli*. (A) Cells move clockwise (left) or counterclockwise (right) along the perimeter of the microchamber as prescribed by the internal circular geometry and asymmetric entrance. (B) Motile cells moving clockwise along the perimeter of the microchamber direct the counter-clockwise rotation of non-motile cells in the center of the chamber. Scale bars, 10 μm.

A related geometry (to Figure 5.8) has been demonstrated for the directional rotation of a free standing microrotor by Hiratsuka *et al*. [18]. In that work, *Mycoplasma mobile* cells, a gliding bacterium, were modified to allow cell surface biotinylation and were directly attached to strepavidin coated rotors. Further, researchers have developed methods to covalently attach motile *E. coli* cell bodies to pre-aligned microarrays so that the cell flagella remain free to induce localized mixing on the surrounding fluid [27]. Other researchers have adsorbed *Serratia marcescens* cells to PDMS surfaces, creating

'bacterial carpets' that were observed to randomly move through the medium via the combined flagellar motion of many cells [28]. In similar work, researchers studied fluid flow in PDMS microchannels coated with and without *S. marcescens* cells and found greater capabilities for mixing in otherwise laminar flow environments in cell-coated channels [16]. These recent studies, intended to suggest means in which to harness the mechanical energy of motile microorganisms, relied on the direct attachment of cells to devices. However, a device powered through the direct attachment of motile cells would have an inherently short lifetime — one that is coupled to the lifetime of the attached cells. As cells die, dislodge or become exhausted, the device would likely need to be refurbished or replaced.

A potential solution to this problem is demonstrated in Figure 5.9A. Here, a microvortex is generated using smooth-swimming motile cells that lodge into grooves along the inner chamber wall. The flagellar motion of cells along the wall coordinated the direction of the vortex and maintained the alignment of cells necessary to continue the rotation of the central fluid. Cells that entered the chamber but did not find their way into grooves became subjected to the microvortex produced by the perimeter cells. In this experiment, a cell was observed to move clockwise along the circumference of the perimeter cells at ~ 70 µm sec^{-1} (~ 2-3 Hz) — roughly 3.5 times the average speed of a self-propelled *E. coli* cell in this medium.
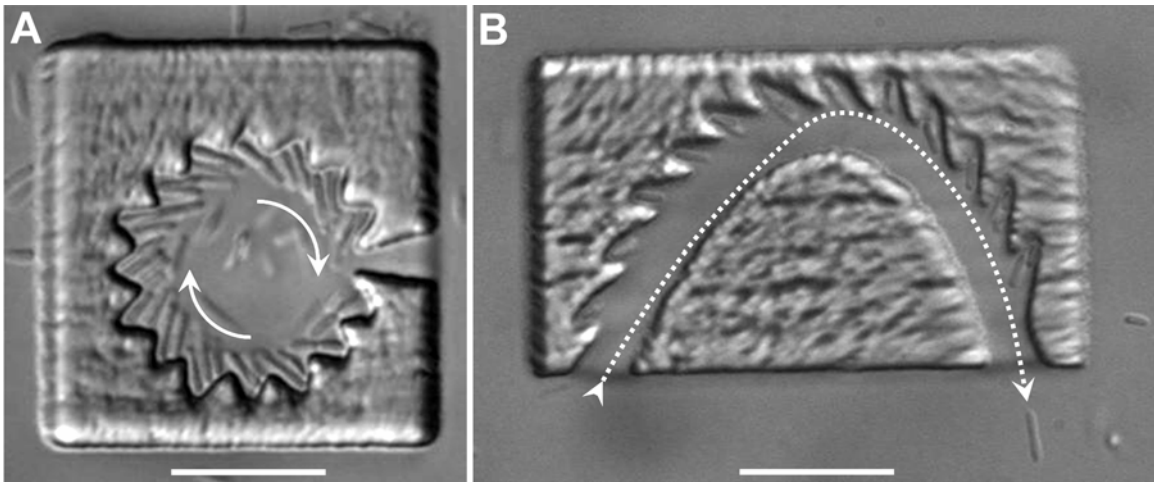
Figure 5.9:   Smooth-swimming *E. coli* cells direct localized fluid movement. (A) Motile
cells trapped within grooves produced a clockwise-directed microvortex that
maintained alignment of cells along the perimeter and clockwise movement
of cells along the perimeter cells (arrows). (B) Smooth-swimming cells
aligned into grooves along a curved microchannel produce a directional
flow that inhibits right to left passage of motile cells. The dotted line traces
the motion path of a single cell through the channel. Scale bars, 10 μm.

Both of the microstructures shown in figure 5.9 use a 'tooth' design to position

cells along the chamber perimeters. The angle of the teeth ($\theta \sim 30\text{-}60°$) allows sideways

movement of the cells in the groove — a solution determined through rapid prototyping.

This may serve two important functions. First, cells are subject to the fluid motion

imposed by neighboring cells which allows cells to be positioned in a coordinated, self-

assembled manner. Thus the microvortex effect shown in Figure 5.9A functions to keep

the cells producing it aligned and in place — a concept that can be extended to the curved

channel shown in Figure 5.9B. Second, cells are observed to be displaced and removed

by new cells entering the microchamber; providing a mechanism that, in principle, allows

the function of such a system well beyond the lifetime of individual cells. If a cell were to

die or otherwise cease swimming in the curved channel for instance, it would likely be

134

expelled from the channel by the directed flow and eventually replaced with a 'fresh' motile cell.

Clearly, the curved channel shown in Figure 5.9B could be connected in a chain to provide directional fluid flow for transport and separations over extended distances. This curved design functioned as an efficient rectifier in which the direction of cell movement was essentially one way. Cells that entered the right end of the channel were (often) shunted into grooves while cells that entered the left end moved rapidly through the extent of the curved channel.

Similar geometric rectifying principles have been suggested for other studies of nanobiotechnological interest. Researchers have begun to explore the reconstitution of molecular motor proteins, such as the microtubule/kinesin system, in microfabricated devices [29-32]. In such studies, microchannels coated with kinesin allowed microtubules to move freely along coated surfaces (this system is described as 'inverted' because, unlike the native configuration, the microtubules are the transported component). As microtubules essentially move randomly on kinesin-coated surfaces, channel geometries have been proposed that result in high efficiency directional movement of microtubules [31]. A similar idea, shown in Figure 5.10, was applied to direct the motion of smooth-swimming *E. coli*. In contrast to methods using closed (kinesin-coated) microchannels for the directional transport of microtubules, the 'open media' characteristic of microstructures shown in Figure 5.10 enables both internal and external geometric influence on rectification.

Rectifying geometries to direct motile microorganisms could serve a number of functions. Rectifying 'units' aligned into a chain could perhaps function as a micro-separations column and provide a means to separate motile species based on phenotypic criteria such as speed and interaction with perimeter walls. Figure 5.10C shows a

proposed geometry for the enrichment of a heterogeneous population *E. coli* (RP437, wt; RP9535, smooth-swimming). Given that smooth-swimming cells have more extensive interactions with chamber perimeters and microchamber geometries than wild type cells, it was hypothesized that this structure or similar column geometries would produce an enrichment of smooth-swimmers at the cube-shaped collection chamber. In this design, cells could enter at each of the rectifying unit interfaces. This design proved not optimal for enrichment of RP9535 in the bottom chamber. Often, wild type cells were observed to interfere with the interaction of smooth-swimming cells to the rectifying geometries along the column. In future work, designs where the rectifying interfaces are closed to the outside medium and column lengths are extended should be evaluated. In addition, these devices should be tested under conditions that provide a clear distinction of RP437 and RP9535 (i.e., by fluorescent labeling).
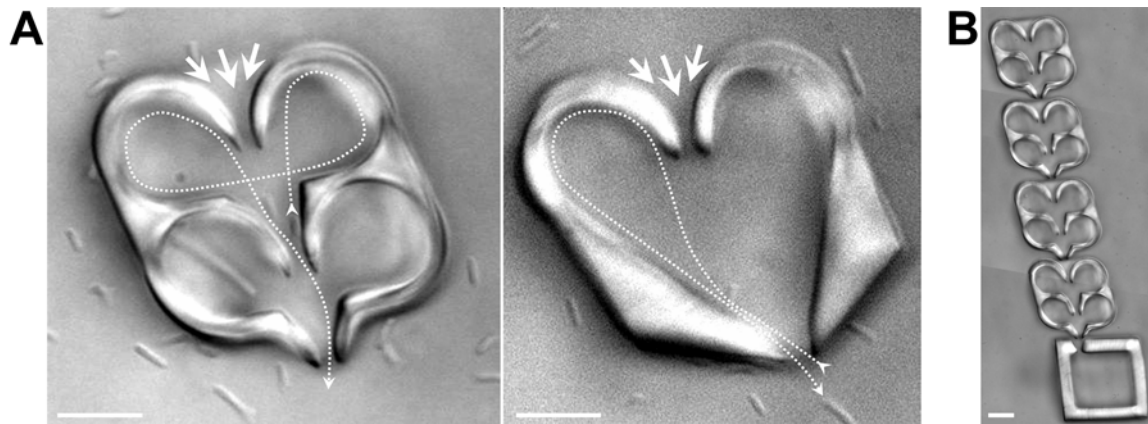
Figure 5.10: Microchamber-rectifying geometries for the unidirectional movement of smooth-swimming *E. coli*. White arrows indicate the direction of cell entry into the chamber — a design intended to bias the entry of swimming cells into the top versus bottom (of the panel) chamber apertures. Dotted lines trace the paths of single cells that have entered the bottom aperture and are redirected to the 'exit'. (C) A proposed geometry for the enrichment of RP9535 (in a population containing RP9535 and RP437) consisting of a chain of rectifying microenclosures leading into a collection chamber. Scale bars, 5 μm.

Nevertheless, the use of rectifying units to direct smooth-swimming cells into circular microchambers (Figure 5.11) resulted in the rapid concentration of smooth-swimming cells (left structures) compared to microchambers without rectifiers (right structures). Figure 5.11B shows the high concentration of cells — nearly complete packing of motile cells — obtained in the left chamber only 12 minutes after cells were introduced into the medium. The high density of smooth-swimming cells in the circular geometry resulted in very rapid and concerted 'vortex-like' motility. Indeed, the ordering of cell bodies is apparent in Figure 5.11A. This motility of bacteria in the circular geometry was suggestive of swarming motility — a smooth-swimming group behavior thought to enable colonization in natural environments [33]. After overnight incubation in T-broth and rinsing of the media solution, the left chamber was tightly packed with non-motile cells in considerable contrast to the 'non-rectified' chamber.
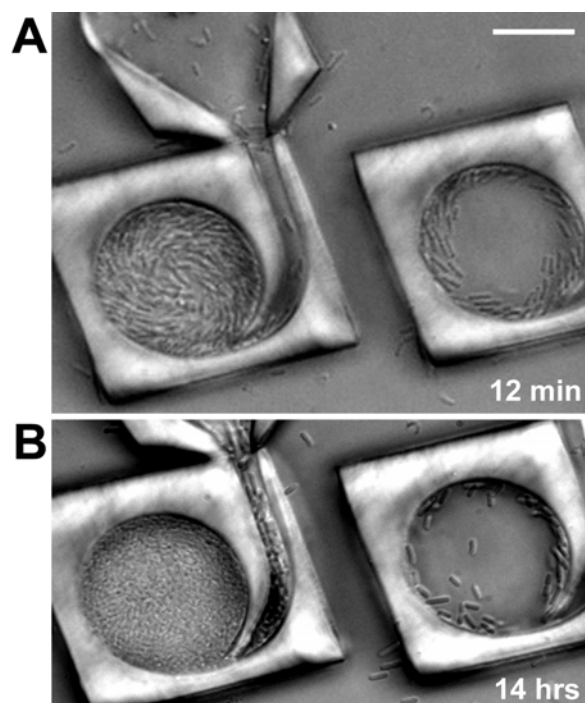
Figure 5.11: Effects of rectification geometries on cell concentration in microchambers. Rapid accumulation of RP9535 was observed in microchambers bridged to the surrounding medium with a rectifying chamber (A, left panel). Panel B shows the results after overnight incubation in nutrient-rich media and rinsing of the solution. A high density of non-motile cells is observed in the left chamber in contrast to the right, 'non-rectified' microchamber. Scale bar, 10 µm.

To begin to quantify the fluidic forces generated in circular chambers of highly concentrated motile cells, microchambers were fabricated over PMMA microparticles, effectively trapping the microspheres inside the circular chamber (Figure 5.12A, left panel). As cells were introduced and began to fill the chamber, the microsphere began to translate in the opposite direction to the moving cells (Figure 5.12A, right panel). In the geometry described here, the rotational velocity of the microsphere depended on the number of cells in the circular chamber — where the fastest measured microsphere velocity (corresponding to the chamber of highest cell count) neared 3 Hz (~ 170 rpm). The rotation of the microsphere could be reversed using a mirror-image geometry (Figure

138

5.12C) — a result predicted from Figure 5.8. As the number of cells in the chamber increased, the circumference of microsphere rotation generally decreased; recent data suggested that a consistent diameter of circumference may be better obtained by the addition of a center 'pole'.
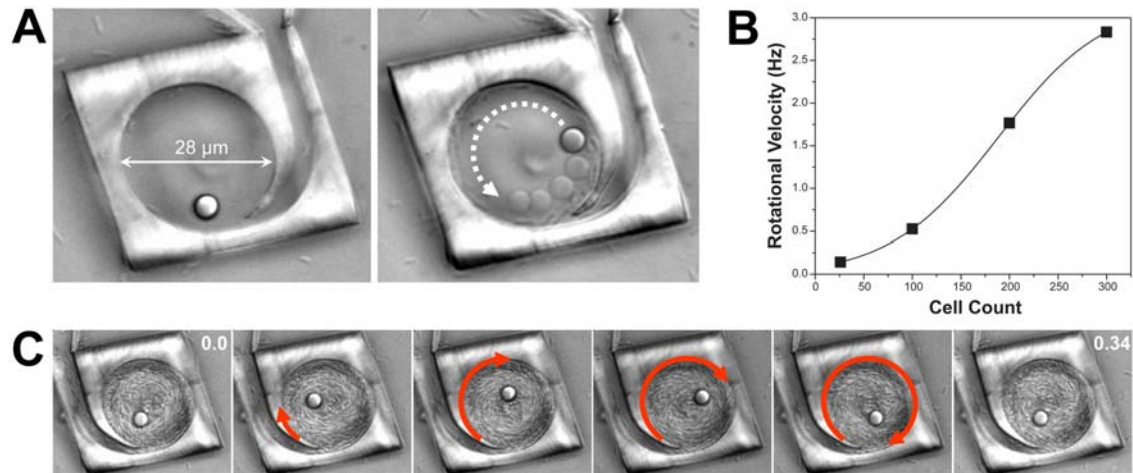
Figure 5.12: Controlled microsphere rotation via directed cell motility. A microsphere is trapped inside a circular microchamber by fabricating the chamber over the microsphere (A, left panel). Perimeter cells directed to swim clockwise in the chamber rotated the microsphere along a counterclockwise trajectory (A, right panel). The rotational velocity of the microsphere increased as the cell count in the microchamber increased. Cell number is based on a combination of manual counting and estimates of the density of cells in a 5 µm tall circular chamber of diameter 28 µm. The smooth curve was obtained from Sigmoidal (Boltzmann) fitting. (C) A single clockwise rotation of a microsphere. The numbers in the first and last panels indicate the elapsed time in seconds.

Continuous movement was observed for at least 6 hours in these chambers using smooth-swimming cells. As indicated in Figure 5.11B, overnight incubation in nutrient media could result in a chamber packed with non-motile cells. It would be of value to determine conditions that allow continuous movement in these chambers for longer periods. This may be accomplished by using less efficient rectifying geometries and

139

frequent flushing of the surrounding media or perhaps by designing a mechanism to flush non-motile cells (which separate into a center plug, Figure 5.8B) out of the chambers. In these and other experiments discussed thus far, decreased motility tended to coincide with increased cell-cell interactions, a process that takes place during the early stages of biofilm formation [34]; as previously suggested, this platform may provide a means to better understand these mechanisms and characterize potential treatments. Further, these conditions could be used to quantitatively study the 'cooperative' motility and fluidic forces generated by the swarmmer phenotype — given the capability to accurately measure cell count and rotational velocities.

These results demonstrate the possibility for harnessing mechanical energy from motile cells. Coupling these chambers to a current-generating geometry may be feasible, though such a system will require significant micromechanical engineering and would only be capable of producing miniscule powers. However, these initial results may provide the foundation to engineer microfluidic systems for directed fluid flow, mixing, and separation using only cell motility — capabilities that would allow a microfluidic device to operate without the need to be addressed by independent pumping or energy sources.

5. 4 CONCLUSION

In this chapter, microchambers composed of crosslinked proteins were evaluated for the capture, incubation, and directed motility of *E. coli* cells. These studies may provide the means to interrogate the behavior of microorganisms under highly controlled conditions with single cell resolution. Insight into the physical and environmental mechanisms that underly phenotypic changes in the bacterial lifecycle (such as population-coordinated behaviors that impact human health and disease) may be achieved

using the strategies presented. It would be of use to fabricate and interrogate many microchambers in parallel, a goal that represents an enormous challenge for serially-based MPE protein photocrosslinking. However, methods have been explored that allow parallel fabrication using MPE, for instance, by incorporation of a microlens array into the fabrication scheme [35]. Additionally, techniques described here offer an ultra-rapid prototyping paradigm for 3D microstructures. Many structure designs can be tested and evaluated in a single day using this approach and, upon optimization of parameters for the given application, microstructures could be fabricated in parallel using an alternative approach such as traditional photo or soft lithography.

Finally, microgeometries that enable the precise placement and rectified movement of motile cells are a step toward the realization of biohybrid microdevices, where a microdevice is powered solely by the energy output of microorganisms. The challenges to fully realize a useful device driven by motile microorganisms remain great, but the principles suggested here for geometric rectification, cell concentration and cell turnover are a significant starting point to develop controlled and autonomous microfluidic flow circuits.

5. 5 REFERENCES

[1]   S. E. Lyshevski, *Nano- and micro-electromechanical systems : fundamentals of nano- and microengineering*, 2nd ed. Boca Raton, Fla.: CRC Press, 2005.

[2]   J. Stelling, "Mathematical models in microbial systems biology," *Curr Opin Microbiol*, vol. 7, pp. 513-8, 2004.

[3]   M. A. Nowak and K. Sigmund, "Evolutionary dynamics of biological games," *Science*, vol. 303, pp. 793-9, 2004.

[4]   J. I. Prosser, B. J. Bohannan, T. P. Curtis, R. J. Ellis, M. K. Firestone, R. P. Freckleton, J. L. Green, L. E. Green, K. Killham, J. J. Lennon, A. M. Osborn, M. Solan, C. J. van der Gast, and J. P. Young, "The role of ecological theory in microbial ecology," *Nat Rev Microbiol*, vol. 5, pp. 384-92, 2007.

[5]   T. P. Curtis, W. T. Sloan, and J. W. Scannell, "Estimating prokaryotic diversity and its limits," *Proc Natl Acad Sci U S A*, vol. 99, pp. 10494-9, 2002.

[6]   M. S. Rappe and S. J. Giovannoni, "The uncultured microbial majority," *Annu Rev Microbiol*, vol. 57, pp. 369-94, 2003.

[7]   M. B. Elowitz, A. J. Levine, E. D. Siggia, and P. S. Swain, "Stochastic gene expression in a single cell," *Science*, vol. 297, pp. 1183-6, 2002.

[8]   B. F. Brehm-Stecher and E. A. Johnson, "Single-cell microbiology: tools, technologies, and applications," *Microbiol Mol Biol Rev*, vol. 68, pp. 538-59, 2004.

[9]   S. Basu, C. W. Wolgemuth, and P. J. Campagnola, "Measurement of normal and anomalous diffusion of dyes within protein structures fabricated via multiphoton excited cross-linking," *Biomacromolecules*, vol. 5, pp. 2347-57, 2004.

[10]   F. K. Balagadde, L. You, C. L. Hansen, F. H. Arnold, and S. R. Quake, "Long-term monitoring of bacteria undergoing programmed population control in a microchemostat," *Science*, vol. 309, pp. 137-40, 2005.

[11]   A. Groisman, C. Lobo, H. Cho, J. K. Campbell, Y. S. Dufour, A. M. Stevens, and A. Levchenko, "A microfluidic chemostat for experiments with bacterial and yeast cells," *Nat Methods*, vol. 2, pp. 685-9, 2005.

[12]   M. B. Miller and B. L. Bassler, "Quorum sensing in bacteria," *Annu Rev Microbiol*, vol. 55, pp. 165-99, 2001.

[13]   B. A. Hense, C. Kuttler, J. Muller, M. Rothballer, A. Hartmann, and J. U. Kreft, "Does efficiency sensing unify diffusion and quorum sensing?," *Nat Rev Microbiol*, vol. 5, pp. 230-9, 2007.

[14]   S. M. Rowe, S. Miller, and E. J. Sorscher, "Cystic fibrosis," *N Engl J Med*, vol. 352, pp. 1992-2001, 2005.

[15]   S. Chattopadhyay, R. Moldovan, C. Yeung, and X. L. Wu, "Swimming efficiency of bacterium Escherichia coli," *Proc Natl Acad Sci U S A*, vol. 103, pp. 13712-7, 2006.

[16]   M. J. Kim and K. S. Breuer, "Enhanced diffusion due to motile bacteria," *Physics of Fluids*, vol. 16, pp. L78-L81, 2004.

[17]   D. B. Weibel, P. Garstecki, D. Ryan, W. R. DiLuzio, M. Mayer, J. E. Seto, and G. M. Whitesides, "Microoxen: microorganisms to move microscale loads," *Proc Natl Acad Sci U S A*, vol. 102, pp. 11963-7, 2005.

[18]   Y. Hiratsuka, M. Miyata, T. Tada, and T. Q. P. Uyeda, "A microrotary motor powered by bacteria," *Proceedings of the National Academy of Sciences of the United States of America*, vol. 103, pp. 13618-13623, 2006.

[19]   H. C. Berg, *E. coli in motion*. New York: Springer, 2004.

[20]   S. Park, P. M. Wolanin, E. A. Yuzbashyan, P. Silberzan, J. B. Stock, and R. H. Austin, "Motion to form a quorum," *Science*, vol. 301, pp. 188, 2003.

[21]   R. S. Shaw, N. Packard, M. Schroter, and H. L. Swinney, "Geometry-induced asymmetric diffusion," *Proc Natl Acad Sci U S A*, vol. 104, pp. 9580-4, 2007.

[22]   M. Conese and J. Rejman, "Stem cells and cystic fibrosis," *J Cyst Fibros*, vol. 5, pp. 141-3, 2006.

[23]   S. Goldman, "Stem and progenitor cell-based therapy of the human central nervous system," *Nat Biotechnol*, vol. 23, pp. 862-71, 2005.

[24]   D. B. Weibel, W. R. Diluzio, and G. M. Whitesides, "Microfabrication meets microbiology," *Nat Rev Microbiol*, vol. 5, pp. 209-18, 2007.

[25]   J. R. Mitchell and D. A. Ledward, *Functional properties of food macromolecules*. London ; New York, N.Y.: Elsevier Applied Science Publishers, 1985.

[26]   S. Takeuchi, W. R. DiLuzio, D. B. Weibel, and G. M. Whitesides, "Controlling the shape of filamentous cells of Escherichia coli," *Nano Lett*, vol. 5, pp. 1819-23, 2005.

[27]   S. Rozhok, Z. Fan, D. Nyamjav, C. Liu, C. A. Mirkin, and R. C. Holz, "Attachment of motile bacterial cells to prealigned holed microarrays," *Langmuir*, vol. 22, pp. 11251-4, 2006.

[28]   N. Darnton, L. Turner, K. Breuer, and H. C. Berg, "Moving fluid with bacterial carpets," *Biophys J*, vol. 86, pp. 1863-70, 2004.

[29]   H. Hess, G. D. Bachand, and V. Vogel, "Powering nanodevices with biomolecular motors," *Chemistry-a European Journal*, vol. 10, pp. 2110-2116, 2004.

[30]   S. G. Moorjani, L. Jia, T. N. Jackson, and W. O. Hancock, "Lithographically Patterned Channels Spatially Segregate Kinesin Motor Activity and Effectively Guide Microtubule Movements," *Nano Letters*, vol. 3, pp. 633-637, 2003.

[31] M. G. van den Heuvel, C. T. Butcher, R. M. Smeets, S. Diez, and C. Dekker, "High rectifying efficiencies of microtubule motility on kinesin-coated gold nanostructures," *Nano Lett*, vol. 5, pp. 1117-22, 2005.

[32] M. G. van den Heuvel, M. P. de Graaff, and C. Dekker, "Molecular sorting by electrical steering of microtubules in kinesin-coated channels," *Science*, vol. 312, pp. 910-4, 2006.

[33] G. M. Fraser and C. Hughes, "Swarming motility," *Current opinion in microbiology*, vol. 2, pp. 630-5, 1999.

[34] R. Van Houdt and C. W. Michiels, "Role of bacterial cell surface structures in Escherichia coli biofilm formation," *Research in Microbiology*, vol. 156, pp. 626-633, 2005.

[35] F. Formanek, N. Takeyasu, T. Tanaka, K. Chiyoda, A. Ishikawa, and S. Kawata, "Three-dimensional fabrication of metallic nanostructures over large areas by two-photon polymerization," *Optics Express*, vol. 14, pp. 800-809, 2006.

Bibliography

Alberts B (2004) Essential cell biology, 2nd edn. Garland Science Pub., New York, NY

Alexander C, Shakesheff KM (2006) Responsive polymers at the biology/materials science interface. Advanced Materials 18:3321-3328

Allen R, Nielson R, Wise DD, Shear JB (2005) Catalytic three-dimensional protein architectures. Anal Chem 77:5089-5095

Arakawa T, Timasheff SN (1984) Mechanism of protein salting in and salting out by divalent cation salts: balance between hydration and salt binding. Biochemistry 23:5912-5923

Balagadde FK, You L, Hansen CL, Arnold FH, Quake SR (2005) Long-term monitoring of bacteria undergoing programmed population control in a microchemostat. Science 309:137-140

Banghart M, Borges K, Isacoff E, Trauner D, Kramer RH (2004) Light-activated ion channels for remote control of neuronal firing. Nat Neurosci 7:1381-1386

Basu S, Wolgemuth CW, Campagnola PJ (2004) Measurement of norma and anomalous diffusion of dyes within protein structures fabricated via muftiphoton excited cross-linking. Biomacromolecules 5:2347-2357

Beebe DJ et al. (2000) Functional hydrogel structures for autonomous flow control inside microfluidic channels. Nature 404:588-590

Berg HC (2004) E. coli in motion. Springer, New York

Berman HM et al. (2000) The Protein Data Bank. Nucleic Acids Research 28:235-242

Bertsch A, Jezequel JY, Andre JC (1997) Study of the spatial resolution of a new 3D microfabrication process: the microstereophotolithog. using a dynamic mask-generator technique. Journal of Photochemistry and Photobiology, A: Chemistry 107:275-281

Bitan G (2006) Structural study of metastable amyloidogenic protein oligomers by photo-induced cross-linking of unmodified proteins. Methods in Enzymology 413:217-236

Brehm-Stecher BF, Johnson EA (2004) Single-cell microbiology: tools, technologies, and applications. Microbiol Mol Biol Rev 68:538-559

Bucknall DG, Institute of Materials Minerals and Mining. (2005) Nanolithography and patterning techniques in microelectonics. Woodhead Pub. on behalf of the Institute of Materials Minerals & Mining ;

Byrne ME, Park K, Peppas NA (2002) Molecular imprinting within hydrogels. Advanced Drug Delivery Reviews 54:149-161

Carter DC, Ho JX (1994) Structure of serum albumin. Adv Protein Chem 45:153-203

Chalfie M, Kain S (2006) Green fluorescent protein : properties, applications, and protocols, 2nd edn. Wiley-Interscience, Hoboken, N.J.

Chang HY, Takei K, Sydor AM, Born T, Rusnak F, Jay DG (1995) Asymmetric retraction of growth cone filopodia following focal inactivation of calcineurin. Nature 376:686-690

Chang JC, Brewer GJ, Wheeler BC (2003) A modified microstamping technique enhances polylysine transfer and neuronal cell patterning. Biomaterials 24:2863-2870

Chang ST, Paunov VN, Petsev DN, Velev OD (2007) Remotely powered self-propelling particles and micropumps based on miniature diodes. Nat Mater 6:235-240

Chattopadhyay S, Moldovan R, Yeung C, Wu XL (2006) Swimming efficiency of bacterium Escherichia coli. Proc Natl Acad Sci U S A 103:13712-13717

Chattopadhyaya R, Meador WE, Means AR, Quiocho FA (1992) Calmodulin Structure Refined at 1.7 Angstrom Resolution. Journal of Molecular Biology 228:1177-1192

Conese M, Rejman J (2006) Stem cells and cystic fibrosis. J Cyst Fibros 5:141-143

Cook WJ, Walter LJ, Walter MR (1994) Drug-Binding by Calmodulin - Crystal-Structure of a Calmodulin Trifluoperazine Complex. Biochemistry 33:15259-15265

Cooperman BS, Dondon J, Finelli J, Grunberg-Manago M, Michelson AM (1977) Photosensitized cross-linking of IF-3 to Escherichia coli 30S subunits. FEBS Letters 76:59-63

Cumpston BH et al. (1999) Two-photon polymerization initiators for three-dimensional optical data storage and microfabrication. Nature (London) 398:51-54

Curtis TP, Sloan WT, Scannell JW (2002) Estimating prokaryotic diversity and its limits. Proc Natl Acad Sci USA 99:10494-10499

Cushing MC, Anseth KS (2007) Hydrogel cell cultures. Science 316:1133-1134

Darnton N, Turner L, Breuer K, Berg HC (2004) Moving fluid with bacterial carpets. Biophys J 86:1863-1870

Davies MJ (2004) Reactive species formed on proteins exposed to singlet oxygen. Photochemical & Photobiological Sciences 3:17-25

Davies MJ, Truscott RJW (2001) Photo-oxidation of proteins and its role in cataractogenesis. Journal of Photochemistry and Photobiology, B: Biology 63:114-125

DeMello AJ (2006) Control and detection of chemical reactions in microfluidic systems. Nature 442:394-402

Denk W, Strickler JH, Webb WW (1990) 2-Photon Laser Scanning Fluorescence Microscopy. Science 248:73-76

Dertinger SKW, Jiang XY, Li ZY, Murthy VN, Whitesides GM (2002) Gradients of substrate-bound laminin orient axonal specification of neurons. Proceedings of the National Academy of Sciences of the United States of America 99:12542-12547

Deubel M, von Freymann G, Wegener M, Pereira S, Busch K, Soukoulis CM (2004) Direct laser writing of three-dimensional photonic-crystal templates for telecommunications. Nature Materials 3:444-447

Duck FA (1990) Physical properties of tissue: a comprehensive reference book, U.S. edn. Academic Press, London ; San Diego

Ehrick JD, Deo SK, Browning TW, Bachas LG, Madou MJ, Daunert S (2005) Genetically engineered protein in hydrogels tailors stimuli-responsive characteristics. Nat Mater 4:298-302

Ehrlicher A et al. (2002) Guiding neuronal growth with light. Proceedings of the National Academy of Sciences of the United States of America 99:16024-16028

El-Ali J, Sorger PK, Jensen KF (2006) Cells on chips. Nature 442:403-411

Elowitz MB, Levine AJ, Siggia ED, Swain PS (2002) Stochastic gene expression in a single cell. Science 297:1183-1186

Formanek F, Takeyasu N, Tanaka T, Chiyoda K, Ishikawa A, Kawata S (2006) Three-dimensional fabrication of metallic nanostructures over large areas by two-photon polymerization. Optics Express 14:800-809

Fraser GM, Hughes C Swarming motility. Current opinion in microbiology (1999) 2:630-635.

Freeman JW, Woods MD, Laurencin CT (2007) Tissue engineering of the anterior cruciate ligament using a braid-twist scaffold design. J Biomech 40:2029-2036

Fromherz P (2002) Electrical interfacing of nerve cells and semiconductor chips. Chemphyschem 3:276-284

Gabrielli D, Belisle E, Severino D, Kowaltowski AJ, Baptista MS (2004) Binding, aggregation and photochemical properties of methylene blue in mitochondrial suspensions. Photochemistry and Photobiology 79:227-232

Gil ES, Hudson SM (2004) Stimuli-responsive polymers and their bioconjugates. Progress in Polymer Science 29:1173-1222

Glezer EN et al. (1997) Three-dimensional optical storage inside transparent materials (vol 21, pg 2023, 1996). Optics Letters 22:422-422

Glezer EN, Mazur E (1997) Ultrafast-laser driven micro-explosions in transparent materials. Applied Physics Letters 71:882-884

Goldman S (2005) Stem and progenitor cell-based therapy of the human central nervous system. Nat Biotechnol 23:862-871

Gonzalez M, Argarana CE, Fidelio GD (1999) Extremely high thermal stability of streptavidin and avidin upon biotin binding. Biomol Eng 16:67-72

Goppert-Mayer M (1931) Elementary processes with two quantum jumps. Annalen der Physik (Berlin, Germany) 9:273-294

Green NM (1975) Avidin. Adv Protein Chem 29:85-133

Grier DG (2003) A revolution in optical manipulation. Nature 424:810-816

Groisman A et al. (2005) A microfluidic chemostat for experiments with bacterial and yeast cells. Nat Methods 2:685-689

Hahn MS, Miller JS, West JL (2005) Laser scanning lithography for surface micropatterning on hydrogels. Advanced Materials 17:2939-2942

Hense BA, Kuttler C, Muller J, Rothballer M, Hartmann A, Kreft JU (2007) Does efficiency sensing unify diffusion and quorum sensing? Nat Rev Microbiol 5:230-239

Herman MA, Fromm D, Kessel D (1999) Tumor blood-flow changes following protoporphyrin IX-based photodynamic therapy in mice and humans. Journal of Photochemistry and Photobiology, B: Biology 52:99-104

Hess H (2006) Materials science. Toward devices powered by biomolecular motors. Science 312:860-861

Hess H, Bachand GD, Vogel V (2004) Powering nanodevices with biomolecular motors. Chemistry-a European Journal 10:2110-2116

Hill RT, Lyon JL, Allen R, Stevenson KJ, Shear JB (2005) Microfabrication of three-dimensional bioelectronic architectures. J Am Chem Soc 127:10707-10711

Hill RT, Shear JB (2006) Enzyme-nanoparticle functionalization of three-dimensional protein scaffolds. Anal Chem 78:7022-7026

Hiratsuka Y, Miyata M, Tada T, Uyeda TQP (2006) A microrotary motor powered by bacteria. Proceedings of the National Academy of Sciences of the United States of America 103:13618-13623

Hsu KL, Pilobello KT, Mahal LK (2006) Analyzing the dynamic bacterial glycome with a lectin microarray approach. Nat Chem Biol 2:153-157

Husain A, Zhang X, Doll MA, States JC, Barker DF, Hein DW (2007) Functional Analysis of the Human N-Acetyltransferase 1 Major Promoter: Quantitation of Tissue Expression and Identification of Critical Sequence Elements. Drug Metab Dispos

Jager EW, Smela E, Inganas O (2000) Microfabricating conjugated polymer actuators. Science 290:1540-1545

Jeon NL, Dertinger SKW, Chiu DT, Choi IS, Stroock AD, Whitesides GM (2000) Generation of solution and surface gradients using microfluidic systems. Langmuir 16:8311-8316

Jiang XY, Xu QB, Dertinger SKW, Stroock AD, Fu TM, Whitesides GM (2005) A general method for patterning gradients of biomolecules on surfaces using microfluidic networks. Analytical Chemistry 77:2338-2347

Jung DR et al. (2001) Topographical and physicochemical modification of material surface to enable patterning of living cells. Critical Reviews in Biotechnology 21:111-154

Kaehr B et al. (2006) Direct-write fabrication of functional protein matrixes using a low-cost Q-switched laser. Anal Chem 78:3198-3202

Kaehr B, Allen R, Javier DJ, Currie J, Shear JB (2004) Guiding neuronal development with in situ microfabrication. Proceedings of the National Academy of Sciences of the United States of America 101:16104-16108

Kaehr B, Shear JB (2007) Mask-directed multiphoton lithography. J Am Chem Soc 129:1904-1905

Kaiser W, Garrett CGB (1961) Two-photon excitation in CaF2:Eu++. Physical Review Letters 7:229-231

Kandel ER, Schwartz JH, Jessell TM (2000) Principles of neural science, 4th edn. McGraw-Hill Health Professions Division, New York

Kawata S, Sun HB, Tanaka T, Takada K (2001) Finer features for functional microdevices. Nature 412:697-698

Keshishian H (2004) Ross Harrison's "The outgrowth of the nerve fiber as a mode of protoplasmie movement". Journal of Experimental Zoology Part a-Comparative Experimental Biology 301A:201-203

Khademhosseini A, Langer R, Borenstein J, Vacanti JP (2006) Microscale technologies for tissue engineering and biology. Proceedings of the National Academy of Sciences of the United States of America 103:2480-2487

Khetani SR, Bhatia SN (2006) Engineering tissues for in vitro applications. Current Opinion in Biotechnology 17:524-531

Kim J, Nayak S, Lyon LA (2005) Bioresponsive hydrogel microlenses. J Am Chem Soc 127:9588-9592

Kim MJ, Breuer KS (2004) Enhanced diffusion due to motile bacteria. Physics of Fluids 16:L78-L81

Klein Y, Efrati E, Sharon E (2007) Shaping of elastic sheets by prescription of non-Euclidean metrics. Science 315:1116-1120

Koshi Y, Nakata E, Yamane H, Hamachi I (2006) A fluorescent lectin array using supramolecular hydrogel for simple detection and pattern profiling for various glycoconjugates. Journal of the American Chemical Society 128:10413-10422

Laitinen OH, Hytonen VP, Nordlund HR, Kulomaa MS (2006) Genetically engineered avidins and streptavidins. Cellular and Molecular Life Sciences 63:2992-3017

Lei M, Gu YD, Baldi A, Siegel RA, Ziaie B (2004) High-resolution technique for fabricating environmentally sensitive hydrogel microstructures. Langmuir 20:8947-8951

Lendlein A, Jiang H, Junger O, Langer R (2005) Light-induced shape-memory polymers. Nature 434:879-882

Levinson HJ (2005) Principles of lithography, 2nd edn. SPIE Press, Bellingham, WA

Lewis JA (2006) Direct ink writing of 3D functional materials. Advanced Functional Materials 16:2193-2204

Lin HJ, Kodadek T (2005) Photo-induced oxidative cross-linking as a method to evaluate the specificity of protein-ligand interactions. Journal of Peptide Research 65:221-228

Liu Z-R, Sargueil B, Smith CWJ (2000) Methylene blue-mediated cross-linking of proteins to double-stranded RNA. Methods in Enzymology 318:22-33

Love JC, Wolfe DB, Jacobs HO, Whitesides GM (2001) Microscope projection photolithography for rapid prototyping of masters with micron-scale features for use in soft lithography. Langmuir 17:6005-6012

Lu HH et al. (2005) Anterior cruciate ligament regeneration using braided biodegradable scaffolds: in vitro optimization studies. Biomaterials 26:4805-4816

Lu Y, Mapili G, Suhali G, Chen S, Roy K (2006) A digital micro-mirror device-based system for the microfabrication of complex, spatially patterned tissue engineering scaffolds. Journal of Biomedical Materials Research, Part A 77A:396-405

Luo Y, Shoichet MS (2004) A photolabile hydrogel for guided three-dimensional cell growth and migration. Nat Mater 3:249-253

Lyshevski SE (2005) Nano- and micro-electromechanical systems : fundamentals of nano- and microengineering, 2nd edn. CRC Press, Boca Raton, Fla.

Mahoney MJ, Anseth KS (2006) Three-dimensional growth and function of neural tissue in degradable polyethylene glycol hydrogels. Biomaterials 27:2265-2274

Mahoney MJ, Chen RR, Tan J, Saltzman WM (2005) The influence of microchannels on neurite growth and architecture. Biomaterials 26:771-778

Maruo S, Nakamura O, Kawata S (1997) Three-dimensional microfabrication with two-photon-absorbed photopolymerization. Optics Letters 22:132-134

Matthew JB, Gurd FR (1986) Stabilization and destabilization of protein structure by charge interactions. Methods Enzymol 130:437-453

Mazor Y, Van Blarcom T, Mabry R, Iverson BL, Georgiou G (2007) Isolation of engineered, full-length antibodies from libraries expressed in Escherichia coli. Nature Biotechnology 25:563-565

Merz M, Fromherz P (2002) Polyester microstructures for topographical control of outgrowth and synapse formation of snail neurons. Advanced Materials (Weinheim, Germany) 14:141-144

Miller MB, Bassler BL (2001) Quorum sensing in bacteria. Annu Rev Microbiol 55:165-199

Ming GL et al. (2002) Adaptation in the chemotactic guidance of nerve growth cones. Nature 417:411-418

Minko S (2006) Responsive polymer materials: design and applications, 1st edn. Blackwell Pub., Ames, Iowa

Mitchell JR, Ledward DA (1985) Functional properties of food macromolecules. Elsevier Applied Science Publishers, London ; New York, N.Y.

Miyata T, Asami N, Uragami T (1999) A reversibly antigen-responsive hydrogel. Nature 399:766-769

Moorjani SG, Jia L, Jackson TN, Hancock WO (2003) Lithographically Patterned Channels Spatially Segregate Kinesin Motor Activity and Effectively Guide Microtubule Movements. Nano Letters 3:633-637

Mora T, Boudaoud A (2006) Buckling of swelling gels. European Physical Journal E 20:119-124

Murphy WL, Dillmore WS, Modica J, Mrksich M (2007) Dynamic Hydrogels: Translating a Protein Conformational Change into Macroscopic Motion. Angew Chem Int Ed Engl 46:3066-3069

Naka Y, Kitazawa A, Akaishi Y, Shimizu N Neurite (2004) Outgrowths of neurons using neurotrophin-coated nanoscale magnetic beads. Journal of bioscience and bioengineering 98:348-352.

Neckers DC (1989) Rose Bengal. Journal of Photochemistry and Photobiology, A: Chemistry 47:1-29

Nowak MA, Sigmund K (2004) Evolutionary dynamics of biological games. Science 303:793-799

Ohyama Y, Kasai K, Nomoto H, Inoue Y (1985) Frontal affinity chromatography of ovalbumin glycoasparagines on a concanavalin A-sepharose column. A quantitative study of the binding specificity of the lectin. J Biol Chem 260:6882-6887

Osada Y, Okuzaki H, Hori H (1992) A Polymer Gel with Electrically Driven Motility. Nature 355:242-244

Park S, Wolanin PM, Yuzbashyan EA, Silberzan P, Stock JB, Austin RH (2003) Motion to form a quorum. Science 301:188

Pearce TM, Williams JC (2007) Microtechnology: meet neurobiology. Lab Chip 7:30-40

Pilobello KT, Krishnamoorthy L, Slawek D, Mahal LK (2005) Development of a lectin microarray for the rapid analysis of protein glycopatterns. Chembiochem 6:985-989

Pitts JD, Campagnola PJ, Epling GA, Goodman SL (2000) Submicron Multiphoton Free-Form Fabrication of Proteins and Polymers: Studies of Reaction Efficiencies and Applications in Sustained Release. Macromolecules 33:1514-1523

Pitts JD, Campagnola PJ, Epling GA, Goodman SL (2000) Submicron Multiphoton Free-Form Fabrication of Proteins and Polymers: Studies of Reaction Efficiencies and Applications in Sustained Release. Macromolecules 33:1514-1523

Prosser JI et al. (2007) The role of ecological theory in microbial ecology. Nat Rev Microbiol 5:384-392

Rajnicek AM, McCaig CD (1997) Guidance of CNS growth cones by substratum grooves and ridges: effects of inhibitors of the cytoskeleton, calcium channels and signal transduction pathways. Journal of Cell Science 110:2915-2924

Rappe MS, Giovannoni SJ (2003) The uncultured microbial majority. Annu Rev Microbiol 57:369-394

Rowe SM, Miller S, Sorscher EJ (2005) Cystic fibrosis. N Engl J Med 352:1992-2001

Rozhok S, Fan Z, Nyamjav D, Liu C, Mirkin CA, Holz RC (2006) Attachment of motile bacterial cells to prealigned holed microarrays. Langmuir 22:11251-11254

Saeta P, Wang JK, Siegal Y, Bloembergen N, Mazur E (1991) Ultrafast electronic disordering during femtosecond laser melting of gallium arsenide. Physical Review Letters 67:1023-1026

Salinas CN, Cole BB, Kasko AM, Anseth KS (2007) Chondrogenic Differentiation Potential of Human Mesenchymal Stem Cells Photoencapsulated within Poly(Ethylene Glycol)-Arginine-Glycine-Aspartic Acid-Serine Thiol-Methacrylate Mixed-Mode Networks. Tissue Engineering 13:1025-1034

Sanjana Neville E, Fuller Sawyer B (2004) A fast flexible ink-jet printing method for patterning dissociated neurons in culture. Journal of neuroscience methods 136:151-163.

Schild HG (1992) Poly (N-Isopropylacrylamide) - Experiment, Theory and Application. Progress in Polymer Science 17:163-249

Scopes RK (1994) Protein purification: principles and practice, 3rd edn. Springer-Verlag, New York

Sharon E, Roman B, Marder M, Shin GS, Swinney HL (2002) Mechanics: Buckling cascades in free sheets - Wavy leaves may not depend only on their genes to make their edges crinkle. Nature 419:579-579

Shaw RS, Packard N, Schroter M, Swinney HL (2007) Geometry-induced asymmetric diffusion. Proc Natl Acad Sci U S A 104:9580-9584

Shear JB (1999) Multiphoton-excited fluorescence in bioanalytical chemistry. Analytical Chemistry 71:598A-605A

Shen HR, Spikes JD, Kopecekova P, Kopecek J (1996) Photodynamic crosslinking of proteins. I. Model studies using histidine- and lysine-containing N-(2-hydroxypropyl)methacrylamide copolymers. Journal of photochemistry and photobiology. B, Biology 34:203-210.

Shen H-R, Spikes JD, Kopeckova P, Kopecek J (1996) Photodynamic crosslinking of proteins. II. Photocrosslinking of a model protein-ribonuclease A. Journal of Photochemistry and Photobiology, B: Biology 35:213-219

Shen HR, Spikes JD, Smith CJ, Kopecek J (2000a) Photodynamic crosslinking of proteins IV. Nature of the His-His bond(s) formed in the Rose bengal-photosensitized crosslinking of N-benzoyl-L-histidine. Journal of Photochemistry and Photobiology, A: Chemistry 130:1-6

Shen HR, Spikes JD, Smith CJ, Kopecek J (2000b) Photodynamic crosslinking of proteins V. Nature of the tyrosine-tyrosine bonds formed in the FMN-sensitized intermolecular crosslinking of N-acetyl-L-tyrosine. Journal of Photochemistry and Photobiology, A: Chemistry 133:115-122

Silva GA et al. (2004) Selective differentiation of neural progenitor cells by high-epitope density nanofibers. Science 303:1352-1355

Spikes JD, Shen H-R, Kopeckova P, Kopecek J (1999) Photodynamic crosslinking of proteins. III. Kinetics of the FMN- and rose bengal-sensitized photooxidation and intermolecular crosslinking of model tyrosine-containing N-(2-hydroxypropyl)methacrylamide copolymers. Photochemistry and Photobiology 70:130-137

Stelling J (2004) Mathematical models in microbial systems biology. Curr Opin Microbiol 7:513-518

Straight RC, Spikes JD (1985) Photosensitized oxidation of biomolecules. Singlet O2 4:91-143

Sun C, Fang N, Wu DM, Zhang X (2005) Projection micro-stereolithography using digital micromirror dynamic mask. Sensors and Actuators, A: Physical A121:113-120

Sun HB, Kawata S (2004) Two-photon photopolymerization and 3D lithographic microfabrication. Nmr - 3d Analysis - Photopolymerization 170:169-273

Sun HB, Tanaka T, Kawata S (2002) Three-dimensional focal spots related to two-photon excitation. Applied Physics Letters 80:3673-3675

Takeuchi S, DiLuzio WR, Weibel DB, Whitesides GM (2005) Controlling the shape of filamentous cells of Escherichia coli. Nano Lett 5:1819-1823

Tanaka T, Sun ST, Nishio I, Swislow G, Shah A (1980) Phase-Transitions in Ionic Gels. Ferroelectrics 30:97-97

Tanielian C, Mechin R (1989) Mechanism and kinetics of the methylene-blue-sensitized photo-oxygenation of polydienes. Journal of Photochemistry and Photobiology, A: Chemistry 48:43-51

Tardivo JP et al. (2005) Methylene blue in photodynamic therapy: From basic mechanisms to clinical applications. Photodiagnosis and Photodynamic Therapy 2:175-191

Taylor AM, Blurton-Jones M, Rhee SW, Cribbs DH, Cotman CW, Jeon NL (2005) A microfluidic culture platform for CNS axonal injury, regeneration and transport. Nat Methods 2:599-605

Terray A, Oakey J, Marr DW (2002) Microfluidic control using colloidal devices. Science 296:1841-1844

Theodossiou T, Hothersall JS, Woods EA, Okkenhaug K, Jacobson J, MacRobert AJ (2003) Firefly Luciferin-activated Rose Bengal: In Vitro Photodynamic Therapy by Intracellular Chemiluminescence in Transgenic NIH 3T3 Cells. Cancer Research 63:1818-1821

Tirumala VR, Divan R, Ocola LE, Mancini DC (2005) Direct-write e-beam patterning of stimuli-responsive hydrogel nanostructures. Journal of Vacuum Science & Technology, B: Microelectronics and Nanometer Structures--Processing, Measurement, and Phenomena 23:3124-3128

Turcu F, Tratsk-Nitz K, Thanos S, Schuhmann W, Heiduschka P (2003) Ink-jet printing for micropattern generation of laminin for neuronal adhesion. Journal of Neuroscience Methods 131:141-148

van den Heuvel MG, Butcher CT, Smeets RM, Diez S, Dekker C (2005) High rectifying efficiencies of microtubule motility on kinesin-coated gold nanostructures. Nano Lett 5:1117-1122

van den Heuvel MG, de Graaff MP, Dekker C (2006) Molecular sorting by electrical steering of microtubules in kinesin-coated channels. Science 312:910-914

Van Houdt R, Michiels CW (2005) Role of bacterial cell surface structures in Escherichia coli biofilm formation. Research in Microbiology 156:626-633

Van Kessel PF, Hornbeck LJ, Meier RE, Douglass MR (1998) MEMS-based projection display. Proceedings of the Ieee 86:1687-1704

Watanabe T et al. (2002) Photoresponsive hydrogel microstructure fabricated by two-photon initiated polymerization. Advanced Functional Materials 12:611-614

Weibel DB et al. (2005) Microoxen: microorganisms to move microscale loads. Proc Natl Acad Sci U S A 102:11963-11967

Weibel DB, Diluzio WR, Whitesides GM (2007) Microfabrication meets microbiology. Nat Rev Microbiol 5:209-218

Weinl C, Becker N, Loeschinger J (2005) Responses of temporal retinal growth cones to ephrinA5-coated beads. Journal of neurobiology 62:219-230.

Weng H, Zhou J, Tang L, Hu Z (2004) Tissue responses to thermally-responsive hydrogel nanoparticles. Journal of Biomaterials Science, Polymer Edition 15:1167-1180

Whitesides GM (2006) The origins and the future of microfluidics. Nature 442:368-373

Wu ES, Strickler JH, Harrell WR, Webb WW (1992) Two-photon lithography for microelectronic application. Proceedings of SPIE-The International Society for Optical Engineering 1674:776-782

Xia YN, Whitesides GM (1998) Soft lithography. Angewandte Chemie-International Edition 37:551-575

Xu C, Zipfel W, Shear JB, Williams RM, Webb WW (1996) Multiphoton fluorescence excitation: new spectral windows for biological nonlinear microscopy. Proc Natl Acad Sci U S A 93:10763-10768

Yeung CK, Lauer L, Offenhausser A, Knoll W (2001) Modulation of the growth and guidance of rat brain stem neurons using patterned extracellular matrix proteins. Neuroscience letters 301:147-150.

Yoshikuni Y, Keasling JD (2007) Pathway engineering by designed divergent evolution. Current Opinion in Chemical Biology 11:233-239

Zaari N, Rajagopalan P, Kim SK, Engler AJ, Wong JY (2004) Photopolymerization in microfluidic gradient generators: Microscale control of substrate compliance to manipulate cell response. Advanced Materials (Weinheim, Germany) 16:2133-2137

Zeck G, Fromherz P (2001) Noninvasive neuroelectronic interfacing with synaptically connected snail neurons immobilized on a semiconductor chip. Proceedings of the National Academy of Sciences of the United States of America 98:10457-10462

Zhang F et al. (2007) Multimodal fast optical interrogation of neural circuitry. Nature 446:633-639

Zhao B, Moore JS (2001) Fast pH- and Ionic Strength-Responsive Hydrogels in Microchannels. Langmuir 17:4758-4763

Zheng JQ, Felder M, Connor JA, Poo MM (1994) Turning of Nerve Growth Cones Induced by Neurotransmitters. Nature 368:140-144

Vita

Bryan James Kaehr was born in New Mexico on March 19, 1975 to James and Theresa Kaehr. He attended Albuquerque public schools, followed by the University of New Mexico, where he earned a Bachelors of Science in Psychology and Sociology (2000) as well as a Bachelors of Science in Biology (2002). In 2002, he enrolled in the Biochemistry graduate program at the University of Texas at Austin.

Permanent address: 8613 Hannett Ave. NE, Albuquerque, NM 87112

This dissertation was typed by the author.